HISTORICAL AND FUTURE ANTARCTIC PRECIPITATION BASED ON CMIP5 MODELS, REANALYSIS DATA AND IN SITU MEASUREMENTS.

MALCOLM TANG SIONG YII

INSTITUTE FOR ADVANCED STUDIES
UNIVERSITY OF MALAYA
KUALA LUMPUR

2020

HISTORICAL AND FUTURE ANTARCTIC PRECIPITATION BASED ON CMIP5 MODELS, REANALYSIS DATA AND IN SITU MEASUREMENTS.

MALCOLM TANG SIONG YII

THESIS SUBMITTED IN FULFILMENT OF THE REQUIREMENTS FOR THE DEGREE OF DOCTOR OF PHILOSOPHY

INSTITUTE FOR ADVANCED STUDIES
UNIVERSITY OF MALAYA
KUALA LUMPUR

2020

ORIGINAL LITERARY WORK DECLARATION

Name of Candidate: Malcolm Tang Siong Yii

Matric No: HHC140020

Name of Degree: PhD

Title of Project Paper/Research Report/Dissertation/Thesis ("this Work"):

Field of Study: Earth Science

I do solemnly and sincerely declare that:

(1) I am the sole author/writer of this Work;
(2) This Work is original;
(3) Any use of any work in which copyright exists was done by way of fair dealing and for permitted purposes and any excerpt or extract from, or reference to or reproduction of any copyright work has been disclosed expressly and sufficiently and the title of the Work and its authorship have been acknowledged in this Work;
(4) I do not have any actual knowledge nor do I ought reasonably to know that the making of this work constitutes an infringement of any copyright work;
(5) I hereby assign all and every rights in the copyright to this Work to the University of Malaya ("UM"), who henceforth shall be owner of the copyright in this Work and that any reproduction or use in any form or by any means whatsoever is prohibited without the written consent of UM having been first had and obtained;
(6) I am fully aware that if in the course of making this Work I have infringed any copyright whether intentionally or otherwise, I may be subject to legal action or any other action as may be determined by UM.

Candidate's Signature Date: 13 October 2020

Subscribed and solemnly declared before,

Witness's Signature Date:
3 November 2020

Name:

Designation:

HISTORICAL AND FUTURE ANTARCTIC PRECIPITATION BASED ON CMIP5 MODELS, REANALYSIS DATA AND IN SITU MEASUREMENTS

ABSTRACT

The study of precipitation in Antarctica is one of the most studied research topics today. The reliability and accuracy of climate models in simulating Antarctic precipitation, however, are still debatable. Measuring precipitation in Antarctica poses many distinctive challenges. This work attempts to establish a comprehensive study of precipitation in Antarctica. The first part of the study assesses a year-long measurements from five precipitation instruments with reanalysis datatsets and satellite data. The tipping bucket gauges (TBGs) were observed to be less sensitive compared to laser-based sensors (LBSs). Case studies of the daily precipitation and seasonal precipitation measurements showed VPF-730 to be the most reliable precipitation sensor among the instruments. The reanalyses had a positive correlation with wind speed, in particular the precipitation measurement from the Japanese 55-year Reanalysis (JRA-55). During strong wind events, the GPCP 1-Degree-Daily (1DD) was unable to fully capture the effect of wind, and hence the relatively low precipitation amount. The Laser Precipitation Monitor (LPM) and Campbell Scientific-700 (CS700H) had instrumental errors during the study. Installing multiple LBSs at different locations (in close proximity) can help identify inconsistency in the readings. For the second part of the study, we assess the precipitation and surface air temperature (SAT) of Antarctica (90 ^{o}S to 60 ^{o}S) using CMIP5 models and the European Centre for Medium-range Weather Forecasts "Interim" reanalysis (ERA-Interim); the National Centers for Environmental Prediction Climate Forecast System Reanalysis (CFSR); JRA-55; and the Modern Era Retrospective-analysis for Research and Applications (MERRA) datasets for 1979–2005. For precipitation, the time series show that the MERRA and JRA-55 have increased significantly from 1979 to 2005, while the ERA-Interim and CFSR have insignificant changes. The reanalyses also have

low correlation with one another (generally less than +0.69). 37 CMIP5 models show increasing trend, 18 of which are significant. The resulting CMIP5 multimodel mean (MMM) also has a significant increasing trend of 0.29 ± 0.06 mm year^{-1}. For SAT, the reanalyses show insignificant changes and have high correlation with one another, while the CMIP5 MMM shows a significant increasing trend. The variability of precipitation and SAT of MMM could affect the significance of its trend. One of the many reasons for the large differences in precipitation is the resolution of the CMIP5 models. The final part of the study involves using CMIP5 models to predict precipitation and SAT trends in Antarctica under four different representative concentration pathways (RCP): RCP 2.6, RCP 4.5, RCP 6.0 and RCP 8.5 for the year 2006-2100. The study shows that for precipitation, the Peninsula has the highest trend regardless of scenarios. For SAT, the interior region has the highest trend, followed by the Weddell Sea off the coast of Halley. For the projection of SAT, the consistency of the CMIP5 models in simulating accurate historical SAT climatology no longer appear in the RCP experiments. However, the consistency of the projection from different models increases as the Greenhouse gases (GHG) concentration increases. The correlation between SAT and precipitation increases as the GHG concentration increases.

Keywords: Antarctica, precipitation, reanalysis, CMIP5, models.

KAJIAN KERPASAN LEPAS DAN MASA DEPAN DI ANTARTIK MENGGUNAKAN MODEL CMIP5, DATASET REANALISIS DAN SUKATAN TAPAK

ABSTRAK

Kajian kerpasan di Antartika telah menarik banyak perhatian baru-baru ini. Keberkesanan model iklim dalam mensimulasikan pemendakan Antartika, bagaimanapun, masih dibahaskan. Kajian kerpasan di Antartika menghadapi banyak cabaran seperti angin dan masalah teknikal lain akibat faktor persekitaran yang mencabar. Kajian ini membandingkan pengukuran kerpasan dari instrumen ukuran dengan data reanalisis, dan kemudiannya membandingkan 49 model iklim Model Intercomparison Project 5 (CMIP5) dengan dataset reanalysis. Dalam bahagian satu, data dari lima instrumen kerpasan di di Stesen Rothera, Semenanjung Antartika dibandingkan dengan data dari satelit dan reanalysis. Alat pengukur tangki (TBGs) secara umumnya kurang sensitif berbanding kepada sensor berasaskan laser (LBSs). Kajian kes menunjukkan bahawa VPF-730 merupakan sensor kerpasan yang paling berkesan di kalangan instrumen-instrumen kerpasan. Kerpasan yang diberikan oleh reanalisis mempunyai korelasi positif dengan kelajuan angin, manakala bacaan dari Reanalysis 55-tahun Jepun (JRA-55) paling dipengaruhi oleh kelajuan angin. Kajian kes juga menunjukkan bahawa apabila kelajuan angin rendah, bacaan kerpasan dari instrumen agak sama dengan bacaan yang diberikan oleh Projek Kerpasan Global Climatology (GPCP) 1 darjah-harian (1DD). Semasa fenomena angin yang kuat, GPCP 1DD tidak dapat mensimulasi sepenuhnya kesan angin maka memberikan bacaan yang rendah. Laser Precipitation Monitor (LPM) dan Campbell Scientific-700 (CS700H) mengalami ralat instrumental semasa kajian yang menyebabkan bacaan kerpasan menjadi sangat tinggi dan rendah. Memasang beberapa buah LBS di lokasi yang berlainan (berdekatan) dapat membantu mengenalpasti ralat dalam pembacaan. Dalam bahagian dua, kita menilai hubungan antara kerpasan dan suhu

permukaan (SAT) Antartika (90°C hingga 60°C) menggunakan model CMIP5 dan reanalisis ERA-Interim, CFSR, JRA-55, dan MERRA dari tahun 1979-2005. Bagi kerpasan, graf siri-masa menunjukkan bahawa MERRA dan JRA-55 telah meningkat dengan ketara dari 1979 hingga 2005, manakala ERA-Interim dan CFSR mengalami perubahan yang tidak signifikan. Reanalisis juga mempunyai korelasi yang rendah antara satu sama lain (umumnya kurang dari +0.69). 37 model CMIP5 menunjukkan trend meningkat, di mana 18 daripadanya adalah signifikan. CMIP5 multi-model mean (MMM) juga menunjukkan trend peningkatan yang ketara sebanyak 0.29 ± 0.06 mm tahun^{-1}. Bagi SAT, reanalisis menunjukkan perubahan yang tidak signifikan dan mempunyai korelasi yang tinggi antara satu sama lain, manakala CMIP5 MMM menunjukkan trend peningkatan yang signifikan. Walau bagaimanapun, variabiliti kerpasan dan SAT MMM boleh menjejaskan sifat trendnya. Kajian terakhir dalam projek ini adalah penggunaan model CMIP5 untuk memahami trend kerpasan dan suhu permukaan di bawah empat fenomena karbon iaitu RCP 2.6, RCP 4.5, RCP 6.0 dan RCP 8.5 untuk tahun 2006-2100. Kajian ini menunjukkan bahawa untuk kerpasan, Semenanjung Antarctika mempunyai trend yang tertinggi untuk kesemua empat fenomena. Untuk kajian suhu permukaan, kawasan pedalaman Antarctika akan mempunyai trend yang tertinggi, diikuti Weddell Sea dan Wilkes Land. Untuk suhu permukaan, konsistensi model CMIP5 dalam meramal trend historical SAT dengan tepat tidak lagi dilihat dalam eksperimen RCP. Walau bagaimanapun, konsistensi ini semakin bertambah dengan peningkatan konsentrasi gas rumah hijau dalam atmosfera.Korelasi antara suhu permukaan dengan kerpasan juga bertambah dengan peningkatan konsentrasi gas rumah hijau.

Kata kunci: Kerpasan, Antartika, model, CMIP5, reanalisis.

ACKNOWLEDGEMENTS

The author would like to thank Professor Dato Dr Azizan Abu Samah and Dr Sheeba Nettukandy Chenoli for their support and help in completing this work. This appreciation also extends to other members of the National Antarctic Research Center including Mr Ooi See Hai, Dr Fadzil, Mr Yunus and Miss Anna.

The author would also like to thank the University of Malaya for the opportunity to conduct valuable research project in various locations such as Bachok and Jang Bogo Station, Antarctica.

The author would like to extend his appreciation to Dr Steve Cowell of the British Antarctic Survey and his team in Rothera Research Station, Antarctic Peninsula. The discussion with Dr Cowell has given tremendous support and to author in his research work.

The author would also like to thank Dr Taejin Choi of the Korean Polar Research Institute (KOPRI) and his team of experts at the Jang Bogo Research Station in Terra Nova Bay, Antarctica. The author appreciates the help and cooperation provided by the Korean researchers during his research stint at the Jang Bogo station.

TABLE OF CONTENTS

LIST OF FIGURES

LIST OF TABLES

LIST OF SYMBOLS AND ABBREVIATIONS

ERA-40	:	40-year ECMWF Reanalysis
ADG	:	Acoustic Depth Gauge
AGPI	:	Adjusted GPI
AAWS	:	Antarctic Automatic Weather System
AMPS	:	Antarctic Mesoscale Prediction System
ARMC	:	Antarctic Meteorology Research Center
AOGCM	:	Atmospheric Ocean Global Circulation Model
ACCESS	:	Australian Community Climate and Earth System Simulator
AWS	:	Automatic Weather System
BCC	:	Beijing Climate Center
BCCR	:	Bjerknes Center for Climate Research
BAS	:	British Antarctic Survey
CIMO	:	Commission for Instruments and Methods of Observation
CO_2	:	Carbon Dioxide
CNRM	:	Centre National de Recherches Météorologiques
CMCC-CM	:	Centro Euro-Mediterraneo sui Cambiamenti Climatici Climate Model
ΔSAT	:	Changes in Air Temperature
Δprecipitation	:	Changes in Precipitation
CFSR	:	Climate Forecast System Reanalysis
CFSv2	:	Climate Forecast System version 2
CPC	:	Climate Prediction Center
CCN	:	Cloud Condensation Nuclei
CPR	:	Cloud Profiling Radar

CCSM	:	Community Climate System Model
CESM	:	Community Earth System Model
CMIP5	:	Coupled Model Intercomparison Project Phase 5
CMAP	:	CPC Merged Analysis of Precipitation
DJF	:	December-January-February
DSP	:	Digital Signal Processing
EOS	:	Earth Observation Systems
ESM	:	Earth System Model
ENSO	:	El-Niño Southern Oscillation
EML	:	Environmental Measurements Limited
ECMWF	:	European Center for Medium-range Weather Forecasts
ERA-Interim	:	European Center for Medium-range Weather Forecasts "Interim" Reanalysis
EC-Earth	:	European Community Earth System Model
AR5	:	Fifth Assessment Report
FIO-ESM	:	First Institute of Oceanography Earth System Model
FGOALS	:	Flexible Global Ocean-Atmosphere-Land System Model
4DVAR	:	Four-dimensional Variational Data Assimilation
GCM	:	General Circulation Model
Geo-IR	:	Geostationary Infrared
GMS	:	Geostationary Meteorological Satellite
GOES	:	Geostationary Operational Environmental Satellites
GFS	:	Global Forecast System
GODAS	:	Global Ocean Data Assimilation System
GPCC	:	Global Precipitation Climatology Center
GPCP	:	Global Precipitation Climatology Project

GEOS	:	Goddard Earth Observing System
GEOS-DAS	:	Goddard Earth Observing System Data Assimilation System
GPI	:	GOES Precipitation Index
GPCP 1-DD	:	GPCP 1-degree daily
GHG	:	Greenhouse gases
HadGEM	:	Hadley Center Global Environmental Model
IR	:	Infrared
IPSL	:	Institut Pierre Simon Laplace
IPCC	:	Intergovernmental Panel on Climate Change
ISCCP	:	International Satellite Cloud Climatology Project
JMA	:	Japan Meteorology Agency
JRA-25	:	JMA 25-year Reanalysis
LPM	:	Laser Precipitation Monitor
LBS	:	Laser-based Sensor
MPI-ECHAM5	:	Max Planck Institute - European Community Hamburg
Meteosat	:	Meteorological Satellites
MODIS	:	Moderate Resolution Imaging Spectroradiometer
MERRA	:	Modern Era Retrospective analysis for Research and Application
MMM	:	Multimodel Mean
NASA	:	National Aeronautics and Space Administration
NARC	:	National Antarctic Research Center
NCEP	:	National Center for Environmental Prediction
NCEP-DOE	:	National Center for Environmental Prediction - Department of Energy
NCEP-NCAR	:	National Center for Environmental Prediction - National Center for Atmospheric Research

NOAA	:	National Oceanic & Atmospheric Administration
NOAA-20CR	:	National Oceanic & Atmospheric Administration 20th Century Reanalysis
NorESM	:	Norwegian Earth System Model
PWS	:	Present Weather Sensor
PGF	:	Pressure Gradient Force
PCMDI	:	Program for Climate Model Diagnosis and Intercomparison
RH	:	Relative Humidity
RCP	:	Representative Concentration Pathway
RMSE	:	Root Mean Square Error
RIS	:	Ross Ice Shelf
RAS	:	Ross Ice Shelf Airstream
SIE	:	Sea Ice Extent
SIV	:	Sea Ice Volume
SPICE	:	Solid Precipitation Intercomparison Experiment
SST	:	Sea Surface Temperature
SAM	:	Southern Annular Mode
SSM/I	:	Special Sensor Microwave / Imager
σ	:	Standard deviation
SAT	:	Surface Air Temperature
SMB	:	Surface Mass Balance
3DVAR	:	Three-dimensional Variational Data Assimilation
TBG	:	Tipping-bucket Gauge
OAP-2DP	:	Two-dimensional Optical Array Spectrometerscope
VPF	:	Visibility and Present Weather Sensor
WMO	:	World Meteorological Organization

WCRP : World Climate Research Program

LIST OF APPENDICES

CHAPTER 1: INTRODUCTION

1.1 Climate of Antarctica: Wind, Temperature and Precipitation

Antarctica is the southernmost continent on Earth, and one of the only two that are not attached to any other continents. It is known for its extreme environment and bitter cold temperatures. The lowest air temperature ever recorded on Earth, -89.2 °C, was recorded at the Russian Vostok Station deep in the interior of Antarctica on July 21, 1983 using ground measurements (Turner et al., 2009a). In August 2010, remote sensing satellite Landsat8 above East Antarctica recorded a surface temperature of -94.7 °C. Scambos reported in a paper published in 2018 that satellite data gathered during the Antarctic polar nights between 2004 and 2016 revealed a region within the high East Antarctic Plateau near Vostok that regularly reached snow surface temperatures of −90 °C and below. These Ultra-cold conditions (below −90 °C) occurred in shallow topographic depressions near the highest part of the ice sheet, at 3,800 to 4,050 meters. Comparisons with nearby automated weather stations suggested that air temperatures during these events were around −94 ± 4 °C. These Ultra-cold conditions occur more frequently when the Antarctic polar vortex is strong (Scambos et al., 2018).

Apart from the extreme temperatures, the continent is also famous for its strong winds. Strong gusts in Antarctica have known to reach over 40 ms^{-1}. The interior of the continent, due to the high elevation (average 4,500 m), has relatively low pressure of only about 600 hPa. Until relatively recently, however, real-time observation of daily measurements in the Antarctic were unavailable due to logistic difficulties and the sheer vastness of the continent. Following the installation of automatic weather stations (AWS) and the establishment of manned research facilities in various locations on the continent, daily measurements are now available to researchers in real-time. Manned research stations can provide shelter and sustenance for long-term research in Antarctica. Nonetheless, the conventional routine for data measurement relies on measurement with limited

temporal basis due to the limited number of manned stations on the continent. The AWS, powered by solar power and battery, is much more abundant throughout the continent. When the Antarctic Automatic Weather Station (AAWS) was conceived in 1980, there were less than ten stations throughout Antarctica. In 2006, there were over sixty stations scattered across the continent. As a result, numerous meteorological measurements are now readily available to researchers. The measurement of temperature at the Rothera research station, for instance, is currently conducted *via* automated sensors attached to data loggers and available for download from the BAS website. Another prominent participant in Antarctic meteorology research is the University of Wisconsin, which hosts the Antarctic Meteorology Research Centre (AMRC) that runs multiple AWS in Antarctica. Other parameters such as pressure, wind direction, sea level pressure, wind speed, and relative humidity are also accessible at 1-minute interval. The deployment of these instruments has helped to further the understanding of Antarctic climate. Nonetheless, the measurement of precipitation still eludes researchers.

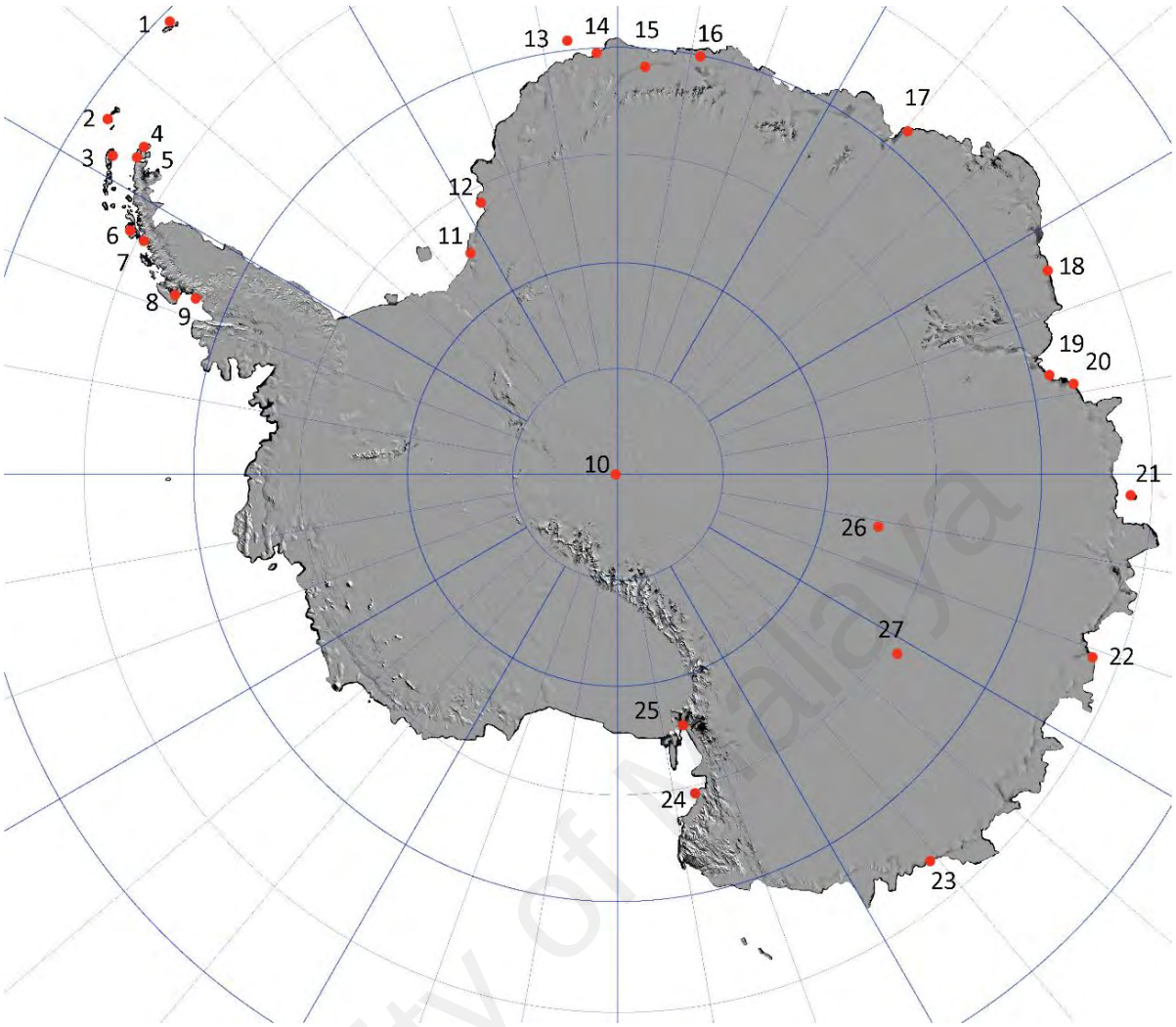

Figure 1.1 Map of manned and permanent stations in Antarctica as of 2020

Table 1.1 Details of manned and permanent stations in Antarctica shown in Figure 1.1

No	Station Name	Country	Location
1	Orcadas	Argentina	60°44′17″S, 44°44′17″W
2	General Bernardo O'Higgins	Chile	63°19′15″S, 57°53′59″W
3	Arctowski	Poland	62°09′37″S, 58°28′24″W
4	Esperanza	Argentina	63°23′51″S, 56°59′52″W
5	Marambio	Argentina	64°14′28″S, 56°37′36″W

6	Palmer	U.S.A	64°46′27″S, 64°03′10″W
7	Vernadsky	Ukraine	65°14′45″S, 64°15′28″W
8	Rothera	U.K.	67°34′08″S, 68°07′29″W
9	San Martin	Argentina	68°07′48″S, 67°06′05″W
10	Amundsen-Scott	U.S.A	90°S, 0°E
11	Belgrano II	Argentina	77°52′25″S, 34°37′39″W
12	Halley	U.K.	75°36′45″S, 26°11′52″W
13	Neumayer III	Germany	70°40′38″S, 8°16′18″W
14	SANAE IV	South Africa	71°40′22″S, 2°50′26″W
15	Troll	Norway	72°00′42″S, 2°32′06″E
16	Novolazarevskaya	Russia	70°46′36″S 11°49′20″E
17	Syowa	Japan	69°00′16″S 39°34′54″E
18	Mawson	Australia	67°36′12″S 62°52′27″E
19	Zhongshan	China	69°22′25″S 76°22′18″E
20	Davis	Australia	68°34′36″S 77°58′03″E
21	Mirny	Russia	66°33′11″S 93°00′35″E
22	Casey	Australia	66°16′57″S 110°31′36″E
23	Dumont d'Urville	France	66°39′46″S 140°00′07″E
24	Jang Bogo	South Korea	74°37′26″S 164°13′44″E
25	McMurdo	U.S.A	77°50′47″S 166°40′06″E
26	Vostok	Russia	78°27′50″S 106°50′15″E
27	Concordia	Italy/France	75°05′59″S 123°19′56″E

1.2 Variability, trends and measurements of Antarctic Precipitation

Precipitation is one of the most important components of the Earth's hydrologic cycle, and is essential for fresh water supply and storage. Precipitation amount, frequency, intensity, type, and duration could be affected by changes in global and regional climate. The Fourth Assessment Report of the Intergovernmental Panel on Climate Change (Bernstein et al., 2008) stresses that the fluctuation of precipitation due to the change in climate could possibly increase the already burdening stress on water resources due to population explosion and land-use. Precipitation fluctuates over a range of space-time scales. Larger space-scale variations often occur at longer time scales, and are related to larger scale phenomena—for instance, the El Niño-Southern Oscillation (ENSO) — in the atmosphere or ocean-atmosphere system. Precipitation is therefore inherently more variable, and more difficult to measure and analyze, than other measured parameters like temperature and pressure.

The Commission for Instruments and Methods of Observation (CIMO) under the World Meteorological Organization (WMO) launched the Solid Precipitation Intercomparison Experiment (SPICE) between 2013 and 2015 in an effort to foster international collaboration in conducting precipitation measurements, data analysis and results sharing. The experiments were conducted at 20 test sites in 15 countries across all continents except Africa and Antarctica. The project received active participation from the instrument manufacturing community—more than twenty types of precipitation instruments were provided by the manufacturers to measure precipitation amount, sow depth, and snow water equivalent. Every instrument had been tested in one or more sites under various weather conditions in order to provide a solid foundation for the results. The project was a resounding success with results published in peer-reviewed journals. The results include suggestions for adjustments that account for the undercatch of solid precipitation due to gauge exposure, specific assessments of the performance of each

measuring instrument, and the assessments of specific operational challenges such as the use of wind shields and heating elements (Nitu et al., 2019).

Precipitation observation in the Antarctic, on the other hand, is notoriously difficult (Bromwich et al., 2004; Genthon et al., 2003; Miles et al., 2008) and understudied. One of the main factors that complicate the measurement of precipitation is strong wind (Cohen et al., 2013; van Lipzig et al., 2004). Even in regions where precipitation falls as rain water, strong wind affects measurements by inducing undercatch and wetting losses (Benning et al., 2005). Studying the effect of snow distribution in Antarctica is highly challenging because it requires the understanding of various other parameters such as the age of the snow, snow moisture, temperature, local topography, and the size of the snow particles (Li et al., 1997). However, in order to address the technical challenges associated with precipitation measurement, it is important to first compares and analyses the performance of precipitation measuring technology already in operation.

1.3 The importance of the study

Increasing concern on climate change has enhanced the demand for knowledge of the space-time distribution of precipitation. Climate model projection predicts increasing temperature due to increasing water vapor in atmosphere following the increase in greenhouse gases (GHG), and this would lead to an increase in precipitation and the efficiency of moisture transport towards the polar region (Uotila et al., 2007). Accurate information on precipitation is required for climate models assessment, biogeochemical modelling, the study of the natural variability of observed climate change (Hulme et al., 1999b), and the preparation of future scenarios for climate change impact research (Hulme et al., 1999a). Antarctica, the largest reservoir of freshwater on Earth, plays a crucial role in the hydrological circulation system of our planet. Understanding the

historical and future precipitation characteristics in Antarctica can be useful for the development of responses to the effect of climate change. In Antarctica, precipitation can be affected by atmospheric dynamics and topography features like fronts, cyclones and the orographic uplift moist air (Bromwich, 1988). The Antarctic ice budget is balanced by the accumulation of precipitation, blowing snow and ice loss due to melting, evaporation and calving of ice along the coast (Monaghan et al., 2006). The surface mass balance (SMB), which is the balance of snow accumulation and melting, has a substantial influence on the global sea level and oceanic conditions (Shepherd et al., 2010). Obtaining ground observation of Antarctic precipitation is therefore essential in the effort of developing an understanding of how climate processes affect precipitation in the region. Understanding the water energy cycle in Antarctica is an important part in estimating the mass balance of ice sheets, gauge potential glacier melting, and imbalances in the Earth system that may build up with the addition of freshwater supply into the ocean. The SMB is defined as the sum of precipitation minus water fluxes and run off. Antarctic precipitation is predicted to increase with global warming (Huybrechts et al., 1991), mitigating the contribution of the Antarctic ice sheet to sea level rise.

Unfortunately, conventional station observation of precipitation is not just rare, but also highly unreliable in Antarctica (Genthon et al., 2003). The shortage of precipitation observation data in Antarctica is because of a combination of many aspects. Strong wind, blowing snow, logistics, and extreme environment are some of the challenges faced by scientists when collecting precipitation measurements. Strong wind is widely regarded as the most difficult of these challenges to overcome, as strong katabatic winds from high land transport snow over vast distances across the landscape. Katabatic winds are pockets of air flowing down over sloping terrain (Parish et al., 1998). It is one of the dominant surface wind patterns in Antarctica, which plays an essential part

in the tropospheric circulation of the southern hemisphere (Renfrew et al., 2002). Katabatic winds carry cold, dense air from the interior of the continent across the unimpeded landscape towards the coast. They usually occur during the austral winter when the lack of sunlight causes a strong surface inversion to develop over the sloping terrain of the interior, providing forcing for the katabatic winds that flow towards the coasts (Parish et al., 2003). Katabatic winds are one of the most important components in the southern hemisphere tropospheric circulation. Strong wind sources like the katabatic winds and cyclones can affect snow volume of an area and affect depth change. Apart from that, topography, especially the Transantarctic Mountains also has an effect on precipitation. The role of topography in the precipitation variability is an important one. Orographic lifting forces snowfall onto the windward slopes, and strong winds from higher elevation then carry the snow along the slopes towards the coast. In the interior, precipitation sensors have to be sensitive enough to register the light precipitation that falls as diamond dusts (Bromwich et al., 2004), while at the same time ignoring the background noise that could overwhelm the snowfall data. At present, measurements of precipitation in real-time are limited and mostly available in manned research stations where researchers collect measurements. Researchers at manned stations sometimes use snow stakes to study precipitation, but the technic is not automated and requires constant man-power. Ice core data is also used for tracking precipitation across the continent. However, the measurement has high spatial variability, not available in real-time, and is only a measure of depth change. Even when observations are available, inaccuracies, biases and inconsistencies are rampant. The advancement in snow sensors technology has helped researchers to better understand and study precipitation in Antarctica. Currently, there are precipitation sensors that can warm up the snow gauge to prevent the ice from blocking the snow gauge. The downside of this technology is that some precipitation might be lost through sublimation and evaporation while

slowly being melted by the heater in the snow gauge (Miles et al., 2008). In addition, low temperatures and hoarfrost could have a negative implication on instruments that are not polar-compatible. A new method had been introduced to measure snowfall event using fluctuations in surface emissivity (Bindschadler et al., 2005). However, the method was not quantitative. Recent advancement in satellite technology has seen the incorporation of quantitative Antarctic precipitation observations using the data provided by the cloud profiling radar (CPR) on board the CloudSat satellite (Liu, 2008; Stephens et al., 2008). However, the CloudSat product began as recently as 2008 and hence could not be used to study historical pattern and trend starting from 1979.

In light of the difficulty in obtaining reliable observation data, scientists have resorted to using mesoscale models and climate models. Antarctic Mesoscale Prediction System (AMPS) has been used to map precipitation in Antarctica but unable to produce verifiable results due to lack of observation data for comparison (Bromwich et al., 2003). There are also climate models such as the Coupled Model Intercomparison Project Phase 5 (CMIP5) models—a compilation of coupled atmosphere–ocean climate models that can be used to assess and study the trends and variability of precipitation in Antarctica—of the World Climate Research Programme (WCRP) in support of the Intergovernmental Panel on Climate Change (IPCC) Fifth Assessment Report (AR5). The precipitation data from CMIP5 includes precipitation from both large-scale and convective clouds, in both solid and liquid phases that fall on to the surface. CMIP models have been around since the early 2000, and there are previous version of the CMIP models like CMIP3 (Connolley et al., 2007) and CMIP1 (Lambert et al., 2001). Numerous scientists have reported on the commendable skill scores of the CMIP5 models in matching climatological features in many different areas of the world (Sheffield et al., 2013; Yin et al., 2013). The

improvement shown by the CMIP5 models, compared to their predecessors, is due to the enhanced description and simulation of physical processes and also enhanced model resolution (Flato et al., 2013). The CMIP5 models consistently simulate Antarctic precipitation to increase in a warming climate (Flato et al., 2013). However, models and different reanalysis datasets vary widely on their representation of the current precipitation rate in Antarctica. The problem that plagues the CMIP5 models is their inability to properly and accurately simulate precipitation compared to reanalysis results.

Owing to the lack of observations in the Antarctic region, researchers usually use any available observations, however sparse it may be, to validate the performance of a model to gain some level of confidence in the model output. In the event where observations are not available, researchers will then turn to reanalysis datasets. Global reanalysis datasets are numerical weather prediction models anchored with multiple meteorological observations (Bromwich et al., 2011). These datasets are generally considered to be more accurate compared to Earth system models (ESMs) because of the inclusion of meteorological observations in reanalysis datasets. There are different types of global reanalysis data sets available for study: the European Centre for Medium-range Weather Forecasts "Interim" reanalysis (ERA-Interim) (Simmons et al., 2007); the National Centers for Environmental Prediction (NCEP) Climate Forecast System Reanalysis (CFSR) (Saha et al., 2010); the Japan Meteorological Agency (JMA) 25-year Reanalysis (JRA-25) (Kobayashi et al., 2015); and others. These datasets provide an excellent tool with which to examine the variability of precipitation over the Antarctic. However, it is important to note that the generation of global reanalysis dataset does not include the observations of precipitation rates (Bromwich et al., 2011). Reanalysis datasets, despite their values and accuracy, are not actual measurements, but rather model results derived from assimilated data. Due to the lack of

observational data as a standard of comparison, it is not possible to confirm the results coming from reanalysis data as the absolute truth.

In addition, the knowledge obtained from the study of the variability and trend of precipitation in Antarctica may be beneficial for researchers in other fields. Biologists who study the flora and fauna of Antarctica, for instance, may need to understand the variability of precipitation and changes in weather pattern and its effects on the animals' breeding and migratory behaviors. Precipitation is one of the main causes for penguin chick mortality (Boersma et al., 2014). Precipitation trend in the western side of Antarctic Peninsula has increased significantly over the past 30 years, and this could have adverse effects on the survival of penguins in the region. Moreover, researchers in the field of geology could also benefit from the study of precipitation variability and trend in Antarctica. The study of precipitation is closely related to the level of sea-level rise because precipitation is the major factor in SMB that mitigates the rise of sea level.

1.4 The objective of this study

The end goal of this project is to assess the ability of CMIP5 models in simulating the historical climatology and climate variability, as well as future prediction of Antarctic precipitation. To carry out this goal, the precipitation of the models will be compared against reanalysis datasets, satellite data and ground instrument. This information will form the basis for future research into the amounts and trends of precipitation in Antarctica. The CMIP5 models output will then be used to analyze Antarctic precipitation from the year 2006-2100 under four different representative concentration pathways (RCPs).

The main objectives of this work are:

(1) To investigate the sensitivity of the Antarctic precipitation measurements based on different sensors.

(2) To examine the historical trends in the Antarctic precipitation and its variability based on various reanalysis datasets and CMIP5 models.

(3) To evaluate the historical runs of the CMIP5 models in simulating the variability and trends of historical precipitation in Antarctica;

(4) To assess Antarctic's projected precipitation and surface air temperature under four different RCPs using CMIP5 models.

1.5 The structure of the thesis

This work will be presented in the conventional thesis format, with the inclusion of two articles published in Institute for Scientific Information (ISI)-cited journals. Chapter 2 will cover the literature review on Antarctica, along with other background information such as earlier research on precipitation, precipitation instruments, climate models, and reanalysis datasets. Chapter 3, 4 and 5 will highlight the methodologies, results, and discussions for three different part of this study:

(a) For the first part of the study, snow gauges and sensors–based precipitation observations installed at Rothera Research Station from March 2014 to February 2015 are compared with reanalysis datasets and Global Precipitation Climatology Project (GPCP) data. The contents of this work were published in the *Polar Research* in an article entitled "*Precipitation instruments at Rothera Station, Antarctic Peninsula: A comparative study*" (Tang et al., 2018a). Temperature and wind speed profiles obtained from AWS (British Antarctic Survey) are also included for comparison.

(b) The second part of the study that will be discussed is an assessment of the historical climatology and trend of Antarctic precipitation from 49 CMIP5 models compared to the reanalysis datasets. The contents of this study were published in the *Polar Science* in an

article entitled "*An Assessment of historical Antarctic precipitation and temperature trend using CMIP5 models and reanalysis datasets*" (Tang et al., 2018b). The goals for development of this analysis are (1) to compare the discrepancy between precipitation amount and trend from CMIP5 models and reanalysis datasets and (2) to identify the correlation between precipitation and temperature from the CMIP5 models.

(c) The final part that we will discuss is the future precipitation and temperature trends of CMIP5 models in Antarctica. The work will evaluate the precipitation and surface temperature output from CMIP5 models in Antarctica under the four RCPs, namely RCP2.6, RCP4.5, RCP6.0 and RCP8.5.

The results presented are this thesis is relevant to precipitation or hydrology study in Antarctica. In addition, the work presented here is also relevant for the evaluation of CMIP5 models, reanalysis datasets and satellite datasets in simulating the variability of precipitation. Chapter 6 highlights the conclusions and recommendations for future work.

CHAPTER 2: LITERATURE REVIEW

2.1 Introduction

Antarctica is one of the least understood regions in the world. This is due to the extreme difficulty in taking meteorological measurements in Antarctica, especially in the interior of the continent. The temporal and spatial distribution of precipitation and the efficiency of precipitation sensors and gauges are some of the questions still left unanswered by researchers. This section provides a literature review on the general information on Antarctica, the study of precipitation in Antarctica, climate models, reanalysis datasets, and satellite data.

2.2 Physical climatology of Antarctica

Antarctica, the continent with the coldest and harshest environment in the world, is one of the least explored corners on the planet. Temperatures average -4°C on the coasts and down as much as -55°C in the interior, with wind speeds up to 20 ms^{-1} in certain areas (King et al., 1997). The lowest air temperature on earth, -89.2 °C, was recorded at the Russian Vostok station deep in the interior of Antarctica in July 1983 (Knuth, 2007). Satellite measurement obtained a new low of -94.7 °C 27 years later on the 10th August 2010.

Antarctica is divided into three main regions – East Antarctica, West Antarctica, and the Antarctic Peninsula, otherwise also known as Peninsula region. The Transantarctic Mountain range sits between the two largest regions, the East and West Antarctica, while floating ice shelves form a considerable part of West Antarctica, the largest being the Filchner-Ronnie and Ross Ice Shelves (RIS). The East Antarctica consists mainly of inland ice sheet plateau that covers roughly 66% (10.35 x 10^6 km^2) of the entire continent. The high elevation of the East Antarctica plateau, with average elevation of over two—or in some areas, over four—kilometres (King et al., 1997), makes it one of the largest

deserts and coldest regions in the world. Areas with altitude of over 2250 m make up 71% of the surface of East Antarctica, and 12% of the surface of West Antarctica (Palerme et al., 2017b). Several countries have set up manned research stations in the interior East Antarctica, including China (Kunlun Station), Russia (Vostok Station) and Japan (Dome Fuji Station). The West Antarctica, otherwise known as Lesser Antarctica, is about five times smaller than the East Antarctica, covering 1.97×10^6 km^2 with average elevation of less than a kilometre (850 m) (King et al., 1997). The lower elevation of the West Antarctica makes it relatively warmer than East Antarctica. Some of the more popular research stations in West Antarctica includes Russkaya (Russia) station and Scott Base (New Zealand). Included in the West Antarctica region is a narrow strip of mountainous land known as the Antarctic Peninsula. Despite being included as part of the West Antarctica, the Antarctic Peninsula is itself a prominent part of Antarctica due to the difference in climate, ecosystem, and geography compared to the West Antarctica. The Antarctic Peninsula, sometimes called "the banana belt" is the warmest region of the continent due to the fact that its narrow strip extends beyond the boundaries of the Antarctic Circle. The Antarctic Peninsula covers only 0.52×10^6 km^2.

Apart from the three main regions of the continent discussed above, the continent holds about 90% of the world's freshwater, most of which are locked as ice covering 97% of the surface of the continent (King et al., 1997). The biggest ice shelf in Antarctica is the RIS, a large area of ice approximately the size of the state of Texas located between the West Antarctica and the Transantarctic Mountains. The RIS is formed from the accumulation of icy rivers flowing down from high elevation down the valleys of the Transantarctic Mountains, precipitation and blowing snow. The RIS is one of the main contributors of large icebergs in the Ross Sea. Some of these icebergs are sufficiently large to affect local weather and ocean currents. The size of the B-15 iceberg, which broke

from the RIS in 2000, was approximately 10,000 km^2 or about the size of the island of Jamaica (Arrigo et al., 2003).

As mentioned above, Antarctica has the most extreme environment on Earth. Studies have shown that the winds in Antarctica can reach 40 ms^{-1}. Observations at many Antarctic stations suggest that topography can substantially influence the local wind field (Bromwich, 1989; Parish, 1988).

One of the most prevalent winds in Antarctica is the katabatic winds. Katabatic winds are cold, dense air that forms on higher elevation and, due to the pull of gravity, flows towards the coast. Up in the higher elevation, the cold air forms a localized high pressure region. The difference in pressure between the high and low elevation area gives rise to a pressure gradient force. The pressure gradient then produces down slope sub-Rossby radius scale katabatic accelerations. In the presence of topographical barriers, the focused katabatic winds can accelerate to extreme speeds. Katabatic winds were first observed during the early expeditions to Antarctica. At Cape Denison, Adélie Land, wind speeds were recorded in excess of 66 ms^{-1}, which according to the scientific community at the time was an exaggerated figure (Nylen et al., 2004). Today, it is recognized that these strong, high speed winds are part of the main features of Antarctica. Katabatic winds are an important feature of the Antarctic climate due to their ability to transport snow, both falling and on-the-ground, over great distances. It is common for katabatic wind that flows down from the Transantarctic Mountains to travel with speed in excess of 20 ms^{-1} or more (King et al., 1997). Apart from world-record temperature and strong wind, the surface pressure and geopotential height field are also notable features of the continent. The high elevation in the interior causes the pressure to be around 600 hPa. On the eastern side of the continent, the high elevation prevents warm, moisture-laden sea air from penetrating deep into the continent. On the western side of the continent lies the RIS. The RIS is

around 35 to 90 meters above sea level. As a result of the relatively lower elevation, the RIS has low pressure and strong winds. The ice on the RIS reflects large amount of radiation back to space.

Another type of phenomenon that is prevalent in the Antarctic is the barrier winds. Barrier winds form when stably stratified flow is directed towards a barrier, or mountain. If the Froude number, the ratio of the flow inertia to the external field, of the three approaching flows is less than one, the barrier blocks the flow and mass convergence occurs (Buzzii et al., 1997; O'Connor et al., 1994). The mass convergence increases the pressure at the base of the barrier, creating a pressure gradient force (PGF) that is directed perpendicular and away from the barrier. The PGF induces a wind that becomes approximately geostrophic and flows parallel to the barrier. This barrier parallel flow is called a barrier wind. Barrier winds most prevalently occur around the regions where there are high, steep barrier e.g. high elevation. Around the RIS, barrier winds form along the base of the Transantarctic Mountains flowing from the southeast towards the northwest (O'Connor et al., 1994; Parish et al., 2006; Seefeldt et al., 2007; Steinhoff et al., 2009).

Apart from barrier winds and katabatic winds, there is another type of circulation known as the Ross Ice Shelf Airstream (RAS). The RAS is essentially the combination of barrier winds and katabatic winds (Parish et al., 2006). It drains cold, dense air from the interior of the continent out towards the coast and over the Ross Sea. As the name suggest, it is most prevalent in and around the RIS area, originating in the Siple Coast confluence zone (Parish et al., 1986), flowing over the western to central RIS to the north over the Ross Sea (Seefeldt et al., 2012). Parish and Bromwich (1998) worked on a case study where a katabatic event caused a 20 hPa drop in pressure over the Antarctic continent and found that the RAS transported around a third of the mass flowed from the

continent passed through the Siple Coast confluence zone to more northerly latitudes (Parish et al., 1998). Just off the coast of the continent lies a belt of low pressure system known as the circumpolar trough. This is the region where declining synoptic-scale lows move from the mid-latitudes, and also the place where many lows develop, particularly mesoscale systems (Turner et al., 2009b; Turner et al., 1998). Around the coast of East Antarctica for example, Casey, Mawson and Dumont d'Urville station, a majority of the winds are due to the interaction between the downslope katabatic winds and these broad scale synoptic circulations (Turner et al., 2009b).

2.3 Precipitation in Antarctica

As the planet warms due to increasing GHG concentration, the atmosphere is able to store higher moisture content and thus, more precipitation is expected. When moist air flows towards the Antarctic, it loses kinetic energy with increasing altitude and water vapour due to condensation (Uotila et al., 2007). The movement of the air can be divided into mean and eddy components by using Reynold averaging: the mean component corresponds to the stationary moisture transport, while the eddy component is the temporally varying component and includes moisture transported by synoptic activity. These two components are approximately equal at the coasts, but the eddy component is the main component for inland precipitation (Cullather et al., 1998). The eddy component varies with altitude and is a major contributor of moisture for the interior of Antarctica. The significant differences between these moisture transport components give rise to the two main precipitation regimes observed in Antarctica (Uotila et al., 2007).

Precipitation is an important part of SMB due to its role as the main input of snow in Antarctica. SMB, otherwise known as *mean net annual surface mass balance*, which is the culmination of several important processes, such as precipitation, hoarfrost, sublimation, melting and runoff, wind souring, and drift deposition. In Antarctica,

precipitation is the main positive and most dominant term in the SMB equation, which can be represented in mathematical term as:

$$SMB = precipitation - sublimation - evaporation - snow\ runoff - blowing\ snow$$

where

$$snow\ runoff = melt + rain + condensation - refreezing$$ (Lenaerts et al., 2019)

Thus, fluctuations in Antarctic precipitation can directly affect global sea level (Genthon et al., 2003). A large part of the continent has positive SMB due to the large precipitation contribution. There are, however, several places that consistently have negative SMB (e.g. blue ice areas) especially on the ice sheets. Unlike the Antarctic Peninsula where the warm temperature contributes to melting, wind erosion and sublimation play a more important role for negative SMB on the West Antarctica and East Antarctica ice sheets. Nonetheless, the annual SMB is generally positive in the long term. Despite the shortage of ground observations, the general climatology of Antarctic precipitation is understood by scientists. Most station data in Antarctica indicate that the surface temperature has been increasing in the second half of the twentieth century (King et al., 1997), while some has been decreasing since the 1980s and the 1990s (Comiso, 2000).

Precipitation climatologies obtained from rain gauges and snow sensors provide useful information about seasonal and regional precipitation attributes, though they are limited by the spatial resolution of the rain gauge network. The coastal areas generally receive more precipitation compared to the interior due to the fact that the coastal regions receive sea breeze with high moisture content and also more cloud condensation nuclei (CCN) from the salty water. Apart from that, the interior is much

drier because the high elevation and steep topography prevent cyclones, the main contributor of precipitation, from going inland. Even if any circulation does penetrate onto the high plateau, there will be very little moisture left for precipitation. In the interior, precipitation generally falls in the form of "diamond dust, tiny ice crystals nucleated from small amount of moisture in the air as radiation cools the air to extremely low temperatures. As a result, a large part of the interior has close to zero or occasionally negative SMB. The Antarctic Peninsula generally has the warmest temperature in Antarctica (about -5 °C in winter and 0 °C in summer) and also receives the most precipitation due to its proximity of moisture-laden ocean breeze from the oceans (King et al., 1997). In addition, the Antarctic Peninsula has high elevation of over 2000 meters that can help increase precipitation from upslope flow. The West Antarctica and RIS, on the other hand, have varying precipitation rates. The RIS is surrounded by the Transantarctic Mountains, the West Antarctic Ice Sheet and the Ross Sea. The average elevation of the ice sheet is around 50 meters. The Transantarctic Mountain range on the RIS western side, meanwhile, has average elevation of over 4500 meters. The difference in elevation creates a pressure difference and a forcing for mesoscale wind features such as katabatic winds, barrier winds, and the RAS. The combination of these features with the synoptic winds from cyclones that traverse the Ross Sea, provide a complex low-level wind field over the RIS (Chenoli et al., 2013). Owing to the lack of topography, the RIS receives less precipitation compared to its surrounding regions. The precipitation on RIS mostly comes from snow blown by katabatic winds from the Transantarctic Mountains, or from the cyclones that originate from the sea. The West Antarctica, on the other hand, has a rugged terrain and therefore higher topographical influence. The topography of West Antarctica has an influence on the cloud cover over the region. In fact, the International Satellite Cloud Climatology Project (ISCCP) has shown that there are more cloud cover over West Antarctica compared to any other regions on Antarctica (Schiffer

et al., 1983). This increased cloud cover would also bring more precipitation. In addition, the West Antarctica and the RIS region is frequented by cyclones (Carrasco et al., 2003). The cyclones will carry moisture from the surrounding ocean inland. The topographic barrier will lift the moisture from the ocean (a phenomenon known as orographic lifting) which will then produce precipitation. The West Antarctica therefore has more precipitation than the RIS due to its topography, especially at the south side of the Transantarctic Mountains and the windward region of the Ross Island, where precipitation has increased due to orographic effects (Monaghan et al., 2005). Besides, cyclone activities off the coast of RIS, especially in the Ross Sea, along with the effect of eddy shedding of vortices that split also bring precipitation onto the leeward side of the Ross Island. The precipitation varies according to seasons. Spring and autumn generally receive the most precipitation on the coast due to the generation of more cyclones from the fluctuation of weather during this periods. The general precipitation pattern of Antarctica is shown in Figure 2.1.

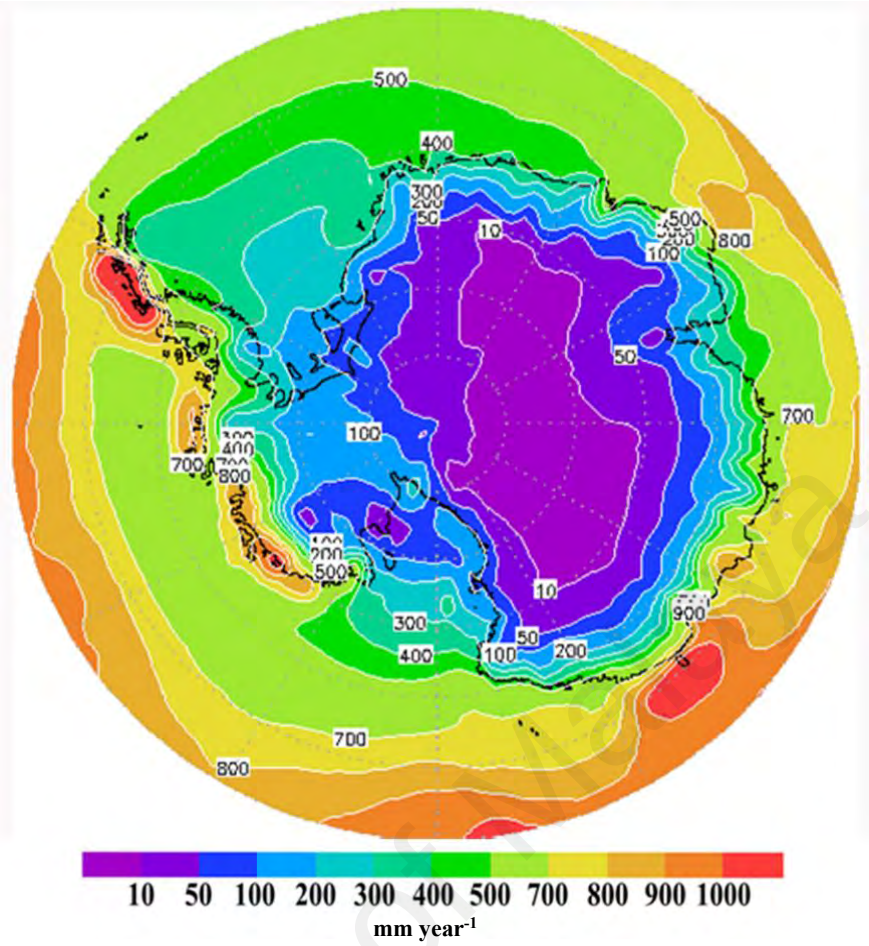

Figure 2.1 Spatial distribution of annual precipitation pattern (annual mean, in mm year^{-1}) of Antarctica, generated from ERA-Interim dataset for the year 1979-2005.

2.4 Studying precipitation in Antarctica

The latent heating associated with precipitation is one of the basic energy sources in the atmosphere. The distribution of precipitation is critical for the modelling and prediction of weather and climate change (Huffman et al., 1997). Capturing consistent and reliable precipitation profiles in Antarctica is one of the main objectives of climate study in the southern continent. In Antarctica, however, logistic challenges, limited accessibility, power, and the unforgiving climate restrict the precipitation profiles to manned research stations. Moreover, the strong winds in Antarctica—which can often travel up to 20 ms^{-1} and blowing in different directions—have a

substantial influence on the accuracy and reliability of the in-situ precipitation measurement instruments (van Lipzig et al., 2004). Nonetheless, the availability of gauge-data which extends back to the early decades of the twentieth century makes it an essential tool in the construction of reliable climatology of Antarctica. The current method of estimating precipitation in Antarctica comes largely from estimation using in situ study of SMB at single points by stakes, ultrasonic sounders, firn and ice cores, snow pits, and ground-penetrating radar. Other techniques include remote sensing techniques, assimilated analyses, and climate models. It is important to note that estimations are different from real-time ground-based observation of precipitation obtained from precipitation measuring gauges and sensors. Several issues especially those risen from the extreme conditions on the continent prevent accurate measurement of precipitation. For a precipitation gauge with an open funnel, an updraft could form at the leading edge of the gauge, leading to an upward deflection of snow particles away from the gauge orifice (Kochendorfer et al., 2017). Flow distortion around the gauge will increase with increasing wind speed, deflecting more snow particles away from the gauge. Previous studies have shown that the relatively slow fall velocity of snow and the creation of flow distortions by precipitation gauges are two main causes for snow undercatch (Folland, 1988). Scientists also measure accumulation using stakes, ice or firn cores and acoustic depth gauges, as proxies for precipitation, but this measurement is not straightforward (Cohen et al., 2013). The literature for direct precipitation measurement in Antarctica is sparse and often limited to only one type of precipitation sensor or short study period (Bellot et al., 2011; Kirchgäßner, 2011; Lachlan-Cope et al., 2001; Palerme et al., 2014). The challenges faced in precipitation observation and measurements in Antarctica is widely known in Antarctic precipitation literatures (Bromwich et al., 2004; Genthon et al., 2003; Miles et al., 2008). Wind is one of the main factors that affect precipitation measurement (Cohen et al., 2013; van Lipzig et al., 2004; Yang, 1999). Even in regions

where precipitation falls as rain water, strong wind affects measurements by inducing undercatch and wetting losses (Benning et al., 2005).

Apart from gauge-based datasets, scientists have also turned to other proxies such as the measurement of snow height using acoustic snow depth gauge, satellite observation, reanalysis datasets and climate models (Bindschadler et al., 2005; Bromwich et al., 2011; Cohen et al., 2013; Fyfe et al., 2013; Palerme et al., 2017b; Palerme et al., 2014). Satellite and radar technologies are not subjected to the harsh environment of the Antarctic and can observe vast regions with increasing resolution. However, there are only one reliable satellite data sets available for the Antarctic: the CloudSat (Stephens et al., 2002). Another product that combines satellite observations and rain gauge measurements is the GPCP (Huffman et al., 1997). The accuracy of the GPCP 1-degree-daily (1DD) product has yet to be tested against in situ precipitation measurements in the Antarctic at the time of writing.

CloudSat relies heavily on a satellite whose narrow orbital track allows it to cover only a limited surface and period, so it is unable to provide continuous and consistent daily measurements of precipitation. For the interior of the Antarctic, the CloudSat algorithm cannot detect small snow particles (Palerme et al., 2017a; Palerme et al., 2014).

Despite the emergence of climate models, reanalysis datasets, and remote sensing techniques, the use of precipitation gauges for the measurement of precipitation remains relevant today. Oceanographic and atmospheric models are very sensitive to their respective forcing data (Jones et al., 2016). Following the increasing use of general circulation models (GCMs) to study Antarctic precipitation, it is imperative to employ ground based measurement as a standard of comparison to ensure that the models are correctly simulating the precipitation in Antarctica if their predictions are to be used with confidence (Turner et al., 1995). This is because climate models are not comparable to

real measurements as they are forced by changes in stratospheric ozone and GHG without the inclusion of observation. Moreover, the resolution of currently-available climate models (range from 1.5° to 3.0°) prohibits a point comparison of precipitation. Reanalysis datasets, on the other hand, have vastly improved its resolution recently—up to 0.75° x 0.75° for ERA-Interim, 0.5° x 0.625° for the JRA-55 and Modern Era Retrospective analysis for Research and Application (MERRA). However, questions remain whether reanalysis datasets can deliver reliable precipitation results. In addition, remote sensing technique such as satellite-based observation suffers from various temporal discontinuities and most do not extend back in time beyond the 1970s at the earliest (New et al., 2001). For remote places like the high latitudes, satellite coverage is comparatively scarce, both in temporal and spatial coverage. Uncertainty remains whether remote sensing techniques can deliver accurate precipitation estimates. Previous comparison of climate models with unreliable field observation may produce inaccurate and unreliable reports (Wang et al., 2016). Thus, in-situ precipitation measurement can be used as a standard for the validation of precipitation observation from satellite and the long term results obtained from climate models and reanalysis datasets.

In order to address the technical challenges associated with precipitation measurement it is imperative to first assess and compare the performance of precipitation measuring tools that are currently available. In this section, we will discuss the several methods of studying precipitation in Antarctica.

2.4.1 Precipitation sensors used in Antarctica

There are two categories of instruments used in this work: Tipping bucket gauge (TBGs) and laser-based sensors (LBSs), also known as disdrometers. A TBG measures

primarily the total amount of falling precipitation, while disdrometers have the ability to measure the nature of individual precipitation particles (Michaelides et al., 2009).

2.4.1.1 Tipping bucket gauge

(a) ***Campbell Scientific Rain Gauge (CS700H)***

The diameter of the orifice for this instrument is 20.0 cm, with a resolution of 0.254 mm. The working principle of this gauge relies on gravity to pull the precipitation particles through the measuring funnel. This gauge is has a heating feature that automatically turns on when the temperature of the funnel drops below 4 ^{o}C. The temperature of the gauge will then be maintained at between 4-10 ^{o}C. This allows the snow to melt and flow through the funnel into the tipping bucket below.

The literature for CS700H is sparse, even for the use in tropics. The instrument had been installed near hydroelectric dam for rainfall monitoring purposes in Vietnam (Pham et al., 2013). The CS700H can be attached to an automated system to enable rainfall data to be transmitted more efficiently. At the time of writing, there has yet to be documentation of the CS700H ever being used for precipitation study in the high latitudes.

(b) ***EML Universal Precipitation Gauge 1000 (UPG-1000)***

The Universal Precipitation Gauge (UPG)-1000, produced by Environmental Measurements Limited (EML), has a nearly identical design to the CS700H, with the exception of a much wider (up to 1000 cm^2) and deeper funnel orifice which aims to capture more snow particles and to minimize the loss of precipitation due to the effect of wind (Dutton et al.). Its aerodynamic design also functions to deflect the wind and to reduce error. The UPG-1000 has a resolution of 0.1 mm. This gauge utilizes low voltage heating element to warm the funnel to melt the snow to prevent the formation of ice. The heating element is controlled by a temperature sensor in the funnel, which turns on the heater when the ambient temperature approaches 0 ^{o}C (Dutton et al.).

Like the CS700H, the literature for the UPG-1000 is sparse. There is yet to be any documentation of the instrument being used for precipitation study in Antarctica at the time of writing.

2.4.1.2 Laser-based sensors

(a) ***Biral Visibility and Present Weather Sensor 730 (VPF-730)***

The Biral Visibility and Present Weather Sensor (VPF)-730 employs an 850 nm infrared (IR) light source to detect precipitation particles. When a precipitation particle passes through the light beam, it causes a scattering that is recorded by a forward scatter receiver and a backscatter receiver. In addition, different types of precipitation scatters the light differently. For instance, liquid precipitation scatters only a tiny portion of the incident beam, while frozen precipitation can cause a significant backscattering of the light beam. Using this principle, the forward scatter functions to calculate the visibility while the backscatter differentiates the type of precipitation. The VPF-730 can be operated under harsh condition (-50 ^{o}C to 60 ^{o}C). The snow measuring resolution of the VPF-730 is 0.0015 mm/hour.

The VPF-730 is more widely used compared to the UPG-1000 and the CS700H. The instrument has been deployed for precipitation studies in Ecuador (Bendix et al., 2008), Canada (Gultepe et al., 2014; Yue et al., 2012), and China . The use of VPF-730 in Antarctica, however, is much rarer. Bellot et al. (2011) used this instrument to study the impact of drifting snow at Cape Prud'homme station, 5 km from the Dumont d'Urville station. The authors suggested that the VPF-730 could not differentiate the between vertically falling snow and particles blown horizontally by wind. Their study proposed a calibration method to quantify the surface flux (Bellot et al., 2011).

(b) ***Campbell Scientific Present Weather Sensor 100 (PWS-100)***

The Campbell Scientific Present Weather Sensor (PWS)-100 is an LBS made up of a Digital Signal Processor (DSP) housing unit attached to a laser unit and two sensors perched on a horizontal arm. Each of the sensor head is 20° off axis to the laser unit axis, one in the horizontal plane and the other in the vertical plane. When a precipitation particle travels between the laser beams, it will be detected by the off-axis receiver in the vertical plane, followed by the second receiver in the horizontal plane. The time of detection between the two receivers is used to calculate the fall speed and size of the particle in addition to the intensity of precipitation. The measuring area for the PWS-100 is 40.0 cm^2 per light sheet, with resolution up to 0.0001 mm precipitation. One of the important features of the PWS-100 is its ability to differentiate between vertically falling snow and particles blown horizontally by wind, due to the way the instrument measures the diffraction made by particles on four horizontal laser planes (Bellot et al., 2011).

Montero-Martinez et al. (2016) compared the PWS-100 with another optical instrument, the Two-Dimensional Optical Array Spectrometer Probe (OAP-2DP) and a tipping rain bucket to study the differences between the instruments. The study showed that the two optical gauges measured much higher amount of precipitation than the tipping bucket. Moreover, the PWS100 is the most sensitive of the instruments, and it is generally more reliable than the OAP-2DP (Montero-Martínez et al., 2016). At the time of writing, there is yet to be any literature on the use of PWS-100 for precipitation measurement in Antarctica.

(c) ***Thies Laser Precipitation Monitor (LPM)***

The Theis Laser Precipitation Monitor (LPM) consists of an infrared laser to measure precipitation particles that pass through its sensors. It is made up of a 780 nm parallel laser source and a receiver made up of a photodiode and a lens. When a

precipitation particle passes through the laser path, its presence blocks the laser path, thus reducing the laser signal that is received by the sensor. Based on this information the instrument is able to compute the sizes of the particles, the falling speed of the particles, and the type of precipitation. It is able to differentiate drizzle, rain, snow, soft hail, hail as well as mixed precipitation. The size of snow particles that can be detected ranges from 0.16 to 8.0 mm, while the instrument accuracy varies (60%-99%) depending on the type of precipitation particles measured. The resolution of this instrument is 0.001 mm.

The LPM is also a much popular rain sensor compared to the other instruments used in this work. It has been used as the standard measuring device in rain simulation work, and sprinkler performance testing where the size of water droplets often fluctuated according to sprinkler's nozzle size and pressure (Iserloh et al., 2012; Lassu et al., 2015; Liu et al., 2016). Zhang et al. (2015) used the LPM to measure solid precipitation alongside the Geonor T-200B precipitation gauge at the Qinghai-Tibetan plateau. The climate of the region is windy and cold, with average annual temperature of -3.8 ^{o}C and wind speed of over 15 ms^{-1}, which is not unlike the climate of Antarctic Peninsula. The author wrote that the optical instruments performed better in recording light precipitation compared to the precipitation gauge. The work also suggested calibration method using the LPM to correct precipitation measurements obtained by other precipitation sensor and gauge (Zhang et al., 2015).

2.4.2 Reanalysis dataset

Atmospheric data assimilation is made up of a series of analysis cycles where background information is merged with observation (of the same period) using statistically-based estimates of their errors to provide an estimation of the state of the atmosphere (the analysis) for that particular time (Uppala et al., 2005). The observation collected usually contains a few types of measurement, while the background information

is taken from a short-range forecast initiated from the most recent previous analysis in the sequence. The concept of reanalysis dataset began with the meteorological data collected for the first reanalysis, the First Global Atmospheric Research Program Global Experiment in 1979, where the collected observations were reanalysed several times in an attempt to enhance the use of data to initialise numerical weather forecasts Researchers found out that reanalysis datasets offer a multivariate, spatially complete and coherent record of the global atmospheric circulation, and are of great importance for meteorological research. With the advancement of technology and computing power, reanalyses of multi-decadal series of past observations have become a widely used resource for the study of atmospheric and oceanic processes and predictability. Apart from meteorology, reanalysis datasets are also used in other industries such as renewable energy, telecommunication and even the migration of birds (Dee et al., 2011). One of the advantages of global reanalysis datasets is that they are unaffected by changes in method due to the way reanalysis datasets are produced, as they are basically generated from fixed, modern versions numerical climate models assimilated with observation data (Bromwich et al., 2011). Another advantage of reanalysis is that the estimated variables are in line with the principles of physics and observations. This is due to the use of a forecast model as the unifying context where different observations from various origins can be assimilated and matched. Reanalysis can analyze and extrapolate information from locally observed parameters, for instance temperature and humidity, to unobserved parameters like precipitation at nearby locations. This feature of reanalysis, however, is dependent on the accuracy, reliability, coverage, physical coherence of the reanalyzed fields, and also the quality of the model itself (Dee et al., 2011).

It is obvious that a single reanalysis will not be enough to satisfy the demand for continual improvement (Saha et al., 2010). There are multiple reanalyses, provide by different institutions around the world, that can be used. Some of the most commonly

used reanalysis datasets include the ERA-Interim (Simmons et al., 2007); the NCEP CFSR (Saha et al., 2010); the JRA-25 (Kobayashi et al., 2015); and MERRA of the National Aeronautics and Space Administration (NASA) of the United States (Rienecker et al., 2011). However, it is worth noting that each reanalysis dataset has its own constraints. In the Antarctic, for instance, the NCEP reanalysis precipitation dataset is under the influence of strong spatial noise and unrealistic low values (Genthon et al., 2003). The reanalysis has been upgraded to the NCEP2 product for the time period 1979 to present, so the precipitation dataset is now free from the influence of spatial noise (Genthon et al., 2003). Some reanalysis, for instance the atmospheric component of the CFSR (1979-2010), spans over only a limited period of time, and should be applied cautiously.

Reanalysis datasets is useful for studying the variability of precipitation over the Antarctic and is often used as a standard of comparison for climate models (Bromwich et al., 2011; Nicolas et al., 2011; Palerme et al., 2017a; Tang et al., 2018b). In the following section we will discuss in details the background of the different types of reanalysis datasets used in this work.

2.4.2.1 The ERA-Interim

The ERA-Interim is a global atmospheric reanalysis dataset offered by the European Centre for Medium-Range Weather Forecasts (ECMWF) as a continuity for the 40-year ECMWF Reanalysis (ERA-40) (Simmons et al., 2007). The ERA-Interim starts from 1st January 1979 to the present, with the aim of offering solutions to difficult problems faced in the previous version of ERA reanalysis, namely the simulation of the hydrological cycle, the characteristics of the stratospheric circulation, and the consistency in time of reanalysed geophysical fields (Dee et al., 2011). The second aim of the ERA-Interim is

to enhance several technical problems in reanalysis, for instance the collection of data, quality control, error remediation, and performance monitoring.

The ERA-Interim is generated using a sequential data assimilation system which moves forward with a 12-hourly repetitive cycle. For every cycle, observation data are merged with earlier information obtained from a forecast model to gauge the evolving state of the global atmosphere and its underlying surface. The process is done by making a variational analysis of the basic upper-air atmospheric parameters that include temperature, wind, humidity, ozone, and surface pressure. This is then followed by a study of basic near surface parameters like 2 meter temperature and 2 m humidity, soil moisture and soil temperature, snow, and ocean waves. The analyses are then used to initialise a short-range model forecast that offers the prior state estimates required in the next analysis cycle. The forecast model plays an important role in the process of data assimilation. The use of model equations allow reanalysis to extrapolate information from locally observed parameters to unobserved parameters in a physically meaningful way. It perform forecasts using the most recent previous analysis as its initial condition, producing the background and atmospheric forcing fields that are necessary for analysis. It should be noted that the amount of retained assimilated information is dependent on the accuracy and skill of the forecast model. Moreover, the forecast estimates a wide range of physical parameters during the production process such as precipitation, turbulent fluxes and radiation field, which are constrained by the observations used to initialise the forecast. The quality of the model physics and analysis will determine the accuracy of the estimates. Assimilation of data provide a consistent documentation of the global atmospheric evolution anchored by observation obtained during the period of reanalysis. Currently, the ERA-Interim offers 6-hourly gridded estimations for three-dimensional meteorological parameters, 3-hourly estimations for surface parameters, and other two dimensional fields.

The ERA-Interim data assimilation system is made up of several important parts. First is the 12-hourly four-dimensional variational data assimilation (4DVAR) of the upper-air atmospheric state. The inclusion of the 4DVAR is one of major improvement in ERA-Interim over its predecessor ERA-40. The 4DVAR uses forecast model to anchor the state evolution within each analysis window. It helps to improve the hydrological cycle and the stratospheric circulation, and enhances temporal consistency at different time scales (Simmons et al., 2007). In addition, the 4DVAR incorporated in the ERA-Interim includes a set of variable estimates that bias-correct satellite-based radiance observations. Consistent use of the model equations in 4DVAR can lead to more effective use of observations (Rabier et al., 1998). Another important characteristic of the 4DVAR is the flow-dependent effect of observations which rises from the use of a forecast model to constrain the analysis (Thépaut et al., 1996). In cases where observations are sparse, for instance in regions of high latitudes, the 4DVAR can perform better than the older 3DVAR. For example, studies have shown that 4DVAR can provide much consistent analyses of the large-scale tropospheric circulation based only on observations of surface pressure compared to 3DVAR (Jean-Noël et al., 2006; Whitaker et al., 2009).

The ERA-Interim is incorporated with an automated bias-correcting scheme for satellite radiance observations. The system utilizes the bias control parameter in the variational analysis. The data assimilation system first detects data events such as the presence of a new satellite data streams. It then initialises, updates, and keep track of bias variables for radiance data from all available satellites. For each sensor channel, the bias corrections are expressed in terms of a small set of predictors that depend on the atmospheric state at the observed location or on the state of the instrument itself. The bias variables determine the linear combination of predictors used for correcting each radiance observation. They are constantly fine-tuned by the variational analysis to reduce

inconsistencies among the available sources of information, including observations from radiosondes and aircraft.

The background error covariances affects the way the analysis sends locally observed information to nearby locations. Besides, the error covariances also influences the way the analysis uses this information to modify estimates of unobserved parameters. This way, it defines the spatial scales and multivariate constraints for all likely modifications to the background state that the variational analysis is able to produce. The background error covariances of the ERA-Interim is mostly identical to the older ERA-40. One significant addition in the ERA-Interim background error covariances is the application of wavelet-like weighing functions which allow variations in spatial correlation scales that depend on both wavenumber and location (Fisher et al., 1995). In the ERA-Interim, background error correlations are computed from statistics of an ensemble of 4DVAR assimilations, from which the background error variances are estimated.

Following the problem faced with the hydrological cycle in the previous ERA-40 (Uppala et al., 2005), a new humidity analysis algorithm was incorporated into the ERA-Interim. The new system applies a nonlinear transformation to the humidity control parameter in order to render the humidity background errors more nearly Gaussian. This is achieved by normalizing the relative humidity by a factor which relies on background approximation of relative humidity and vertical level. The scheme also prohibits the increase of humidity in the stratosphere by establishing minute humidity bias above the target tropopause.

The ERA-Interim reanalysis is generated using the ECMWF Integrated Forecasting System which has a forecast model alongside three coupled components for atmosphere, land surface, and ocean waves. The forecast model has gone through various upgrades and changes over the years. For the atmospheric model, the new reanalysis uses a 30-

minute time step and has a spectral T255 horizontal resolution, which is around 79km grid. This is another major improvement from the older ERA-40 which uses the T159 resolution (about 125km). However, the vertical resolution remains the same, which is 60 model layers with the top of the atmosphere located at 0.1 hPa.

In addition, a newly revised scheme for cloud, with modifications made to the model physics with the aim of improving the simulation of hydrological cycle, has also been incorporated in the ERA-Interim. Improvements have been made on the formation of ice sedimentation, cloud-top entrainment, cumulus subsidence, the conversion of supersaturated profiles, cloud erosion, and the numeric of the cloud scheme. All these changes were made with the objective of stabilizing the model atmosphere with less vertical motion by increasing the activity of the convection scheme.

Apart from that, a moist boundary-layer scheme has also been introduced. The new scheme utilizes the moist conserved variables liquid water static energy and total water. This new scheme produces more stratocumulus in previously underpredicted areas. Kohler et al. (2011) show that the new boundary-layer scheme can improve the sharpness of the inversion marginally (Köhler et al., 2011).

Lastly, the number of observations merged into the ERA-Interim has increased significantly over the years. In 1989, the average number of observations per day was around 10^6 observations, and the number increased to about 10^7 observations per day in 2010. A vast portion of these data comes from satellite observation. This includes clear-sky radiance measurements from polar-orbiting sounders and imagers, geostationary sounders and imagers, atmospheric motion vectors calculated from geostationary satellites' data, scatterometer wind data, and ozone retrievals from multiple types of satellite-borne sensors. Measurements of atmospheric refraction collected from GPS radio occultation started to be included in 2001. Beside satellite observation, ERA-

Interim also involves measurements from conventional observation systems. Ground-based measurements of air temperature, wind and humidity from radiosondes, pilot balloons, and aircrafts are assimilated into the final product.

2.4.2.2 JRA-55

The JRA-55 is produced by the JMA as an improvement over its predecessor, the JRA-25. It is important to note that at the time of writing, the JRA-55 has three different datasets: The Japanese 55-year Reanalysis (JRA-55, ds628.0), The Japanese 55-year Reanalysis using conventional data only (JRA-55C, ds628.2), and The Japanese 55-year Reanalysis AMIP-type Simulation (JRA-55AMIP, ds628.4). While the JRA-55C and JRA-55AMIP do not extend beyond 1 January 2013, the JRA-55 has been updated through July 2016. The JRA-55 started in 1958, the time when regular radiosonde observations began on a global basis. It is the first comprehensive reanalysis to cover the past 50 years since the ERA-40, and the first reanalysis to adopt the 4DVAR system (Kobayashi et al., 2015). The primary aims of the JRA-55 are to mitigate the problems faced in the previous JRA-25 and to offer a comprehensive atmospheric reanalysis that is suitable for multidecadal studies.

The JRA-55 is, in many ways, similar to the ERA-Interim. The observations used in the JRA-25, for example, come mainly from observations used in ECMWF's ERA-40 and is later inherited by the JRA-55 (Kobayashi et al., 2015). JRA-55 is the first reanalysis to assimilate the new Atmospheric Motion Vectors and Clear Sky Radiances data from Geostationary Meteorological Satellite and Multi-functional Transport Satellite. An important part of quality control applied in JMA's data assimilation process is "Dynamic QC" whereby the threshold value is defined as a variable linearly dependent on local horizontal gradient and tendency of the first-guess fields (Onogi, 1998). Another important aspect of quality control is data filtration. In order to reduce the chances of

assimilating duplicated data, The JRA-55 chooses the ERA-40 observational dataset due to its accuracy and reliability. Due to this reason, the quality control scheme of the JRA-55 is often considered much improved compared to the JRA-25. For certain region (like Japan), the JRA-55 includes conventional observations prior to 2002 obtained from JMA's archive. The improved quality control scheme also reduces the amount of observations assimilated in the JRA-55 compared to JRA-25.

The JRA-55 uses the bias-correction scheme for radiosonde temperature called Radiosonde Observation Correction using Reanalysis version 1.4 as described by Haimberger (2008), which was subsequently upgraded to version 1.5 by 2007 (Haimberger et al., 2008). Again, the JRA-55 is highly dependent on ECMWF products, as bias estimates are generated by calculating the departure values from ERA-40 or ERA-Interim using a statistical break detection protocol (Dee et al., 2011). For cloud, the JRA-55 uses an enhanced cloud scheme described by Krzemiski et al. (2009). It does not simulate the effects of clouds on satellite radiances, and hence cloud-contaminated observations can be identified and filtered before the assimilation (Krzeminski et al., 2009).

The JRA-55 runs in a 6-hourly analysis cycle, with the exception of snow depth analysis which is conducted at 18 UTC daily. The forecast model uses the most recent previous analysis as initial conditions, thereby generating background and atmospheric forcing fields that are necessary for analysis. The horizontal resolution of the model is based on the TL319 (approximately 55 km, with 60 vertical levels) version of JMA assimilation system, which is an improvement over the older JRA-25. Similar to the ERA-Interim, the atmospheric component of JRA-55 uses the 4DVAR system (Kobayashi et al., 2015). The JRA-55 has a bias-correction for satellite radiances and uses GHG history

data, three-dimensional daily ozone data and quality control information from previous reanalyses (Ebita et al., 2011).

2.4.2.3 CFSR

The CFSR runs from January 1979 to December 2010. It is a reanalysis developed by the NCEP. The CFSR analysis runs at 6-hourly and 9-hourly intervals (Saha et al., 2010). Prior to the official release of the operational version of CFSR, a trial (beta) version of the reanalysis, called CFSR-Lite, was released for testing. The beta-CFSR had only uncoupled atmospheric model at 210 km (or 1.90^{o}) resolution.

The CFSR project included observations from two periods: 1979-present; and then be extended back in time to 1947 or earlier. For the 1978-1997 phase, a majority of the observations were obtained from earlier works. As for the 1997-2009 phase, most observations were taken from the NCEP archives. It is worth noting that the CFSR also included a lot of special observations. The African Monsoon Multidisciplinary Analysis, for instance, was included in the CFSR since 2006. In 1992, the Aircraft Communications, Addressing and Reporting System was incorporated into the CFSR.

The NCEP operational Global Data Assimilation System has directly assimilated satellite radiances for long time, but the CFSR is the first NCEP global reanalysis to do so. The atmospheric analysis scheme used in CFSR, the Grid-point Statistical Interpolation scheme, is similar to that used by the MERRA reanalysis (Saha et al., 2010). The implementation of Grid-point Statistical Interpolation scheme has brought about three important improvement to the CFSR. Firstly, the Grid-point Statistical Interpolation scheme applies flow dependence to the background error variances that could enhance climatological estimates. Secondly, the First-Order Time Extrapolation to the Observation algorithm is also included in the Grid-point Statistical Interpolation scheme. Lastly, the quality control algorithm, the non-linear Variational Quality Control, replaced

the old quality control program that was used in the older models. The Grid-point Statistical Interpolation scheme also has a variational satellite bias-correction scheme. At 38 km, the CFSR has the highest horizontal resolution among all the reanalysis datasets (Saha et al., 2010).

2.4.2.4 MERRA

The MERRA is the second reanalysis product released by NASA's Global Modeling and Assimilation Office. It runs from January 1979 and ended in 2016. The introduction of MERRA was inspired by the fact that multiple aspects of the hydrological cycle simulated in other reanalyses were insufficient for climate and weather studies (Rienecker et al., 2011). It is available for download in netCDF and HDF formats.

Unlike the ERA-Interim, JRA-55, and CFSR, the MERRA uses a version 5.2.0 Goddard Earth Observing System (GEOS) atmospheric model and data assimilation system (DAS). This system was intended for the NASA instrument teams and the scientific community. With this in mind, the GEOS-DAS emphasizes more on temperature, moisture, and wind fields, as well as climate-quality reanalyses (Schubert et al., 1993). The GEOS-DAS system is based on finite-volume dynamics which include moist physics with prognostic clouds (Bacmeister et al., 2006), a modified version of the relaxed Arakawa-Schubert convective scheme (Moorthi et al., 1992), shortwave radiation scheme (Chou, 1999), and the longwave radiation scheme (Chou et al., 2001). Two atmospheric boundary layer turbulent mixing scheme are also included. The GEOS-5 incorporates both an orographic gravity wave drag scheme and a scheme for non-orographic waves (Rienecker et al., 2011). The MERRA is available in 0.5° x 0.667° resolution, with 72 vertical levels. Different from the other reanalysis datasets that use the 4DVAR, the MERRA uses the 3DVAR assimilation system with a 6-hourly update cycle. Also, unlike the CFSR which uses the Gridpoint Statistical Interpolation scheme,

the GEOS-5 uses an Incremental Analysis Update method as described by (Bloom et al., 1996). This method has help to mitigate the spindown issue in precipitation during the early stages of the forecast and thereby enhancing the stratospheric circulation.

One of the similarities between MERRA and other reanalysis is the extensive use of satellite radiance from space-borne sensors like the Atmospheric Infrared Sounders on Aqua spacecraft. Besides, MERRA also uses similar observation data as the CFSR and ERA-Interim. Nonetheless, the processing of these data gives rise to the differences in output of the reanalyses. Following the launch of the Advanced TIROS Operational Vertical Sounder in 1998, and the launch of Atmospheric Infrared Sounders and Advanced Microwave Sounding Unit-A in 2002, the number of observations available for reanalysis increased to around 4 million in a 6-hourly cycle, among which half were rejected due to quality control. As for traditional observation data such as radiosonde data, MERRA uses the same data that were quality-controlled for CFSR and corrected by the Global Modeling and Assimilation Office. The features and attributes of all the reanalyses discussed above are summarized in Table 2.1.

Table 2.1 Summary of atmospheric reanalysis products. * JRA-55C, ds628.2 and JRA-55AMIP, ds628.4 ** JRA-55, ds628.0

Name	Institution	Period	Resolution	Data assimilation scheme
ERA-Interim	ECMWF	1979-present	0.70° , 60 levels	4DVAR
JRA-55	JMA	1958-2013 * 1958-present **	0.57°, 60 levels	4DVAR
CFSR	NCEP	1979-2010	0.34°, 64 levels	3DVAR, GSI
MERRA	NASA	1979-2016	0.50° , 72 levels	3DVAR, GSI

2.4.2.5 Using reanalysis dataset for precipitation study in Antarctica

Attempts to quantify Antarctic precipitation using reanalysis datasets had been conducted by various authors. Bromwich et al. (2011) used ERA-Interim, JRA-25, CFSR, NCEP-2 and MERRA to assess precipitation variability over the Antarctic and the surrounding Southern ocean for the period 1989-2009. The study shows that the reanalyses are prone to spurious trends due to modifications made to observations, though other factors may also contribute to the inhomogeneity. In particular, the NCEP2, JRA-25 and MERRA tend to show spurious precipitation data (Bromwich et al., 2011). In a follow-up work, Nicolas et al (2011) added the CFSR reanalysis to the list of spurious reanalysis. Two reanalyses (CFSR and ERA-Interim) show insignificant positive trend over the study period, while the NCEP-2 show the largest (and significant) positive trend. The earlier study reported that the ERA-Interim provides the most reliable reanalysis for Antarctic precipitation (Bromwich et al., 2011). The authors concluded that the ERA-Interim could likely be the most reliable of the reanalyse for precipitation study in

Antarctica for the period 1989-2009. However, the authors cautioned the use of reanalysis datasets for climate change assessment (Nicolas et al., 2011).

Following this work, numerous authors have begun using ERA-Interim as the standard for comparison for precipitation study in Antarctica. Cohen et al (2013) compared the ERA-Interim and NCEP/NCAR Reanalysis-2 precipitation values to the ground-based measurements from nine AWS around RIS from 2008-2012 (Cohen et al., 2013). The study shows that the ERA-Interim often produced more precipitation events (two to four times as much over the varying time periods) compared to NCEP-2 reanalysis in six of the AWS. The author suggested that the ERA-Interim has a weaker southerly component for air coming from the Ross Sea onto the RIS, and this weaker cyclonic circulation over RIS could explain the differences in total precipitation amount. In addition, the higher spatial resolution of the ERA-Interim also implies that it could better simulate the orographic effect of the Transantarctic Mountain compared to NCEP-2. The reanalyses were able to show significant relationships with five of the nine AWS. When compared to the Acoustic Depth Gauge (ADG) measurements, it was found that the ERA-Interim had more matching events with the AGD compared to NCEP-2, though neither reanalysis showed consistently higher correlations with the ADG event sizes (Cohen et al., 2013).

Palerme et al. (2017) compared ERA-Interim dataset with CloudSat and CMIP5 models for precipitation study in Antarctica for the period 1986-2005. The study revealed that compared to CloudSat estimation, the ERA-Interim underestimated precipitation over the Southern Ocean and the coastal areas, but overestimated precipitation in the interior. In addition, the author also noted ERA-Interim differed with seasonal variability observed in CloudSat especially during the winter. Owing to the lack of observation data in the interior, the reliability of ERA-Interim to produce accurate precipitation over the interior is debatable (Palerme et al., 2017b). In another work, Palerme et al. (2017) used

CloudSat data to compare against four reanalysis datasets: ERA-Interim, JRA-55, CFSR, MERRA, and MERRA-2 on Antarctic snowfall. The study period of the work covered only 2007-2010, due to the limited availability of CloudSat data (which started in 2008), and MERRA (which ended in 2010). The mean snowfall rate over Antarctica north of 82^{o}S simulated by the reanalyses between 2007 and 2010 ranged from 165 to 225 mm per year, while CloudSat observations indicate a value of 172 mm per year. The ERA-Interim was the closest reanalysis to observation. However, the other reanalyses were able to replicate the seasonal and interannual variability of Antarctic snowfall reported in CloudSat observations (Palerme et al., 2017a). According to Palerme et al. (2017), ERA-Interim produces consistent seasonal and interannual variability, and the moisture budget in ERA-Interim is closer to equilibrium compared to other data sets.

Wang et al. (2016) published their work which compared spatial and interannual variability of SMB of multiple in-situ observations and 29 observational records with those from ERA-Interim, JRA-55, MERRA and regional atmospheric climate models. Their study showed that in terms of snow accumulation, the JRA-55 captured the interannual variability better than ERA-Interim at six out of 29 study sites in Antarctica (Wang et al., 2016). For the East Antarctic plateau, the ERA-Interim failed to offer realistic estimate of precipitation seasonality. However, it showed significant correlation with interannual variability of observed snow accumulation measurements at 28 of the 29 locations. While the ERA-Interim had the highest correlation with ice-core records, MERRA showed the highest skill for capturing the interannual variation of observed SMB. The ERA-Interim showed no significant SMB trend over the period 1979-2012, while the MERRA and JRA-55 showed significant positive trend. Overall, the authors suggested that the ERA-Interim proved to be the most reliable reanalysis for interannual variability in the observed precipitation (Wang et al., 2016).

2.4.3 Forecast model: CFSv2

The Climate Forecast System version (CFSv2) model from the NCEP is a quasi-global, fully coupled atmosphere-ocean-land model that forces observation from soil moisture and hydrologic states (Saha et al., 2014). It is the continuation of the CFS version 1 model, which was a combination of four independent systems: the NCEP-DOE Global Reanalysis 2; the global ocean data assimilation system (GODAS); the NCEP's Global Forecast System (GFS); and the Modular Ocean Model version 3. The CFSv2 is essentially an enhanced version of the CFSv1, with added new features such as upgraded four-level soil model, interactive three-layer sea-ice model, and historically prescribed CO_2 concentrations. The ocean and sea-ice models in the CFSv2 are similar to those used in the CFSR reanalysis (Saha et al., 2010). The atmospheric model, however, is different from the CFSR in that it has a spectral triangular truncation of 126 waves in the horizontal and a finite differencing in the vertical with 64 sigma-pressure hybrid layers (Saha et al., 2014).

Previous works have shown that the CFSv2 ensemble mean precipitation skill was not admirable after the first month of reforecast, but overall was better compared to other global forecast models (Yuan et al., 2011). Research has shown that the precipitation reforecast errors in the reanalysis can enhance the simulation of soil moisture over the central North America with hydrologic models after bias correction (Mo et al., 2012). Dirmeyer et al. (2013) have shown that precipitation biases appears in both the reanalysis and reforecasts (Dirmeyer, 2013). In a study published recently to evaluate the skills of CFSv2, it is found that CFSv2 performed poorly for precipitation and 2-meter temperature simulation in Antarctica, as it simulates precipitation anomalies with opposite signal compared to the Climate Prediction Center (CPC) Merged Analysis of Precipitation (CMAP) analysis (Silva et al.). At the time of writing, the CFSv2 has yet to be used for in-situ precipitation comparison study in Antarctica.

2.4.4 CMIP models

The CMIP models are one of the most widely used suite of climate models for studying climate around the world. The models are the result of contributions made by research centers and universities in Europe, Americas and Asia. In this section, the history, models' description and differences are discussed in detail.

2.4.4.1 History

In 1995, the Coupled Model Intercomparison Project models —a compilation of coupled atmosphere–ocean global climate models (AOGCMs)—of the WCRP was launched. The launch of the model aims to initiate a community-based infrastructure to support climate model validation, model intercomparison, process diagnosis, climate change attribution, climate change projection and as an update on the present state of the planet's climate, in support of the IPCC AR5 assessment report. There are previous versions of the CMIP models, including CMIP3 (Connolley et al., 2007) and CMIP1 (Lambert et al., 2001). Each version of CMIP models serves as the foundation for the IPCC assessment report. For instance, the results based on CMIP1 were used in the IPCC's Second Assessment Report, released in 1995; the results based on CMIP2 were the foundation of the IPCC's Third Assessment Report, released in 2001; the results based on CMIP3 were used to inform the IPCC's Fourth Assessment Report, released in 2007; and the results based on the CMIP5 are being used to inform the IPCC's AR5, released in 2014 (Zhou et al., 2014). It is worth noting that the CMIP4 is regarded as a transition program between CMIP3 and CMIP5. Due to this reason it is considered relatively less influential.

During the launch of first phase of CMIP (CMIP1), there were 21 global coupled atmosphere-ocean-ice models archived at the United States Department of Energy Program for Climate Model Diagnosis and Intercomparison (PCMDI) at the Lawrence Livermore National Laboratory (Meehl et al., 2000). About half of the

models use flux adjustment of anomaly coupling—an algorithm to adjust the fluxes of heat, water, and momentum at the air-sea interface to compensate for errors in the model components and to minimize climate drift. Various researchers have written on the excellent model skills of the CMIP models in matching climatological features in various regions. Lambert et al. (2001) used 15 CMIP1 models to simulate the global climate and found that the models were able to reproduce major features of the observed distribution of the basic climate parameters (Lambert et al., 2001). However, the variability among models is large especially for oceanic variables. Higher resolution models (1^o x 1^o) in the CMIP1 suite of models did not necessarily provide better results compared to low resolution models (4^o x 5^o) (Lambert et al., 2001). In 2003, Stephenson et al. (2003) published a work using 17 CMIP1 models to investigate the North Atlantic Oscillation. The author wrote that 13 of the 17 models were able to simulate the North Atlantic Oscillation surface temperature quadrupole pattern that centred over Northwest Europe, northwest Atlantic, south-eastern USA and the Middle East. In addition, 10 of the 17 models produced North Atlantic Oscillation indices that vary similar to the observations (Stephenson et al., 2003).

In the second phase of the CMIP (CMIP2), launched in 1997, the models were incorporated with carbon forcing, aimed to compare climate changes simulated by the models for an idealized change in forcing of 1% per year increase in carbon dioxide (CO_2) (Meehl et al., 2000). However, as compared with the first phase of CMIP, some of the models do not use flux adjustments at the ocean-atmosphere interface (Covey et al., 2003). An overview on CMIP2 models was summarized in a report by Covey (2003), which examined the output from 18 CMIP2 models. The author found that models that do not use flux adjustments can give results that are almost as stable as, and agree with observations nearly as well as, the flux-adjusted

models. Despite still exhibiting climate drift from the lack of flux adjustment, the errors from the non-flux-adjusted models are within the bounds required for useful model simulations on time scales of 100 years or more. The differences in results between the models are still significant. In addition, the models do not yield the same results when subjected to identical scenario of 1% per year increase in CO_2 (Covey et al., 2003).

Following the introduction of CMIP2, an additional version of CMIP (known as the CMIP2+) was also launched. The CMIP2+ marked the first time that every field from each model component (atmosphere, ocean, land and sea-ice) for the control as well as 1% CO_2 increase experiments was collected and made available for analysis. However, the collection effort was hampered by technological limitation, especially in terms of storage and data transfer (Meehl et al., 2005). In addition, modelling groups were given short notices and hence had limited time to perform the vast number of experiments (numbering about 30 at the time) as the date for the IPCC Third Assessment Report approached. As a result, only a limited amount of CMIP2+ output was collected and stored in the PCMDI archive (Meehl et al., 2005). This therefore affected the popularity of the CMIP2+ models, and prompted the WGCM to recognize the importance of proper organization and coordination.

In 2003, the WGCM launched the new CMIP3 models. The new CMIP3 models included twentieth-century (starting from pre-industrial years in late 1800s) simulation to year 2000 with anthropogenic and natural forcings, six climate change experiments with multiple values of carbon concentration running from 2000-2100 or beyond (until year 2300), century control run with all forcings held constant, and other enhancements (Meehl et al., 2007). The size of the experiment output from the models was considered monumental at the time that online transfer became impractical. In order to accommodate and archive the large output data, hard disks

were distributed the different modeling groups by the PCMDI. The results were then copied into the hard disks in netCDF format before sent to PCMDI to be stored (Meehl et al., 2007). The introduction of CMIP3 marked the first time such a large set of AOCGM climate change simulation has been made openly available for analysis. The climate output was also, for the first time, released instantly upon completion to allow researchers worldwide the access to examine and study the output easier (Taylor et al., 2012). Laepple et al. (2008) used CMIP3 models to predict annual global temperature and northern hemispheric mean surface air temperature (SAT), compared against predictions from complex forecast model. The result showed that the global and northern hemispheric mean temperatures was expected to rise from 2007-2011 (Laepple et al., 2008). In another report, Biasutti et al. (2008) used 19 CMIP3 models to investigate the variability of sea surface temperature (SST) and rainfall in Sahel, Sahara desert for the twentieth and twenty-first century. The author wrote that for the historical (pre-industrial) simulation, most CMIP3 models are able to simulate the relationship that links Sahel rainfall anomalies to tropical SST anomalies at interannual time scale. As the climate continues to warm in the twenty-first century, the warming of the Indo-Pacific would induce droughts in the Sahel. Nonetheless, for the prediction of future rainfall, most models simulate a wetting of the Sahel, which goes against the warming of SST in Pacific. The author suggested that the existing mechanism that controls rainfall could be altered in the future due to a change in GHG concentration, or that SST is not the only factor that affects rainfall in Sahel. The author concluded that the ability of CMIP3 models to perform high quality historical simulation may be insufficient for a trustworthy prediction of the future (Biasutti et al., 2008).

With the introduction of new versions of CMIP models, researchers began comparing the different versions of CMIP. Numerous improvements and

enhancements had been incorporated into newer versions of CMIP models, so comparing the different versions of CMIP models became an important step to determine the level of improvement achieved by the models. An example of CMIP comparison is the work published by Zhou et al. (2014) which studies models from the CMIP1, CMIP2, CMIP3, and CMIP (Zhou et al., 2014). The author summarized that in CMIP1, the surface heat and salinity fluxes were often needed adjustment and the effects of clouds remained uncertain. In the CMIP2, sea-ice and land surface components were introduced into the models. This led to more realistic modeling of land surface processes and consequently better simulated temperature, salinity and sea-ice. However, the effects of clouds, hydrological balance over land surface and heat flux at ocean surface remained uncertain. In CMIP3, the problem of clouds and humidity were addressed and led to enhanced coupled models. For this version, the simulation of the ENSO was enhanced, and most models are now capable of simulating results that are close to observation that soon the idea that no single model could ever be considered "best" was proposed. In the CMIP4, most Coupled General Circulation models that were in CMIP3 had stopped using flex adjustments. Several models have also added in the treatment of the carbon cycle (Zhou et al., 2014).

2.4.4.2 The CMIP5 models

The main focus of this work is the use of models from the latest CMIP5 experiments for the assessment of precipitation variability. The CMIP5 models were launched by the WGCM in 2008 following the success of the CMIP3. The CMIP5 has gone on to become the most participated model suite among the CMIPs, as it involves over 50 climate system models and earth system models from over 20 modeling groups worldwide (Taylor et al., 2012). Despite the increasing number of models from various modeling groups, most models are similar because they essentially describe and model the same system, while incorporating the same biases

and parameterizations. A significant portion of the discussion in this section will be devoted to review the fundamentals and basics of CMIP5.

Figure 2.2 shows the relationship between CMIP5 and the different organizations that coordinate international climate research activities: the WCRP organizes and runs the CMIP, while the research activities based on CMIP are run by the research community made up of scientists from all over the world so that the outcome from the research can be used to inform the ongoing IPCC process. The CMIP5 aims to offer a multimodel context for:

1. Assessing the mechanisms responsible for model differences in poorly understood feedbacks associated with carbon cycle and clouds;

2. Investigating climate "predictability" and examine the predictive capacities of forecast systems on decadal timescales; and

3. Investigate the reason why models give different output despite forced under the same conditions.

The CMIP5 is divided into three main parts. The first part is the long-term integration where the integration time is over a century (Taylor et al., 2012). This part is further divided into two main experiments:

1. The atmospheric model intercomparison project protocol first described by (Gates, 1992) and

2. The climate system model experiment.

The atmospheric model intercomparison project experiment specifies the observed SST and sea-ice for the past century. The integrations usually begins with multicentury preindustrial control (quasi equilibrium) integrations. The long-term experiments in the CMIP5 is built upon the successful CMIP3 experiments, but include extra runs to offer a more thorough comprehension of the variability of climate change (Taylor et al., 2012).

The second part of the CMIP5 is the near-term integration, where decadal (10 to 30 years) predictions are conducted. These predictions include external forcing changes (e.g. GHG), anthropogenic aerosols, solar variability, volcanic eruptions, and the initial state of the ocean to perform decadal predictions (Meehl et al., 2009). The short-term integrations usually start with observed ocean and sea-ice conditions. Unlike the long-term experiments, the near-term prediction experiments are a new feature in the CMIP where the models will respond not just to climate forcing like rising concentration of CO_2, but also predict to a certain extent the outcome of climate change, including the unforced component of climate evolution (Taylor et al., 2012).

The third and final part of the CMIP5 is high-resolution atmospheric model experiments which conduct historical study spanning the period 1979-2008 and prediction study spanning the period 2026-2035. The CMIP5 time-slice option allows a wider range of modelling research groups to participate in and contribute to CMIP5 (Zhou et al., 2014).

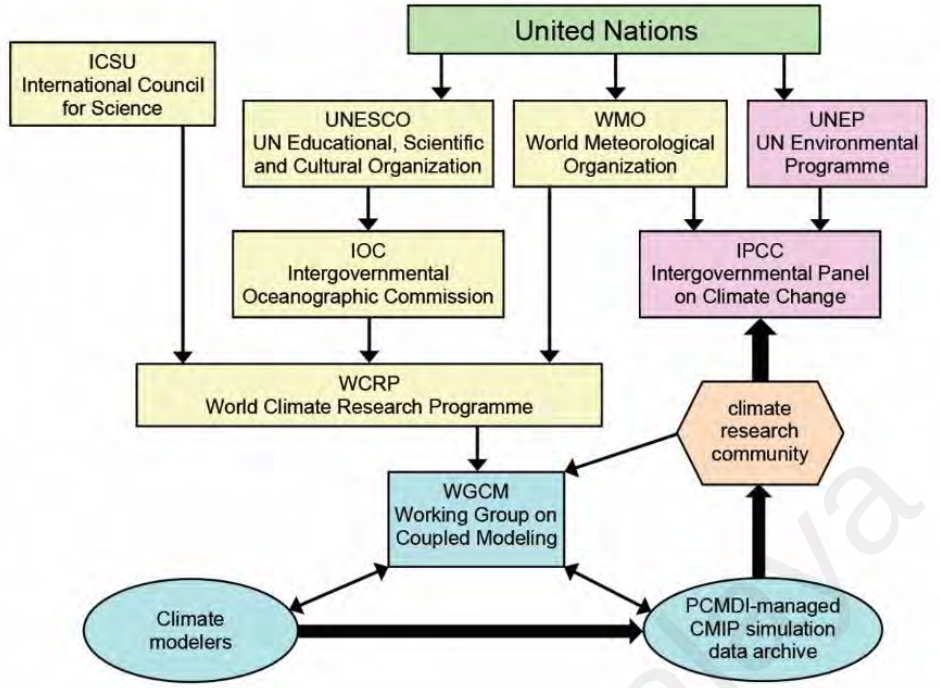

Figure 2.2 The link between CMIP5 and institutions that coordinate international climate research and IPCC, modeling centers and the research community.

The standard AOGCMs and Earth System Models of Intermediate Complexity in CMIP5 models can be forced under various concentrations of GHG and include an interactive representation of the atmosphere, ocean, land and sea-ice (Petoukhov et al., 2005). It is worth noting that for long-term simulations as mentioned in item (1) in the previous paragraph, some AOGCMs, known as the Earth System Models, will for the first time in CMIP be coupled to biogeochemical components in order to "complete" the carbon cycle in the models, thereby providing a more realistic representation of the entire climate system (Taylor et al., 2012). The biogeochemical components in the Earth System Models include the important fluxes of carbon between the ocean, atmosphere and terrestrial biosphere carbon reservoirs, thereby enable the Earth System Models to use time-evolving emissions of constituents from which concentrations can be computed interactively. The Earth System Models may

in some cases also include interactive prognostic aerosol, chemistry and dynamical vegetation components (Taylor et al., 2012).

Owing to the large amount of simulation required for all the models, the integrations for both the century and decadal time scales are categorized into the "core" set surrounded by one or two "tiers". This categorization aims to produce a huge number of runs to allow a proper model intercomparison within each experiment, and hence creating a credible multimodel dataset for analysis. The long-term experiments listed in the core and the surrounding tiers are shown in Figure 2.3 below.

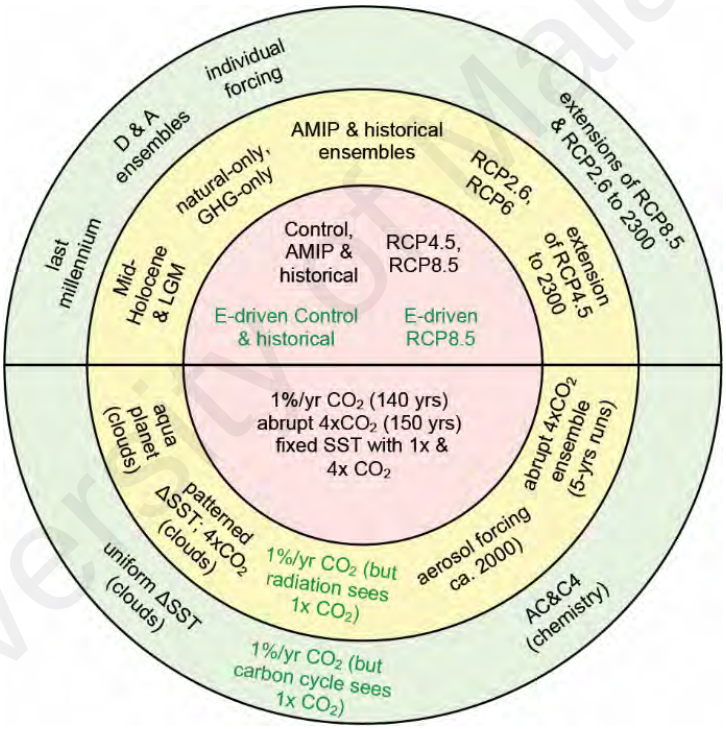

Figure 2.3 The "core" and "tier" experiments available in CMIP5 long-term experiments. Pink shade marks the most important experiments, while tier 1 is marked by yellow shade, while tier 2 is marked by green shade (Taylor et al., 2012).

The most important experiments i.e. those that are critical for assessing the models and could provide prediction on future climate change are listed in the innermost circle (Figure 2.3). These experiments include an AMIP run, a coupled control run,

and a "historical" run, which starts from the year 1850 to near present (year 2005), forced by observed atmospheric composition changes and, for the first time, including time-evolving land cover. There are also two additional future prediction experiments in the core set (RCPs). The RCP runs are forced with specified concentrations of GHG in the year 2100 relative to pre-industrial values, specifically +4.5 Wm^{-2} and +8.5Wm^{-2}. The RCPs are named after the specific concentration of GHG that they represent (RCP 4.5 named after GHG concentration of +4.5 Wm^{-2} by year 2100). The RCP 4.5 assumes that global annual GHG emissions peak around 2040 at +4.5 Wm^{-2}, followed by a stabilization in GHG concentration, while the RCP 8.5 assumes the GHG concentration continue to increase throughout the twenty-first century and reaching +8.5Wm^{-2} by the year 2100 (Moss et al., 2010). The RCP 8.5 is also known as high emission scenario, while the RCP 4.5 is known as the midrange mitigation emissions scenario. The tier 1 experiments, marked by yellow shade, are critical for studying specific aspects of climate model forcing, response and processes. Exist within this tier are two other RCP runs: the RCP 2.6 and RCP 6.0, which carries the same definition as their RCP 4.5 and RCP 8.5 counterparts. Also, the RCP 4.5 in tier 1 is further extended by two centuries to the year 2300. The tier 2 integrations (green shade) are in-depth study of the experiments in tier 1. For Earth System Models in tier 1 and 2 runs, there are two carbon cycle feedback experiments:

1. Climate change is suppressed so the carbon cycle response only reflects changing CO_2 influences unrelated to climate change; and

2. The climate responds to CO_2 increase, but the CO_2 increase is hidden from the carbon cycle.

By following the schematic shown in Figure 2.3 from the core to the tiers, researchers would be able to explore the basics of CMIP5 projections to more

specialized simulations. For each experiment, researchers would begin from the core and make it the tier integrations based on their specific research interests.

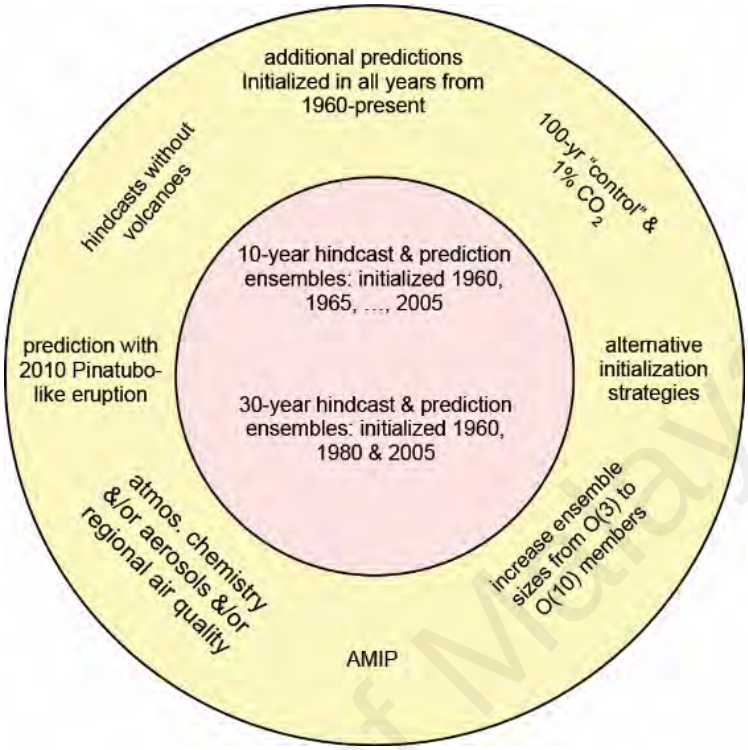

Figure 2.4 The "core" and "tier" experiments available in CMIP5 short-term experiments. Pink shade marks the most important experiments, while tier 1 is marked by yellow shade (Taylor et al., 2012).

Similar to long-term experiments, the short-term experiments are also divided into core and tier runs, as shown in Figure 2.4. There are two sets of core runs: a set of 10-year hind casts started from observed climate states near the years 1960, 1965 and every 5 years up to 2005. The 10-year runs allow researchers to study the skills of the forecast system in predicting climate statistics for times when the initial climate state may exert some considerable influence. Other core integrations extend the 10-year simulations initialized in 1960, 1980, and every 20 years up to 2005, ending with two 30-year hind casts, and one 30-year prediction by the year 2035 (Taylor et al., 2012). The tier 1 experiments for near-term runs include a relatively short "control" run of about a century, along with a 1% year^{-1} CO_2 increase experiment to

offer a calibration of the models' internal variability and response to rising CO_2 (Taylor et al., 2012).

Last but not least, there is also the prospect for an atmospheric chemistry/pollutant experiment in the near-term runs. It is worth noting that the near-term experiments' objectives are to enhance the understanding of predictability, reveal the advantages of different data assimilation methods, and expose the limitations of the existing ocean observation network. Several approaches have been tested to assimilate ocean observations into the models with little success and acceptance. In addition, the quality and completeness of ocean observations may be insufficient to realize but a fraction of the predictability inherent in the system. Owing to this reason, the forecast systems for CMIP5 cannot be seen as operational, much less offer better simulations compared to long-term runs (Taylor et al., 2012). The overall predictive skill of a forecast system is judged by the quality of observations, the capabilities of assimilation method, and the skill of the model itself. Users are reminded that decadal predictions with climate models are in exploratory stage and the model output should therefore be used with caution. As already mentioned above, the CMIP5 data represents the mean value over each individual grid cell, which is approximately 100km on a side. Therefore, when comparing CMIP5 result simulations against observation at point locations, one should consider the mismatch in spatial representativeness of data values.

2.4.4.3 CMIP5 and other versions of CMIP

(a) ***Similarities***

Code-sharing occurred in CMIP3, and the practice has become more ubiquitous in CMIP5. This partly explains why some models give similar or almost similar results. For instance, for the atmospheric component, the Chinese Beijing Climate Center (BCC) models use the French ARPEGE which is also present in the Centre National

de Recherches Meteorologiques (CNRM) model. The Australian Community Climate and Earth System Simulator (ACCESS) models (ACCESS1-0, ACCESS1-3) are based on the Hadley Center Global Environmental Model version 2 (HadGEM2) atmospheric model, while the Norwegian Earth System Model (NorESM) and the First Institute of Oceanography Earth System Model (FIO-ESM) are built using the basics of Community Earth System Model version 1 (CESM1). The atmospheric component of the BCC comes from Community Climate System Model version 3 (CCSM3), while the atmospheric model of the Flexible Global Ocean-Atmosphere-Land System Models (FGOALS-g2, FGOALS-s2) shares some parameterizations from CCSM. The CNRM and European Community Earth System Model (EC-EARTH) use the ARPEGE/IFS/ECMWF atmosphere model, while the Italian model, Centro Euro-Mediterraneo sui Cambiamenti Climatici Climate Model (CMCC-CM) uses an MPI-ECHAM5 model. For ocean model, the Bjerknes Centre for Climate Research (BCCR) and NorESM use the MYCOM ocean model, while the Institut Pierre Simon Laplace (IPSL) model and CNRM model use ocean models based on NEMA, ORCA or OPA. It can be said that a lot of these models maintain a predecessor-successor relationship, which is summed up in a report by (Knutti et al., 2013).

(b) ***Difference 1: spatial resolution***

Compared to the CMIP3, the CMIP5 contains more comprehensive models and experiment runs that covers a wide range of scientific studies, as already discussed in earlier section. Another critical improvement that can be observed in the CMIP5 is enhanced spatial-resolution in the models. For most models, the spatial resolution range from 0.5^{o} to 4^{o} for the atmosphere component, and 0.2^{o} to 2^{o} for the ocean component. About 50% of the atmospheric models with have an average latitudinal resolution smaller (better) than 1.3^{o}, a vast improvement compared to the CMIP3 where only one model had this resolution. For the ocean components, about 50% of

the models in CMIP3 had average latitudinal resolution larger (coarser) than 1°, while only two of over 30 models in CMIP5 that have resolution coarser than 1°. Flato et al. (2013) credited the enhanced simulation ability of the CMIP5 models to improved resolution (Flato et al., 2013). This notion has been supported by numerous other studies (Boyle et al., 2010; Delworth et al., 2012; Neale et al., 2013; Watterson et al., 2014). However, the improvement of simulation with the improvement in resolution only works in certain parameters (Watterson et al., 2014). For instance, several studies have found that the enhancement of CMIP5 models for precipitation is somewhat modest (Mass et al., 2002; Mishra et al., 2014; Pope et al., 2002). In fact, high resolution models often suffer from the "double-penalty" issue, where a metric penalizes a simulation for missing a feature of high precipitation in the observation while also for simulating it at a location where the observation have less precipitation.

(c) ***Difference 2: documentation and additional fields***

PCMDI provides better documentation and information for each models and experiment conditions in the CMIP5. The lack of documentation, or the difficulty of obtaining documentation for the experiments was one of the main problem that plagued the CMIP3. To remedy this, the model output files in CMIP5 are equipped with information and details, in the output files' metadata, of the runs, resolutions, dates of runs, and the time span of the experiments so users could have quick access to the information.

The process of compiling the type of scientific questions in preparation for CMIP5 experimentation was done by soliciting a list of requested output from various potential users. In previous versions of CMIP most of the atmospheric components had already been requested. For the CMIP5 additional variables in the ocean components have been added, in addition of aerosol, biogeochemical and cryospheric

fields (Taylor et al., 2012). Moreover, many of the CMIP5 models can produce a new set of variables using specialized "satellite simulator" codes. These codes, contained in the Cloud Feedback Model Intercomparison Project Observation Simulator Package, could help ease the comparison between CMIP5 models and CloudSat/Cloud-Aerosol Lidar and Infrared Pathfinder Satellite Observations and ISCCP observations. In total, there are about 60 atmospheric fields, 77 ocean fields, 58 land surface and carbon cycle variables, 74 ocean biogeochemistry variables, 38 sea-ice variables, 14 land ice and snow fields, and 100 clouds variables in the CMIP5 experiments. Most of these variables are available as annual means (57), monthly means (390), daily means (53), or every 3 or 6 hours. Apart from adding extra fields, there was also request by the IPCC's Task Group on Data and Scenario Support for Impact and Climate Analysis to sample some of the fields on an hourly basis. However, the request was eventually turned down due to two reasons:

1. Modeling groups could not guarantee accurate performance and behavior of the models at hourly time scale; and

2. The size of the output would be enormous and may require considerable storage capacity.

The additional model output means that the entire CMIP5 archive is much larger than all its predecessors. The CMIP3, for instance, utilizes about 36 terabytes of storage. The CMIP5, with all its core experiments, tier experiments, long- and near-term experiments, the extra models and the models' finer spatial-resolution, requires over 3 petabytes of storage, or 3000 terabytes of storage, which is about a hundred times the size of the CMIP3 archive.

(d) Using CMIP5 models for precipitation study in Antarctica

The precipitation data from CMIP5 includes precipitation from both large-scale and convective clouds which falls in both solid and liquid forms. Fyfe et al. (2012) studied the summer (December-February) precipitation in Antarctica using 29 CMIP5 models and suggested that the austral summer precipitation in polar region of the southern hemisphere has been increasing since 1957. The author merged the historical simulations up to 2005 with either historical extension simulations or the RCP 4.5 from 2006 until 2010. In addition, the results also suggested that rather than natural climate variability, anthropogenic influences especially the emission of GHG and ozone-depleting compounds had a profound effect on precipitation across the mid- and high latitudes of the southern hemisphere (Fyfe et al., 2012).

Palerme et al. (2016) conducted a study using 40 CMIP5 models, ERA-Interim reanalysis data and CloudSat satellite precipitation to assess the present (1986-2005) and future (2006-2099) Antarctic precipitation under four RCPs scenarios. The author reported that there is a positive trend in historical Antarctic precipitation shown by all but one of the CMIP5 models. Over the coast, the models are able to simulate snowfall rates that are in agreement with CloudSat and ERA-Interim, though they overestimate the snowfall in the interior. The author also cautioned that almost all the models overestimated current Antarctic precipitation, some by as much as 100%, when compared against the ERA-Interim and CloudSat. For future precipitation prediction, precipitation is expected to vary from -6.5% to 43.0% for the whole Antarctic continent, depending on the models and the different RCPs. The increase in Antarctic precipitation, on average, is expected to be around 5.5% (RCP 2.6) to 24.5% (RCP 8.5) (Palerme et al., 2017a).

Agosta et al. (2015) used 41 CMIP5 models alongside six reanalyses: ERA-Interim; JRA-55; MERRA; National Center for Environmental Prediction-Department of Energy (NCEP-DOE); National Center for Environmental Prediction –National Center for Atmospheric Research (NCEP-NCAR); and National Oceanic and Atmospheric Administration 20th Century Reanalysis (NOAA-20CR) to evaluate the CMIP5 fields that will be used as input for Regional Climate Models. The results show that the precipitation trend, rate and pattern in Antarctica predicted by the most of the models is inconsistent with the results obtained from the reanalysis datasets. Less than 10 CMIP5 models show reasonable biases compared to ERA-Interim, among which the ACCESS1-3 is the best model for forcing Regional Climate Models over Antarctica, followed by ACCESS1-0, CESM1-BGC, CESM1-CAM5, NorESM1-M, CCSM4 and EC-EARTH. In addition, the air temperature at 850 hPa has a strong correlation with austral summer precipitation (Agosta et al., 2015).

2.4.5 Satellite observations

The use of satellite data for precipitation study in the high latitude regions began in the mid-1990s (Carleton et al., 1993). One of the advantages of satellite observations is that satellites provide extensive spatial coverage especially over bodies of water such as oceans and lakes where no precipitation gauges can be installed. Moreover, satellite and radar technologies are free from the harsh condition of the Antarctic climate and be used to survey large swath of land and ocean. However, there are only two reliable satellite data available for the Antarctic region, namely the GPCP and CloudSat (Huffman et al., 1997; Stephens et al., 2002). CloudSat data is determined by satellite whose narrow orbital track allows it to cover only limited surface and period (Palerme et al., 2014). Because of this reason, CloudSat is unable to supply continuous daily measurement of precipitation. In the interior of the Antarctic where precipitation often falls as diamond dust, the CloudSat

algorithm is unable to detect these small snow particles (Palerme et al., 2017a). Palerme et al. (2014) used two new CloudSat products to generate the first model-independent, multi-year climatology of Antarctic precipitation north of 82°S (Palerme et al., 2014).

The GPCP was set up by the WCRP in 1986. The main objective of the GPCP is to offer monthly mean precipitation data on a global 2.5° x 2.5° latitude-longitude grid for the period 1979 to present. The basic concept of the GPCP is to merge precipitation data acquired from three main sources: microwave estimates from the Special Sensor Microwave/Imager (SSM/I) from the Defence Meteorological Satellite; the IR precipitation estimates from USA, Europe, and Japan geostationary satellites or polar-orbiting satellites; and rain gauge data analysed by the Global Precipitation Climatology Centre (GPCC) into a final product (Huffman et al., 1997). The GPCP product, GPCP 1DD Version 1.3 is also used as one of the standard of comparison in this work. In the following section, a brief description of GPCP is presented.

2.4.5.1 GPCP dataset

As mentioned in the previous section, the GPCP is the combination of SSM/I data, IR estimates from satellites, and rain gauge data. Each input dataset has advantages and disadvantages, and the concept of GPCP is to take advantage of the strength of each dataset to provide an accurate precipitation climatology for the world. It should be noted that the original release of the GPCP does not include coverage for the high latitudes. Newer versions, like the 1DD version 1.2 and version 1.3, do provide precipitation data for the Arctic and Antarctic. The original GPCP release (version 1) covers only 1987 through to 1995. The version of GPCP used in this work, GPCP 1DD version 1.3, offers precipitation estimates on a 1° grid for the whole planet on a 1-day time step from 1 October 1996 to 31 October 2015. The GPCP 1DD dataset

has been selected for this work because at the time of writing (June 2017), the GPCP 1DD product has not been used in any validation work for precipitation measurement in Antarctica. Moreover, the dataset is of much finer temporal and spatial resolution compared to its 2.5° monthly counterpart, making it the perfect satellite product to be used as a comparison standard. In the following section, we will discuss briefly on the three sources that make up the GPCP dataset: geostationary IR (geo-IR) data, SSM/I radiances, and precipitation gauges.

(a) Geostationary Infrared data

Precipitation data from geostationary infrared data are essentially geo-IR images taken from Geostationary Operational Environmental Satellites (GOES) owned by the USA, Meteorological satellites (Meteosat) owned by the European community, and the Geostationary Meteorological Satellite (GMS) owned by Japan every 3 hours from their orbit, thus offering good temporal resolution of precipitation systems and coverage of the diurnal cycle. The global IR rainfall estimates are then produced from a merger of these data at the Climate Prediction Center using the GOES precipitation index (GPI) technique (Arkin et al., 1987), which associates cold cloud-top area to rain rate. The main problem faced by the geostationary satellites is the poor coverage in the regions of high latitudes. This is because geostationary satellites orbit the Earth in circular orbits that are orientated in the plane of the Earth's equator.

(b) SSM/I radiances

The second source for the GPCP is the SSM/I radiances from the Defence Meteorological Satellite. The concept of this technique is to utilize the emission of microwave energy. The ability of an object to emit microwave energy is determined by the temperature and the internal scattering properties of the said object. The concept has been used by scientists to monitor the passive microwave emission of Earth using satellite since 1973. The usual observation frequencies are at or near 6,

19, 23, 37, and 85 Gigahertz, corresponding to spectral windows in atmospheric absorption (Bindschadler et al., 2005). The emission from the earth's surface, when observed from a space-borne satellite, will be modified by the atmosphere in between the satellite and the earth, mainly by hydrometeors. Ice hydrometeors, for example, scatter upwelling radiant energy at higher SSM/I frequency, an effect that offer strong correlation with surface rainfall and is detectable over both land and water. This would alter the resulting microwave brightness temperatures that can be picked by the SSM/I sensor. The GPCP uses two SSM/I estimations; one for ocean regions where the water has low emissivity; the other for land areas. The microwave estimates from the water and land algorithms are combined by taking the histogram-based emission estimates over water and the scattering-based estimates of land to produce a global estimate. In 1990, the first operational SSM/I on the Defence Meteorological Satellite Program F-8 satellite was damaged because of improper shielding from solar radiation. As a result, the on-board 85-Gigahertz scattering index unit failed to work. The problem was remedied the following year with the launching of the F-10 and F-11 spacecraft which carried the new SSM/I units into orbit. The main problem faced by the SSMI/I radiances is that the SSM/I observations have poor temporal coverage, averaging only 1.2 images per day in the tropics and subtropics with one satellite.

(c) Precipitation gauges

Gauge reports are considered the most accurate source of data. However, precipitation gauges can only be installed on land, and therefore cannot provide accurate measurement of precipitation over bodies of water. Moreover, gauges installed at a particular location represents a point value rather than an average over a predestined space (grid). To facilitate comparison between gauge data and model data, the data from the gauges have to be converted to area means. For data-merging in GPCP, a variant of the SPHEREMAP interpolation routine is employed to

interpolate the station data to regular grid points (Willmott et al., 1985), which are then averaged to produce area-mean monthly total precipitation on 2.5° grid cells.

(d) Merging of SSM/I, IR, and gauge data

The combination of the three main sources in GPCP is illustrated in Figure 2.5. The merger technique is aimed at taking the strengths of each source to produce merged global monthly precipitation fields that are superior to any of the individual source.

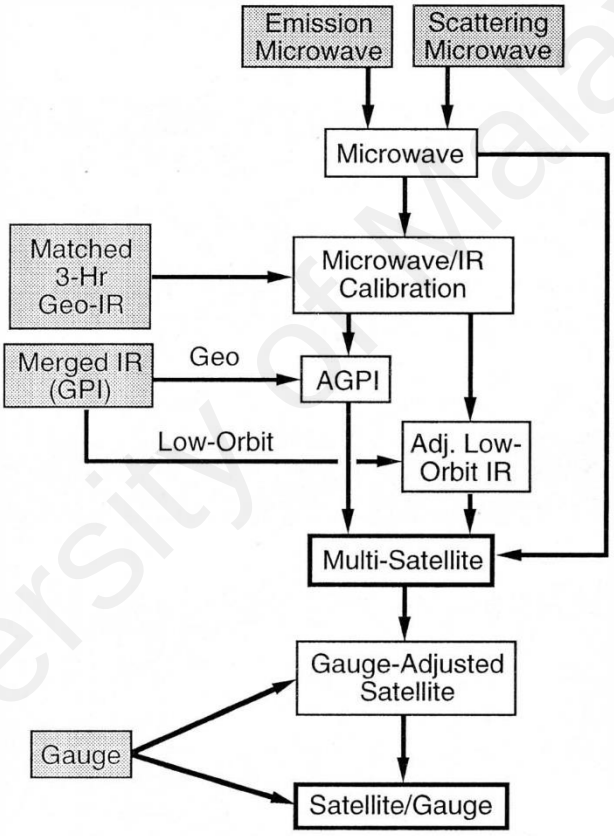

Figure 2.5 Schematic flow of satellite-gauge-model precipitation combination technique (Huffman et al., 1997)

The microwave estimates are about time- and space-matched with geo-IR observations to derive a microwave/IR calibration ratio for each grid box, which is smoothly filled in regions where the SSM/I is missing but the geo-IR is available. In contrast, in areas of light precipitation an adjustment is added, and in areas lacking

geo-IR data, the low-orbit IR in the GPCP-merged IR dataset is adjusted using a varying interpolation of the microwave/geo-IR adjustment ratio. The spatially varying arrays of adjustment coefficients are then applied to the full set of GPI estimates to give the adjusted GPI (AGPI). Studies have shown that the AGPI estimates could help reduce known biases in the GPI over subtropics and over land, and that the AGPI estimates perform better than either the microwave or GPI estimates alone (Adler et al., 1993). The multi-satellite estimate is produced from the merging of AGPI, adjusted low-orbit IR, and microwave.

There are two versions of GPCP data sets available: GPCP V2.3 and GPCP 1DD V1.3. The latter version, which will be used in this work, provides precipitation estimates on a 1° grid over the entire globe on a one-day time-step from 1 October 1996 to 31 October 2015 (at the time of writing), while the former uses a 2.5° × 2.5° grid. The daily 1° × 1° precipitation GPCP data for Rothera (67°S, 68°W) was obtained from the Research Data Archive of the NCAR website. At the time of writing, the GPCP 1DD product has yet to be used for a precipitation study in Antarctica.

2.5 Summary

In summary, new technology can help scientists and researchers in their quests to understand weather patterns and climatology in many parts of the world, including regions inaccessible to humans. Satellite technology, for example, has enabled the monitoring of climate in many regions of the world today, including the open ocean and the polar region like Arctic and Antarctica. Reanalysis dataset, on the other hand, can simulate accurate historical weather patterns and trends with the incorporation of measured data. Lastly, climate models like the CMIP suite of models can be compared against reanalysis datasets for the prediction of weather pattern in the future.

CHAPTER 3: DATA, INSTRUMENTATION AND METHODOLOGY

3.1 Precipitation Instruments at Rothera Station, Antarctic Peninsula: A Comparative Study.

3.1.1 Introduction

For the first part of this work, a Campbell Scientific CS700H heating gauge, contributed by the National Antarctic Research Centre (NARC), was set up during the summer (December to February) of 2014-2015. Precipitation measurement obtained from the CS700H and four different types of precipitation sensors hosted at Rothera Research Station in the Antarctic Peninsula from the period March 2015 to February 2016 were analysed and compared with reanalyses data sets, namely ERA-Interim, JRA-55, the NCEP′s CFSv2 model, as well as the GPCP 1DD satellite product data set. Figure 3.1 shows the CS700H system that was later deployed at Rothera. The CS700H was installed without a wind shield.

Figure 3.1 The CS700H rain gauge system contributed by the NARC

On the other hand, the EML UPG-1000 gauge was installed with a wind shield to reduce the influence of wind. The shield, named the Alter screen, is developed by EML. The Alter screen has swinging leaves to prevent the accumulation of snow.

Figure 3.2 The UPG-1000 system installed at Rothera.

Figure 3.3 shows the VPF-730 system in Rothera. The VPF-730 is one of the longest-serving instruments installed at the research station.

Figure 3.3 The VPF-730 system installed at Rothera.

Figure 3.4 The PWS-100 system installed at Rothera.

Figure 3.5 The LPM system available at Rothera

3.1.2 Location and study period

Rothera station is one of five British Antarctic Survey research stations in the British Antarctic Territory. It is located at Rothera Point (67°33’S, 68°7′W) on Adelaide Island, Antarctic Peninsula (Figure 3.6). It began operation in 1975 and has a wide array of meteorological measurements in operation. The average temperatures at the station in summer range from 0 to + 5°C (winter from −20°C to −5°C), with winds that can reach up to 40 ms^{-1}. For this work, all instruments, except for the UPG-1000, were installed close to one another in order to provide a similar environment for all the instruments. The UPG-1000 was installed behind one of the buildings, at the request of the manufacturer, about 100 m away from the rest of the instruments, to provide extra shelter against very strong wind events. The measurements from the gauges were logged every minute and made available on the British Antarctic Survey website. For this report, the period of study is from 19 March 2015 to 4 February 2016.

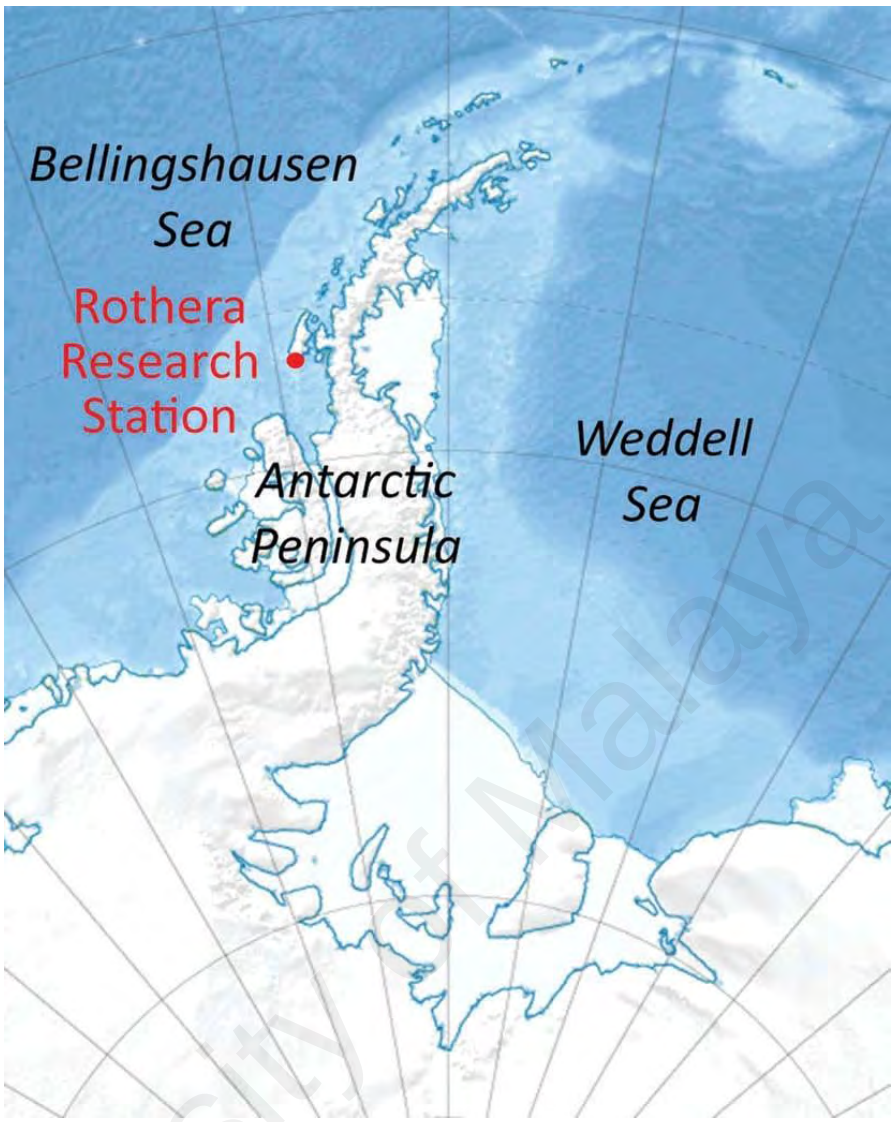

Figure 3.6 Location of Rothera Station (67° 34'S, 68° 08'W). (Modified from a map by Kikos, CC BY-SA 3.0, https://creativecommons.org/licenses/by-sa/3.0, from Wikimedia Commons.)

3.2 An assessment of historical Antarctic precipitation and temperature trend using CMIP5 models and reanalysis datasets

3.2.1 Introduction

The current method of data collection in Antarctica relies on precipitation measurement with limited temporal basis, with distances between measurements sometimes exceeding 1300 km (Knuth et al., 2010). This makes instrumental-based measurement of precipitation in Antarctic highly unreliable (Genthon et al., 2003). A non-

quantitative method of measurement had been developed to measure snowfall by sensing the fluctuation in surface emissivity (Bindschadler et al., 2005). Quantitative Antarctic precipitation detection, on the other hand, had been developed following the installation of the Cloud Profiling Radar onboard the CloudSat satellite (Liu, 2008; Stephens et al., 2008). The recent CloudSat products had been incorporated in a study to produce a model-independent, multi-year climatology of Antarctic precipitation north of 82°S (Palerme et al., 2014). However, the CloudSat product started only in 2008 and could not be used to compare with CMIP5 nor the ERA-Interim for the historical study starting from 1979. Nicolas and Bromwich (2011) used monthly mean precipitation from the GPCP Version 2 to study the precipitation changes in Antarctica alongside reanalysis datasets. The study shows that GPCP produce significantly higher precipitation estimates compared to ERA-Interim, and at least 40% more precipitation than the CMAP analysis (Nicolas et al., 2011).

For Antarctica, CMIP5 models consistently predicted that the precipitation would increase as the global climate warms (Stocker et al., 2013). Fyfe et al. (2012) assessed the summer (DJF) precipitation in the Antarctic using 29 CMIP5 models and reported that the austral summer precipitation in the high latitude of the southern hemisphere has been increasing since 1957 (Fyfe et al., 2012). Palerme et al. (2017) used 40 CMIP5 models, as well as ERA-Interim reanalysis data and CloudSat satellite precipitation data to investigate the historical (1986–2005) and projected (2006–2099) Antarctic precipitation under four RCP scenarios. The work suggested that there is a positive, albeit statistically insignificant, trend in historical Antarctic precipitation shown by all but one of the CMIP5 models (Palerme et al., 2017b). A work by Agosta et al. (2015) used 41 CMIP5 models alongside six reanalyses to evaluate the Antarctic SMB. The work concluded that air temperature at 850 hPa has a strong correlation with austral summer precipitation and austral winter sea ice. However, the precipitation trend, rate and pattern in Antarctica

predicted by the models is inconsistent with the results obtained from the reanalysis datasets (Agosta et al., 2015). A recent study using the ERA-Interim also shows that from 1979 to 2016, the poleward moisture flux into the Antarctic did not show a significant long-term trend (Oshima et al., 2017). In addition, the abovementioned contributions were based on limited numbers of CMIP5 models output due to model availability at the time of writing. Moreover, some of these studies used the ERA-Interim as the benchmark for measuring precipitation (Agosta et al., 2015; Palerme et al., 2017a; Palerme et al., 2017b). Due to the lack of observational data for comparison, the reliability of ERA-Interim to simulate precipitation especially over the Antarctic plateau is debatable (Nicolas et al., 2011). It is therefore prudent to choose several reanalyses to represent a "best estimate" rather than selecting a particular reanalysis dataset as the precipitation benchmark.

For this work, we assess the precipitation and SAT of the historical CMIP5 model runs from 1979 to 2005. We assessed the historical record simulated by 49 CMIP5 models and compare the output with the four reanalysis datasets: ERA-Interim, MERRA, CFSR, and JRA-55.

3.2.2 Data

Monthly mean precipitation of historical experiment (1979–2005, 27 years) for the CMIP5 AOGCM were downloaded from the PCMDI website (http://cmip-pcmdi.llnl.gov/cmip5/). The list of models used for this work is tabulated in Table 3.2. These models were forced by observed changes in GHG, ozone concentrations, aerosols and solar variability (Turner et al., 2013). All the data were used at their original resolution to obtain the unaltered results from the models. For the calculation of multi-model mean (MMM), the models were interpolated onto a common 2.5° × 2.5° longitude-latitude horizontal grid before performing the analysis. For models with more than one ensemble

member, the model output is the mean of the ensemble members. For the reanalysis datasets, we downloaded the MERRA, CFSR, JRA-55, and ERA-Interim from the NCAR and ECMWF website. The area of study covers 90°S- 60°S, including the landmass and the Southern Ocean.

3.3 Future precipitation and surface air temperature in Antarctica simulated by CMIP5 models.

3.3.1 Introduction

Precipitation dataset in the CMIP5 models includes precipitation in both solid and liquid phases that falls on to the surface, and from all types of clouds (both large-scale and convective). Studies on CMIP5 models have shown that the models have generally improved over the previous CMIP3 (Flato et al., 2013). Unlike older versions of CMIP models, i.e. CMIP3 and CMIP1 (Lambert et al., 2001), CMIP5 models include two core experiments aimed at investigating the projection of climate change in the 21st century. These core experiments are based on two RCP: RCP 4.5 and RCP 8.5. The RCPs are named after the specific concentration of GHG that they represent, for instance, the RCP 4.5 is named after GHG concentration of +4.5 Wm^{-2} by year 2100, and that global annual GHG emissions peak around 2040 at +4.5 Wm^{-2}, followed by a stabilization in GHG concentration. The RCP 8.5, on the other hand, assumes the GHG concentration continue to increase throughout the twenty-first century and reaching +8.5Wm^{-2} by the year 2100 (Moss et al., 2010). There are two addition RCP experiments i.e. the RCP 2.6 and RCP 6.0, which are known as tier-one experiments (Taylor et al., 2012).

For Antarctica, variability of precipitation will affect the SMB and consequently the Antarctic ice sheet and global sea level. Antarctic precipitation is expected by the CMIP5 models to increase as the global climate warms (Pachauri et al., 2014). The study of CMIP5 RCP experiments have been conducted by various authors for different regions

of the world (Eyring et al., 2013; Palerme et al., 2017b). However, the literature on precipitation RCP projections in Antarctica is relatively scarce. Wu and Polvani (2015) used 24 CMIP5 models to study the short- and long-term projections (RCP 2.6 and RCP 8.5) of summer precipitation in the southern hemisphere subtropics. The work showed that over the next five decades, there is no significant change in summer precipitation trends. The author attributed the insignificant trend to be the result of recovering ozone layer, specifically the ozone hole, over the southern hemisphere (Wu et al., 2015). Palerme (2017) used 40 CMIP5 models alongside the ERA-Interim reanalysis data and CloudSat satellite precipitation data to investigate the historical (1986-2005) and projected (2006-2099) Antarctic precipitation and temperature under four RCP scenarios. The work suggested that for precipitation amount, the mean Antarctic precipitation increment varied from 7.4 % (RCP 2.6) to 29.3% (RCP 8.5). The study also suggested that the precipitation in the interior is larger than at the coastal regions. As for temperature, the CMIP5 models predicted an increase from 1.0 ^{o}C to 3.9 ^{o}C for RCP 2.6 ad RCP 8.5, respectively (Palerme et al., 2017b). Little et al. (2016) used 19 CMIP5 models to investigate circum-Antarctic temperature biases and warming projections under the RCP 2.6 and RCP 8.5. The study revealed that across the ensemble there is a strong, RCP-independent, correlation between Weddell Sea and Ross Sea warming (Little et al., 2016).

Some of these works, however, are not continental-wide study, or do not focus on precipitation and SAT. In addition, there is no in-depth studies on the time series and spatial trend of precipitation and temperature, which is essential for identifying how the variability of temperature and precipitation would behave in different regions in Antarctica. Moreover, these works used limited numbers of CMIP5 models output due to model availability at the time of writing. It is also important to study the relationship between SAT and precipitation.

The aim of this work is to assess and quantify projected precipitation and SAT trends in Antarctica in the 21st century (year 2006-2100) that would result under four different scenarios: RCP 2.6, RCP 4.5, RCP 6.0 and RCP 8.5.

3.3.2 Data

Monthly mean precipitation of the four RCPs experiments (2006-2100, 95 years) from the CMIP5 were obtained from the PCMDI website (http://cmip-pcmdi.llnl.gov/cmip5/). It should be noted that the not all CMIP5 models have the complete set of RCP 2.6, RCP 4.5, RCP 6.0 and RCP 8.5 experiments. At the time of writing, 43 CMIP5 models have the RCP 8.5 and RCP 4.5 experiment for precipitation, followed by 29 models that have RCP 2.6, and 20 for RCP 6.0. For SAT, 43 models have the RCP 4.5, 42 models have RCP 8.5, 29 models have RCP 2.6, and 21 models have RCP 6.0. This discrepancy is due to the fact that unlike the RCP 4.5 and RCP 8.5, the RCP 2.6 and RCP 6.0 are not considered as part of the core experiments in the CMIP5 (Taylor et al., 2012). The complete list of models with the RCPs experiments are listed in Table 3.1, while the modeling details of all the CMIP5 models used in this work is tabulated in Table 3.2. The models were forced by changes in GHG under the four RCP scenarios, changing ozone concentrations following anticipated ozone recovery, aerosols and solar variability. The models' output were retained in the original resolution in order to obtain pristine results. One of the metrics that will be used extensively in this work is the MMM calculated from the mean of all the CMIP5 models. Research have shown that when compared with observational data, the MMM often report a lower root mean square error (RMSE) than most, if not all, individual models (Lambert et al., 2001). For the calculation of spatial MMM results, the models were interpolated onto a common $2.5^{o} \times 2.5^{o}$ longitude-latitude horizontal grid prior to data analysis process. For models that contain several ensemble members, the mean of the ensemble members will be calculated to be the model output.

Table 3.1 List of CMIP5 models with RCP 2.6, RCP 4.5, RCP 6.0 and RCP 8.5

Model	200601-210012			
	RCP2.6	**RCP4.5**	**RCP6.0**	**RCP8.5**
ACCESS1-0		✓*		✓*
ACCESS1-3		✓*		✓*
BCC-CSM-1-1	✓*	✓*	✓*	✓*
BCC-CSM-1-1-m	✓*	✓*	✓*	✓*
BNU-ESM	✓*	✓*		✓*
CanCM4		✓*		
CanESM2	✓*	✓*		✓*
CCSM4	✓*	✓*	✓*	✓*
CESM1-BGC		✓*		✓*
CESM1-CAM5	✓*	✓*	✓*	✓*
CESM1-WACCM	✓*	✓*		✓*
CMCC-CESM				✓*
CMCC-CM		✓*		✓*
CMCC-CMS		✓*		✓*
CNRM-CM5	✓*	✓*		✓*
CSIRO-MK3-6-0	✓*	✓*	✓*	✓*
EC-EARTH	✓*	✓*		✓*
FGOALS-g2	✓*	✓*		✓*
FGOALS-S2				✓*
FIO-ESM	✓*	✓*	✓*	✓*
GFDL-CM2p1		✓*		✓

GFDL-CM3	✓*	✓*		✓*
GFDL-ESM2G	✓*	✓*	✓*	✓*
GFDL-ESM2M	✓*	✓*	✓*	✓*
GISS-E2-H	✓*	✓*	✓*	✓*
GISS-E2-H-CC		✓*		✓*
GISS-E2-R	✓*	✓*	✓*	✓*
GISS-E2-R-CC		✓*		✓*
HadCM3		✓*		
HadGEM2-AO	✓*	✓*	✓*	✓*
HadGEM2-CC		✓*		✓*
HadGEM2-ES	✓*	✓*	✓*	✓*
INMCM4		✓*		✓*
IPSL-CM5A-LR	✓*	✓*	✓*	✓*
IPSL-CM5A-MR	✓*	✓*	✓*	✓*
IPSL-CM5B-LR		✓*		✓*
MIROC4h		✓*		
MIROC5	✓*	✓*	✓*	✓*
MIROC-ESM	✓*	✓*	✓*	✓*
MIROC-ESM-CHEM	✓*	✓*	✓*	✓*
MPI-ESM-LR	✓*	✓*		✓*
MPI-ESM-MR	✓*	✓*		✓*
MRI-ESM1				✓*
MRI-CGCM3	✓*	✓*	✓*	✓*
NorESM1-M	✓*	✓*	✓*	✓*
NorESM1-ME	✓*	✓*	✓*	✓*

Table 3.2 List of the CMIP5 models and reanalysis datasets used in this study.

Models	Institution/Organization	Resolution (longitude x latitude)	Number of ensemble	Country
ACCESS 1-0	CSIRO (Commonwealth Scientific and Industrial Research Organization, Australia), and BOM (Bureau of Meteorology, Australia)	1.25° × 1.88°	3	Australia
ACCESS 1-3	CSIRO	1.25° × 1.88°	3	Australia
BCC-CSM1-1	Beijing Climate Centre (BCC), China Meteorological Administration (CMA)	2.80° × 2.80°	3	China
BCC-CSM1-1-m	BCC, CMA	2.80° × 2.80°	3	China
BNU-ESM	College of Global Change and Earth System Science, Beijing Normal University	2.80° × 2.80°	1	China
CanCM4	Canadian Centre for Climate Modelling and Analyses (CanCM)	2.80° × 2.80°	10	Canada
CanESM2	CanCM	2.80° × 2.80°	5	Canada

CCSM4	National Centre for Atmospheric Research (NCAR)	0.90° × 1.25°	6	USA
CESM1-BGC	NCAR	0.90° × 1.25°	1	USA
CESM1-CAM5	NCAR	0.90° × 1.25°	3	USA
CESM1-FASTCHEM	NCAR	0.90° × 1.25°	3	USA
CESM1-WACCM	NCAR	1.90° × 2.50°	4	USA
CMCC-CESM	Centro Euro-Mediterraneo per I Cambiamenti Climatici (CEM-CC)	3.40° × 3.75°	1	Italy
CMCC-CM	CEM-CC	0.75° × 0.75°	1	Italy
CMCC-CMS	CEM-CC	3.70° × 3.75°	1	Italy
CNRM-CM5	Centre National de Recherches Meteorologiques (CNRM)	1.40° × 1.40°	10	France
CNRM-CM5-2	CNRM	1.40° × 1.40°	1	France
Csiro-Mk3-6-0	CSIRO and the Queensland Climate Change Centre of Excellence	1.87° × 1.88°	10	Australia
EC-EARTH	EC-Earth Consortium	1.00° × 1.00°	9	Europe
FGOALS-g2	LASG, Institute of Atmospheric Physics, Chinese Academy of Sciences	2.80° × 2.80°	5	China

FGOALS-s2	LASG, Institute of Atmospheric Physics, Chinese Academy of Sciences	1.70° × 2.80°	2	China
FIO-ESM	The First Institute of Oceanography, SOA, China	2.81° × 2.81°	3	China
GFDL-CM2p1	Geophysical Fluid Dynamics Laboratory (GFDL)	2.00° × 2.50°	10	USA
GFDL-CM3	GFDL	2.00° × 2.50°	5	USA
GFDL-ESM2G	GFDL	2.00° × 2.50°	1	USA
GFDL-ESM2M	GFDL	2.00° × 2.50°	1	USA
GISS-E2-H	NASA Goddard Institute for Space Studies (GISS)	2.00° × 2.50°	5	USA
GISS-E2-H-CC	NASA GISS	2.00° × 2.50°	1	USA
GISS-E2-R	NASA GISS	2.00° × 2.50°	6	USA
GISS-E2-R-CC	NASA GISS	2.00° × 2.50°	1	USA
HadCM3	Met Office Hadley Centre (MOHC)	2.50° × 3.75°	10	U.K
HadGEM2-AO	MOHC	1.25° × 1.88°	3	U.K
HadGEM2-CC	MOHC	1.25° × 1.88°	1	U.K
HadGEM2-ES	MOHC	1.25° × 1.88°	5	U.K
INMCM4	Institute for Numerical Mathematics	1.50° × 2.00°	1	Russia

IPSL-CM5A-LR	Institut Pierre-Simon Laplace (IPSL)	1.90° × 3.75°	6	France
IPSL-CM5A-MR	IPSL	1.30° × 2.50°	3	France
IPSL-CM5B-LR	IPSL	1.90° × 3.75°	1	France
MIROC4h	Japan Agency for Marine-Earth Science and Technology, Atmosphere and Ocean Research Institute (JAMSTEC) and National Institute for Environmental Studies (NIES)	0.56° × 0.56°	3	Japan
MIROC5	JAMSTEC and NIES	1.40° × 1.40°	5	Japan
MIROC-ESM	JAMSTEC and NIES	2.80° × 2.80°	3	Japan
MIROC-ESM-CHEM	JAMSTEC and NIES	2.80° × 2.80°	1	Japan
MPI-ESM-LR	Max Planck Institute for Meteorology (MPI-M)	1.87° × 1.88°	3	Germany
MPI-ESM-MR	MPI-M	1.87° × 1.88°	3	Germany
MPI-ESM-P	MPI-M	1.87° × 1.88°	2	Germany
MRI-CGCM3	Meteorological Research Institute (MRI)	1.00° × 1.13°	3	Japan
MRI-ESM1	MRI	1.00° × 1.13°	1	Japan

NorESM1-M	Norwegian Climate Centre (NCR)	1.90° × 2.50°	3	Norway
NorESM1-ME	NCR	1.90° × 2.50°	1	Norway
Reanalysis	Institute/Organization			
ERA-Interim	European Centre for Medium-Range Weather Forecasts	0.75° × 0.75°		Europe
CFSR	National Centers for Environmental Prediction	0.50° × 1.00°		USA
JRA-55	Japan Meteorological Agency	0.50° × 0.63°		Japan
MERRA	National Aeronautics and Space Administration	0.50° × 0.63°		USA

CHAPTER 4: RESULTS

4.1 Results for precipitation instruments comparison study

4.1.1 Precipitation measurement

Generally, the LBSs are able to detect more precipitation while the TBGs detect less precipitation. The VPF-730 was the most sensitive among the five instruments as it was able to detect more precipitation days than all other instruments: 276 precipitation days from a total of 348 observation days (henceforth denoted as 276/348); followed by the LPM (248/348), the PWS-100 (191/348), the UPG1000 (152/348) and the CS700H (60/348). The reanalyses, on the other hand, indicated no less than 310 precipitation days during the study period. The reanalyses were also quite consistent with one another, with JRA-55 indicating the most precipitation days (328 precipitation days), followed by ERA-Interim (313 precipitation days) and the CFSv2 model (312 precipitation days). An interesting observation that can be drawn from Table 4.1 is that the number of precipitation days indicated by the GPCP 1DD in autumn 2015 and winter 2015 is closer to the number detected by the precipitation instruments, while the reanalyses indicate a much higher number of precipitation days.

Table 4.1 Number of precipitation days measured by each instrument (UPG-1000, PWS-100, VPF-730, LPM, CS700H), reanalysis data sets (ERA-Interim, JRA-55), CFSv2 model and the GPCP during the study period (19 March 2015 to 4 February 2016). Note: The GPCP data were available up to 31 October 2015 at the time of writing.

	TBGs		LBS			Reanalyses		Forecast model	Satellite
	UPG-1000	CS700H	PWS-100	VPF-730	LPM	ERA-Int	JRA-55	CFSv2	GPCP
Autumn 2015	40	24	43	55	53	68	71	66	53
Winter 2015	33	6	51	74	61	84	81	78	49
Spring 2015	44	19	57	82	74	85	89	85	44
Summer 2015/16	35	11	40	65	60	76	87	83	NA[a]
Total	152	60	191	276	248	313	328	312	146

[a] Not available.

The LPM registered the highest mean daily precipitation during the study period (mean = 5.76 mm, σ [standard deviation] = 14.59 mm), followed by the PWS-100 (mean = 5.72 mm, σ = 17.18 mm), the VPF-730 (mean = 5.10 mm, σ = 11.60 mm), the UPG-1000 (mean = 2.29 mm, σ = 6.36 mm) and the CS700H (mean = 0.459 mm, σ = 15.27 mm). The JRA-55 had the highest mean daily precipitation at 13.75 mm, followed by CFSv2 (6.30 mm) and ERA-Interim (3.97 mm). The GPCP 1DD mean daily precipitation (2.27 mm) and standard deviation (3.17 mm) were closer to the instruments than to the

reanalyses. It is important to note that the daily mean precipitation amount of the GPCP 1DD and reanalyses are not comparable to the reading from the instruments on account of their coarse resolution, as will be shown later in the monthly and seasonal precipitation section. The precipitation readings from the GPCP 1DD and the reanalyses are more suitable to be compared on a longer time-scale. A t-test showed that the differences in mean daily precipitation were insignificant between the LBS instruments. This means that the different LBSs produced results with very minor differences among themselves. In contrast, there were significant differences among the TBGs and among the reanalyses. The GPCP 1DD precipitation was significantly lower than all the data sets ($p < 0.05$), with the sole exception of UPG-1000 ($p = 0.69$).

Figure 4.1 shows the monthly precipitation derived from the five precipitation instruments, the reanalyses and the GPCP 1DD (for which the data stop at October 2015). One important observation from Figure 4.1 is the high precipitation amount registered by the PWS-100 in August 2015 due to the extreme precipitation on 4–6 August 2015. The details of this extreme event will be discussed in the case studies and discussion sections. Among the instruments, the LPM had the highest mean monthly precipitation (154.94 mm), followed by the PWS-100 (153.9 mm), the VPF-730 (137.33 mm), the UPG-1000 (61.68 mm) and the CS700H (12.37 mm).

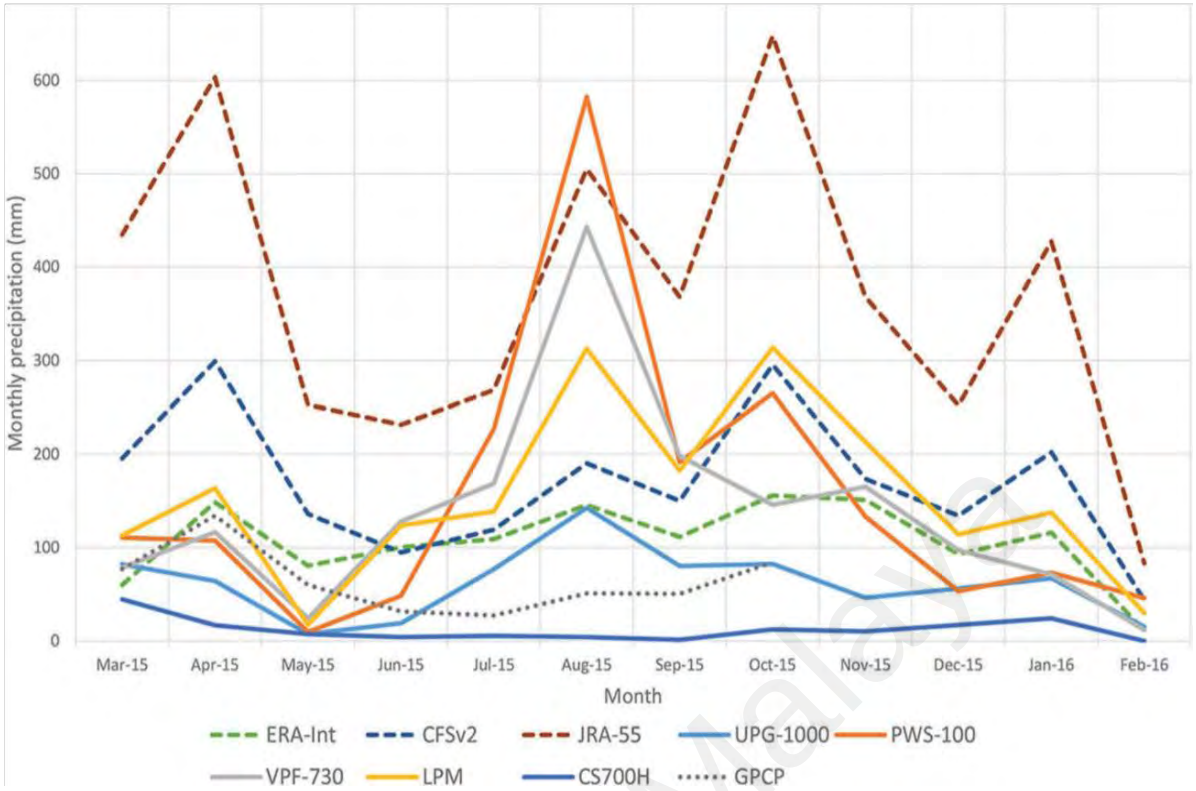

Figure 4.1 Monthly precipitation for all the precipitation instruments, reanalyses, model and the GPCP 1DD. Supplementary information available in table format in Appendix section (Supplementary 1).

Maximum precipitation occurred in the months of August (winter 2015) and October (spring 2015), while minimum precipitation occurred in the month of May (autumn 2015). ERA-Interim and CFSv2 produced results that match closely with the instrumental precipitation measurement. JRA-55, however, showed a much higher precipitation compared to the other reanalysis and precipitation instruments (except for August). JRA-55 also yielded the highest monthly mean precipitation (370.10 mm), followed by CFSv2 (169.45 mm) and ERA-Interim (106.82 mm). The mean monthly precipitation for the GPCP 1DD was 64.51 mm, which was closer to the measurements made by the instruments.

The resolution of the reanalysis data sets and the GPCP 1DD played a large role in the readings. For the reanalyses, the coarse resolution did not capture the complicated terrain

of the Antarctic Peninsula surrounding Rothera, especially the high elevation on Adelaide Island, and therefore did not accurately replicate the orographic effect. For the GPCP 1DD, as with all merged-satellite precipitation products, the inherent difficulty of converting sparse satellite data into meaningful precipitation estimates confined in a high-resolution grid is caused by several factors. The geostationary IR detector senses the changes of clouds rather than precipitation itself, and surface precipitation is determined indirectly through the measurement of brightness temperature via microwave and infrared satellite. These proxies of precipitation are then fed into an algorithm that includes cloud-reflected energy from radar and sparse, in situ direct gauge measurements to produce the final GPCP precipitation estimate (Huffman et al., 1997). Moreover, satellite products employed in the GPCP algorithm tend to miss light precipitation events (Behrangi et al., 2012; Behrangi et al., 2014).

A correlation study was used to determine the similarity in terms of temporal pattern between two sets of data. It is important to note that a significant correlation shows that two data sets have a degree of similarity in terms of data pattern and trend, but are not necessarily similar in terms of magnitude or precipitation amount. A correlation index (shown in Table 4.2) shows how consistent two data sets are with one another, and therefore whether they are useful for the purpose of validation. The correlation indices between the monthly precipitation logged by the instruments, reanalyses and the GPCP 1DD are tabulated in Table 4.2. Table 4.2 shows that all the reanalyses have more than + 0.50 correlation with at least one of the precipitation instruments. From another perspective, it is clear that with the exception of the CS700H, the instruments show correlation indices over + 0.60 with at least one reanalysis. JRA-55, for instance, has a + 0.6491 correlation with the UPG-1000 and + 0.4880 correlation with the PWS-100. The GPCP 1DD has high correlation with reanalysis JRA-55 (+0.7637) and model CFSv2 (+0.8811), while having correlation less than + 0.50 with the precipitation instruments.

Table 4.2 Correlation table for the precipitation measured by the precipitation instruments (UPG-1000, PWS-100, VPF-730, LPM, CS700H), reanalysis data sets (ERA-Interim, JRA-55), CFSv2 model and GPCP. Numbers in boldface are values that are significant α = 95% (p≤ 0.05)

	UPG-1000	PWS-100	VPF-730	LPM	CS700H	ERA-Int	CFSv2	JRA-55	GPCP
UPG-1000	1.00	0.87	0.81	0.78	0.19	0.52	0.50	0.65	0.056
PWS-100		1.00	0.94	0.80	−0.21	0.51	0.30	0.49	−0.15
VPF-730			1.00	0.78	−0.28	0.59	0.22	0.41	−0.25
LPM				1.00	−0.066	0.81	0.62	0.76	0.12
CS700H					1.00	−0.066	0.42	0.36	0.45
ERA-Int						1.00	0.72	0.76	0.35
CFSv2							1.00	0.97	0.88
JRA-55								1.00	0.76
GPCP									1.00

4.1.2 Seasonal variation

All instruments, except the CS700H, and reanalyses show that spring (September–November) 2015 had the most precipitation days, while the day with the least precipitation was evenly distributed between winter (June–August) 2015 and autumn (March–May) 2015 (Figure 4.1).

However, Figure 4.2 shows that the precipitation amount for winter exceeded that of spring. Precipitation seasonal means and standard deviations are tabulated in Table 4.3. The seasonal mean precipitation measured by the VPF-730 and the PWS-100 were closest to the value obtained from ERA-Interim for autumn 2015, spring 2015 and summer 2015/16. The GPCP 1DD, on the other hand, was closest to precipitation values obtained from the UPG-1000 in winter 2015 and spring 2015. The LPM and the PWS-100 yielded

extremely high precipitation readings, resulting in high precipitation means and standard deviations. These anomalies will be further discussed in a later section.

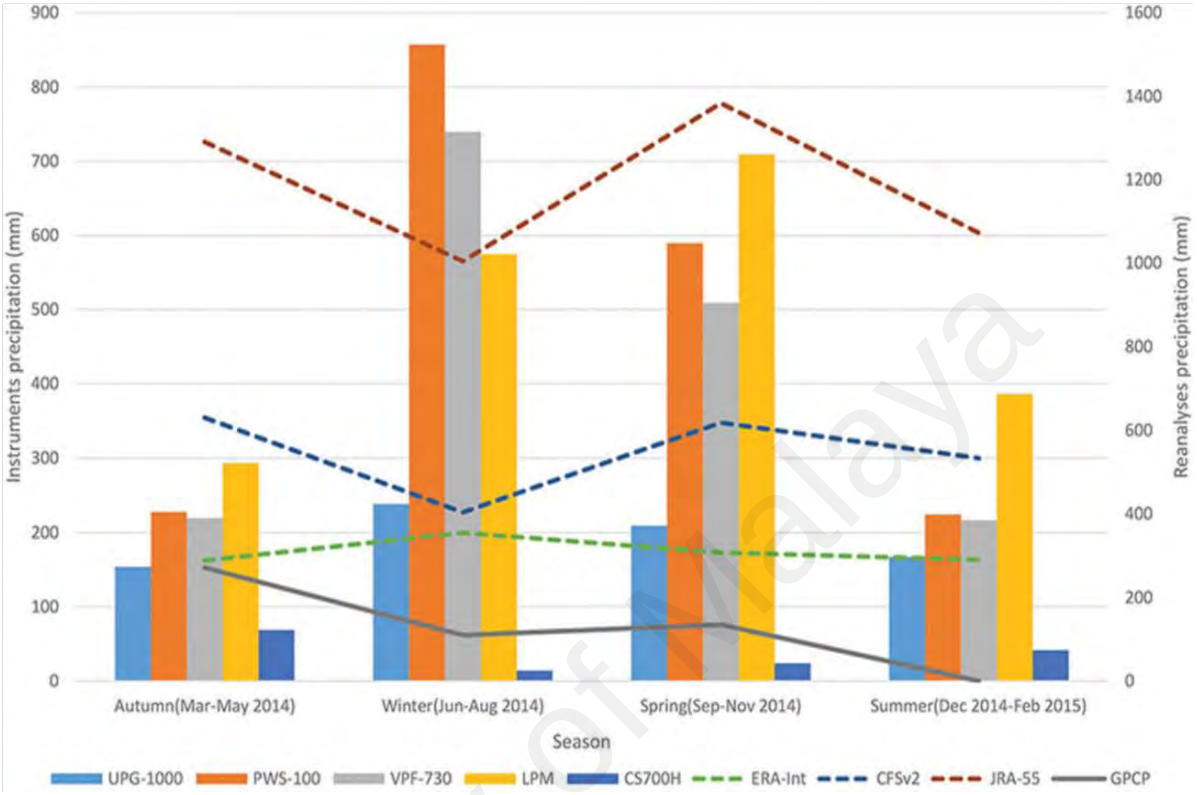

Figure 4.2 Seasonal precipitation for the precipitation instruments, reanalysis data sets and model.

Table 4.3 Mean and standard deviation of precipitation for autumn, winter, spring and summer.

		Autumn		Winter		Spring		Summer	
		Mean (mm)	Standard deviation (mm)	Mean (mm)	Standard deviation (mm)	Mean (mm)	Standard deviation (mm)	Mean (mm)	Standard deviation (mm)
TBGs	UPG-1000	2.08	6.83	2.59	8.06	2.30	5.38	1.84	4.60
	CS700H	0.93	4.00	0.15	0.63	0.264	0.896	0.63	2.37

LBS	VPF-730	3.00	7.00	8.04	15.84	5.59	12.19	2.38	4.97
	PWS-100	3.08	7.51	9.42	26.75	6.48	15.12	2.47	6.76
	LPM	4.14	8.83	6.61	16.98	8.06	18.84	4.25	9.59
Reanalyses	JRA-55	17.44	21.63	10.92	16.63	15.20	19.02	11.79	14.09
	ERA-INT	3.90	4.42	3.86	5.22	4.60	4.82	3.19	4.75
Forecast model	CFSv2	8.52	9.05	4.39	5.82	6.80	6.88	5.87	6.54
Satellite	GPCP	3.67	4.27	1.19	1.87	2.21	2.48	--	--

4.1.3 Case studies

To gain a better understanding of the operation of the different instruments and the environmental factors that affect precipitation measurement, the case studies of precipitation measurement presented below compare the precipitation measurements from the different instruments and reanalyses against wind speed and temperature data obtained from an automated weather station at Rothera. For the case studies, periods with strong wind and precipitation days were chosen: 19 March 2015 to 5 April 2015; 27 July 2015 to 18 August 2015; and 21 December 2015 to 5 January 2016.

4.1.3.1 19 March 2015 to 6 April 2015

This period was chosen because all the instruments were active and performing at their best. Figure 4.3 shows the daily mean temperature, daily mean wind speed and daily precipitation from 19 March 2015 to 6 April 2015. As expected, all readings from the instruments were positively correlated with one another (> + 0.80) and with those from the reanalyses (> + 0.70). The GPCP 1DD had a correlation ranging from + 0.4328 to + 0.6127 with the precipitation instruments and reanalyses. More interestingly, all the

precipitation data sets were positively correlated (ranging from + 0.4844 to + 0.7078) with the daily wind speed, and slightly less positively correlated (ranging from + 0.2942 to + 0.5060) with daily temperature. This shows that wind fluctuations had an important effect on the amount of precipitation measured. The instruments' precipitation measurements on 21 March 2015, 29–30 March 2015 and 5 April 2015 were much lower compared to those of the reanalyses.

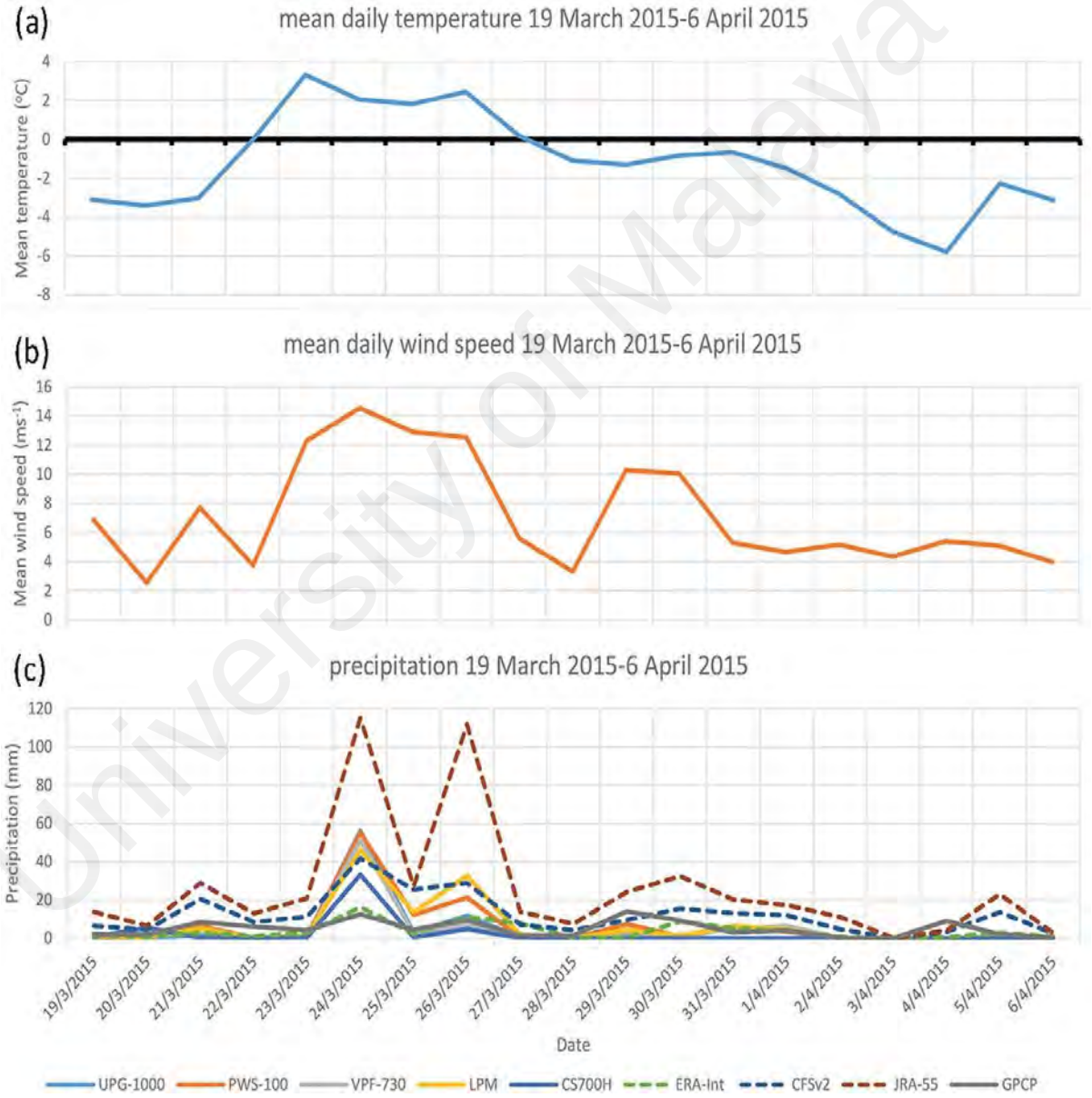

Figure 4.3 (a) Daily temperature, (b) mean wind speed and (c) daily precipitation at Rothera 19 March 2015 to 6 April 2015. The wind and temperature data were obtained via automated sensors connected to a CR1000 data logger at Rothera.

The wind speed on 24 March 2015 exceeded 12 ms^{-1}. In spite of the strong wind, the TBGs captured significant amounts of precipitation (up to 56.0 mm and 33.2 mm for the UPG-1000 and the CS700H, respectively) – higher values than the precipitation measured by ERA-Interim (16.1 mm). JRA-55 registered close to 120.0 mm of precipitation on 24 March 2015, which was more than seven times higher than the ERA-Interim precipitation readings. It is worth noting that precipitation is the result of the interaction between various meteorological parameters – including wind, pressure, temperature, and cyclone activity – and temperature is only a contributing factor in this complex cycle. Simple correlations between temperature and precipitation alone may not be sufficient to present the complexity of the entire precipitation cycle.

4.1.3.2 27 July 2015 to 18 August 2015

These dates were chosen because of the precipitation days and a strong wind event from 4 to 6 August 2015. Similar to the previous case study, the precipitation measurements were positively correlated with both temperature (ranging from + 0.4144 to + 0.5272) and wind speed (ranging from + 0.6060 to + 0.8110), with the sole exception of the LPM. The reading for the LPM during this period was removed because of a blockage to the instrument's laser head. Also similar to the previous case study, the CFSv2 had a positive correlation (+ 0.8264) with wind speed. The reanalyses data sets showed high amounts of precipitation while the actual instruments registered only very small amounts of precipitation. For this period, the GPCP 1DD was positively correlated with the UPG-1000 (+ 0.7061), the PWS-100 (+ 0.7657), the VPF-730 (+ 0.8504), the CFSv2 (+ 0.7234) and the JRA-55 (+ 0.7092).

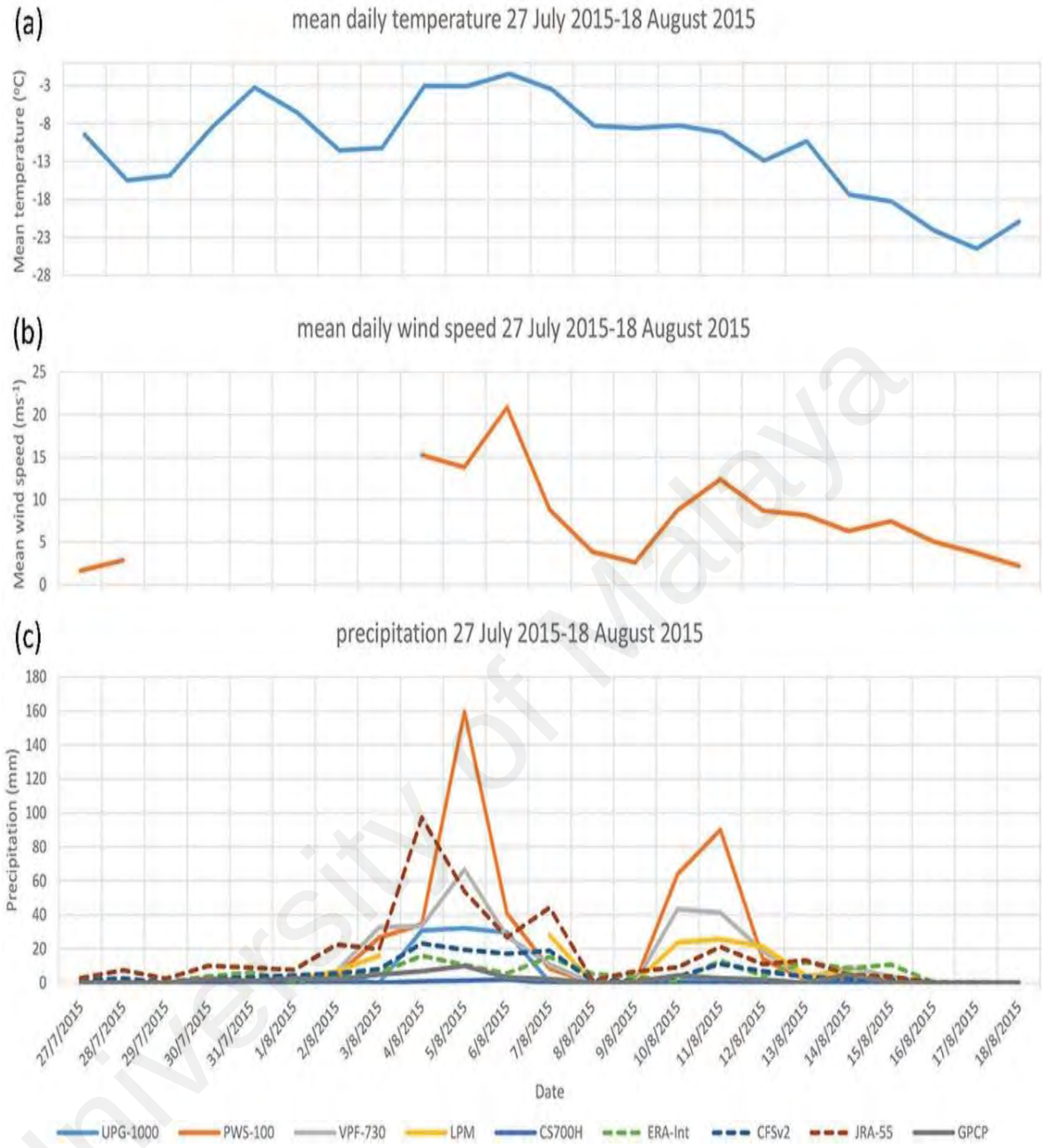

Figure 4.4 (a) Daily temperature, (b) mean wind speed and (c) daily precipitation at Rothera 27 July 2015 to 18 August 2015. The wind and temperature data were obtained via automated sensors connected to a CR1000 data logger at Rothera.

As can be seen in Figure 4.4, there were three strong wind episodes from 4 to 6 August 2015. Three of five instruments detected the most precipitation on 5 August, whereas the reanalyses registered the most precipitation on 4 August, and again on 7 August, when all

the instruments registered low precipitation. The strong wind events on 4–6 and 10–11 August caused the LBSs to report high precipitation readings. As mentioned above, the LPM laser's head was blocked by snow on 4–6 August, causing the reading to become exceedingly high (over 1000 mm). Comparing the instruments' results revealed the inconsistency of the LPM reading, confirming the existence of error. For the 10–11 August case, the LPM was fully functional but did not indicate any precipitation, while the readings registered by the PWS-100 and the VPF-730 were high. It should be noted that the CS700H was malfunctioned during this period and failed to deliver reliable readings.

4.1.3.3 21 December 2015 to 5 January 2016

For this period, temperature was positively correlated with the instruments (up to + 0.5550) and the reanalyses (+ 0.4951 to + 5562). Wind speed, on the other hand, had a low correlation with the reanalyses and model (ERA-Interim: + 0.3538; CFSv2: + 0.2019; JRA-55: + 0.1554). An important observation that can be drawn from Figure 4.5 is the precipitation measurement by the VPF-730 on 23–24 December 2015, which happened on two relatively warm, windy days when all other instruments registered no precipitation readings.

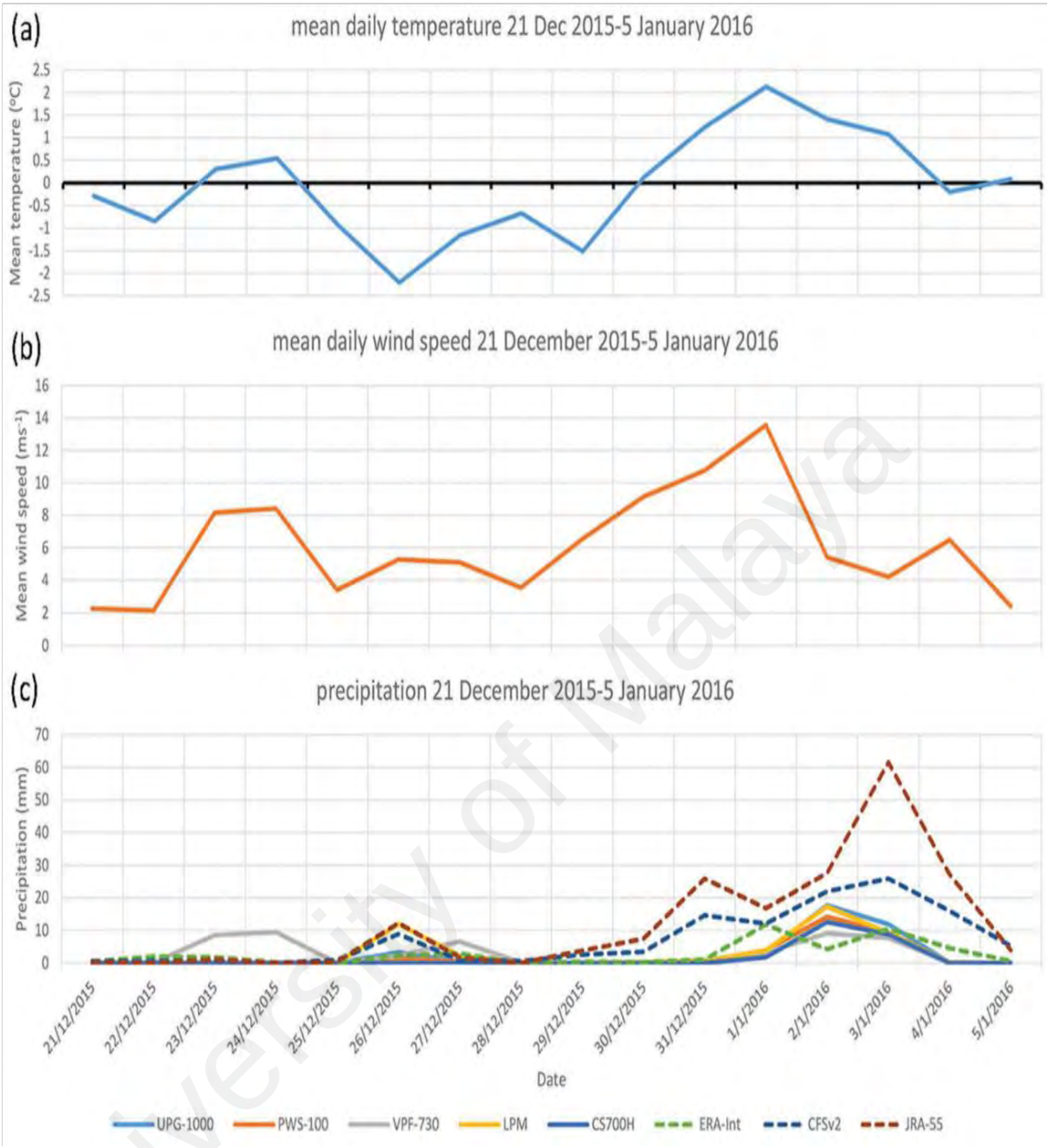

Figure 4.5 (a) Daily temperature, (b) mean wind speed and (c) daily precipitation at Rothera 21 December 2015 to 5 January 2016. The wind and temperature data were obtained via automated sensors connected to a CR1000 data logger at Rothera.

Another interesting observation of the influence of wind on the reanalyses can be seen during the 28 December 2015 to 4 January 2016 period: all the instruments showed an increase in precipitation from 1 to 3 January 2016, with the most precipitation measured on 2 January 2016. The two reanalyses, on the other hand, showed different precipitation

patterns. The precipitation of the reanalyses increased with increasing wind speed, especially during the period 29 December 2015 to 1 January 2016 (Figure 4.5). The different reanalyses registered peak precipitation on different days: the ERA-Interim peak precipitation occurred on 30 December, while the JRA-55 and CFSv2 peak precipitation occurred on 3 January. ERA-Interim is widely considered to be the most accurate reanalysis for studying precipitation in the Antarctic. However, while all the in situ instruments in our study showed consistent results on 2 January 2016, the ERA-Interim suggested a different picture. This could be due to the fact that the instruments produce point measurements while ERA-Interim shows a mean of a wider area.

4.2 Results for an assessment of CMIP5 historical precipitation and SAT

4.2.1 Precipitation

4.2.1.1 Time series of area average for 60°S -90°S

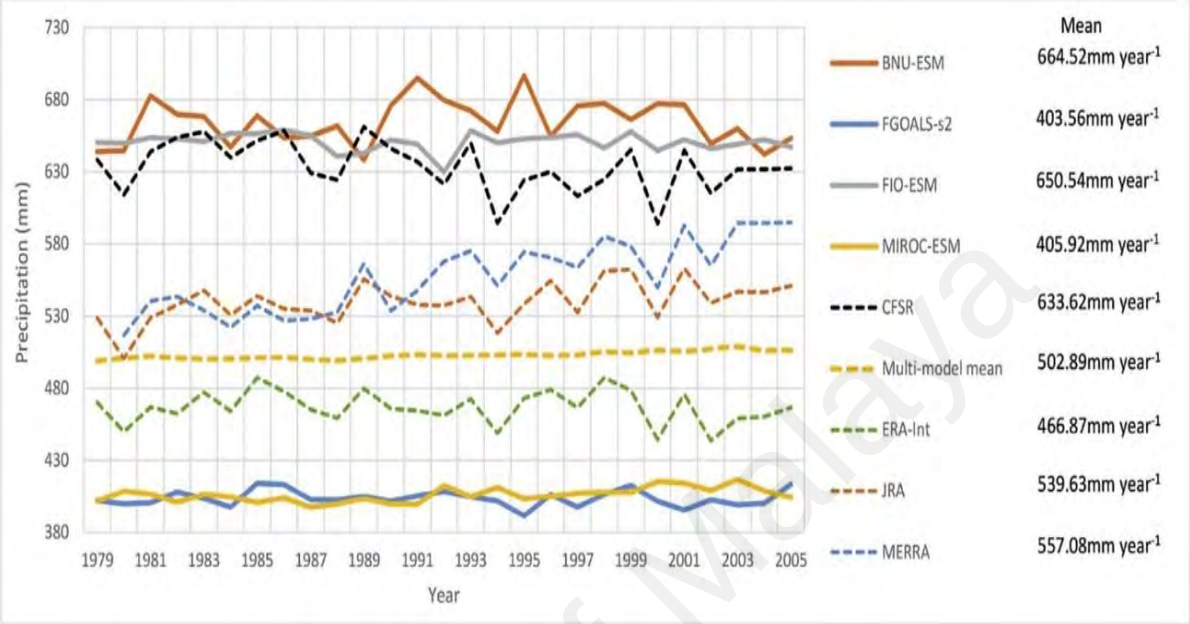

Figure 4.6 Time series of annual precipitation 1979-2005 (mm year^{-1}) for 60°S - 90°S

Figure 4.6 shows the precipitation time series from 1979 to 2005. The four reanalyses are able to show a common precipitation temporal pattern—although there is a significant difference in precipitation amount—especially from 1987 onward. The CFSR mean precipitation amount (633.60 mm year^{-1}, standard deviation, σ = 17.80 mm) is significantly higher than the other three reanalyses. The ERA-Interim, widely considered to be the most accurate reanalysis dataset available for Antarctic precipitation (Bromwich et al., 2011; Nicolas et al., 2011; Palerme et al., 2017a; Palerme et al., 2017b), is lowest among the reanalyses in terms of mean precipitation amount (466.90 mm year^{-1}, σ = 11.68 mm). The mean precipitation of JRA-55 is 539.60 mm year^{-1} (σ = 13.96 mm) and MERRA 557.10 mm year^{-1} (σ = 24.63 mm). The correlation between the four reanalysis data is widely varied and is tabulated in Table 4.4.

Table 4.4 Correlation coefficient for between the reanalysis datasets and the CMIP5 MMM.

Correlation	ERA-Interim	CFSR	JRA-55	MERRA	MMM
ERA-Interim	1.00	0.69[a]	0.65[a]	0.17	−0.26
CFSR		1.00	0.47[a]	−0.08	−0.36
JRA-55			1.00	0.67[a]	0.38[a]
MERRA				1.00	0.77[a]
MMM					1.00

[a] Significant at 95% confidence level

The four reanalyses also show different precipitation trend from 1979 to 2005, with the MERRA and JRA-55 showing a significant increasing precipitation trend (+2.76 ± 0.76 mm year^{-1}, 0.90 ± 0.62 mm year^{-1}, respectively) while the ERA-Interim (+0.20 ± 0.60 mm year^{-1}) and CFSR (+0.84 ± 0.86 mm year^{-1}) both showing insignificant trend. The insignificant trend for ERA-Interim is in agreement with the results from earlier authors such as (Palerme et al., 2017a) and (Oshima et al., 2017). For MERRA, the introduction of Advanced Microwave Sounding Unit in late 1998 and 2001 has resulted in a two-step upward shift in precipitation estimate (Nicolas et al., 2011). The large differences in precipitation amount and trend among the reanalyses make it difficult to select a particular set of reanalysis as the precipitation standard.

The annual mean precipitation for the CMIP5 models range from 403.6 mm year^{-1} (FGOALS-s2, σ = 5.53 mm) to 664.50 mm year^{-1} (BNU-ESM, σ = 15.72 mm) (Figure 4.6), while the CMIP5 MMM has a mean precipitation of 502.90 mm year^{-1} (σ = 2.60 mm). This is in contrast to the report by (Palerme et al., 2017b), whose work shows that

on the continent, the CSIRO model has the lowest mean precipitation rate while the GISS-E2-H has the highest precipitation rate. There are nine models that project precipitation amount lower than the four reanalyses (refer Supplementary 2), while only two models that show more precipitation amount compared to the CFSR. There are several models that fall within the multimodel mean standard deviation, which is an estimation of intrinsic variability (Marshall et al., 2015). However, 38 of the total 49 CMIP5 models (77.6%) are within the reanalyses precipitation range.

As for the precipitation trend, the regression analysis on the trend shows that 37 models have increasing precipitation trend from 1979 to 2005, 18 of which are significant ($p \leq .05$), while 12 models show a decreasing trend. Among the CMIP5 models, the model that shows the largest positive trend is GFDL-CM2p1 ($+1.03 \pm 0.16$ mm year^{-1}). The trends of the CMIP5 models are shown in Figure 4.7. The resulting MMM has a significant increasing precipitation trend of $+0.29 \pm 0.06$ mm year^{-1} or 2.90 ± 0.61 mm decade^{-1}. The lower boundary of this value is comparable to the value reported by (Palerme et al., 2017b) (+2.30 mm decade^{-1}), but significantly larger than the value given by (Monaghan et al., 2006)(+1.90 mm decade^{-1} from 1955 to 2004). Nonetheless, the value of precipitation trend may fluctuate between 0.19 and 0.23 mm year^{-1} depending on the length of study period and the number of CMIP5 models involved. It should also be noted that the t-value from the regression analysis is dependent on the standard error of the trend which, in the case of MMM, is a very small value, resulting in a significant result. Apart from that, this MMM is the mean calculated from 49 CMIP5 models; at least 9 models more than those used in the work of other researchers, and hence the effect of smoothing could be even more apparent. Based on a report by Fyfe et al. (2012), the CMIP5 mean precipitation shows a positive trend starting from the 1960s and flattening in the 2000s (Fyfe et al., 2012). The flattening of the precipitation trend in the 2000s

coincides with the reduction in ozone-depleting substances (Salby et al., 2012). However, the continual increase of GHG is expected to offset the effect of ozone recovery.

One important observation in Figure 4.6 is the spike of precipitation shown by the CFSR reanalysis at the end of 1998, early 1999. This sudden surge of precipitation is caused by the incorporation of Advanced TIROS Operation Vertical Sounder observation system data following the launch of the NOAA-15 satellite into the CFSR reanalysis in 1998 (Zhang et al., 2012). Another important observation is the divergence of MERRA and JRA-55 precipitation trend in the year 1990–1991, when the MERRA reanalysis experience a significant increase in precipitation amount. This increase coincides with the introduction of SSM/I F-10 observation system into the MERRA in December 1990 (Rienecker et al., 2011).

4.2.1.2 Seasonal variation of precipitation

The reanalyses are able to simulate the seasonal precipitation of Antarctic fairly well, as shown in Figure 4.8. All the reanalyses have a high correlation with one another (> +0.98), with the exception of MERRA, which shows a slightly different precipitation curve especially during the winter–spring (June–November) seasons. For the reanalyses, the maximum precipitation is observed during autumn (March-April-May, range from CFSR, 57.62 mm to ERA-Interim, 44.22 mm) while summer (December-January-February) receives the least precipitation (CFSR, 44.93 mm; ERA-Interim, 32.77 mm). Three of the four reanalyses show more precipitation amount compared to MMM (Figure 4.8(b)). Similar to Figure 4.6, there are several CMIP5 models that underestimate (eight models) (refer Supplementary 3) and overestimate (two models) the seasonal precipitation amount. There are three models that receive peak precipitation in May (HadGEM2-CC, HadGEM2-ES, HadCM3) instead of April, and five models that receive highest precipitation in March (CCSM4, CESM1-BGC, CESM1-CAM5, GISS-E2-R,

GISS-E2-RCC). The FIO-ESM lacks the decrease that appears in the month of June, one that was visibly captured by other CMIP5 models (refer Supplementary 3). As a result, these four CMIP5 models have the lowest correlation (ranging from +0.70 to +0.88) with the four reanalyses, while the other 45 CMIP5 models have correlation > +0.90 with the reanalyses. The resultant MMM also has a high correlation (> 0.98) with the four reanalyses.

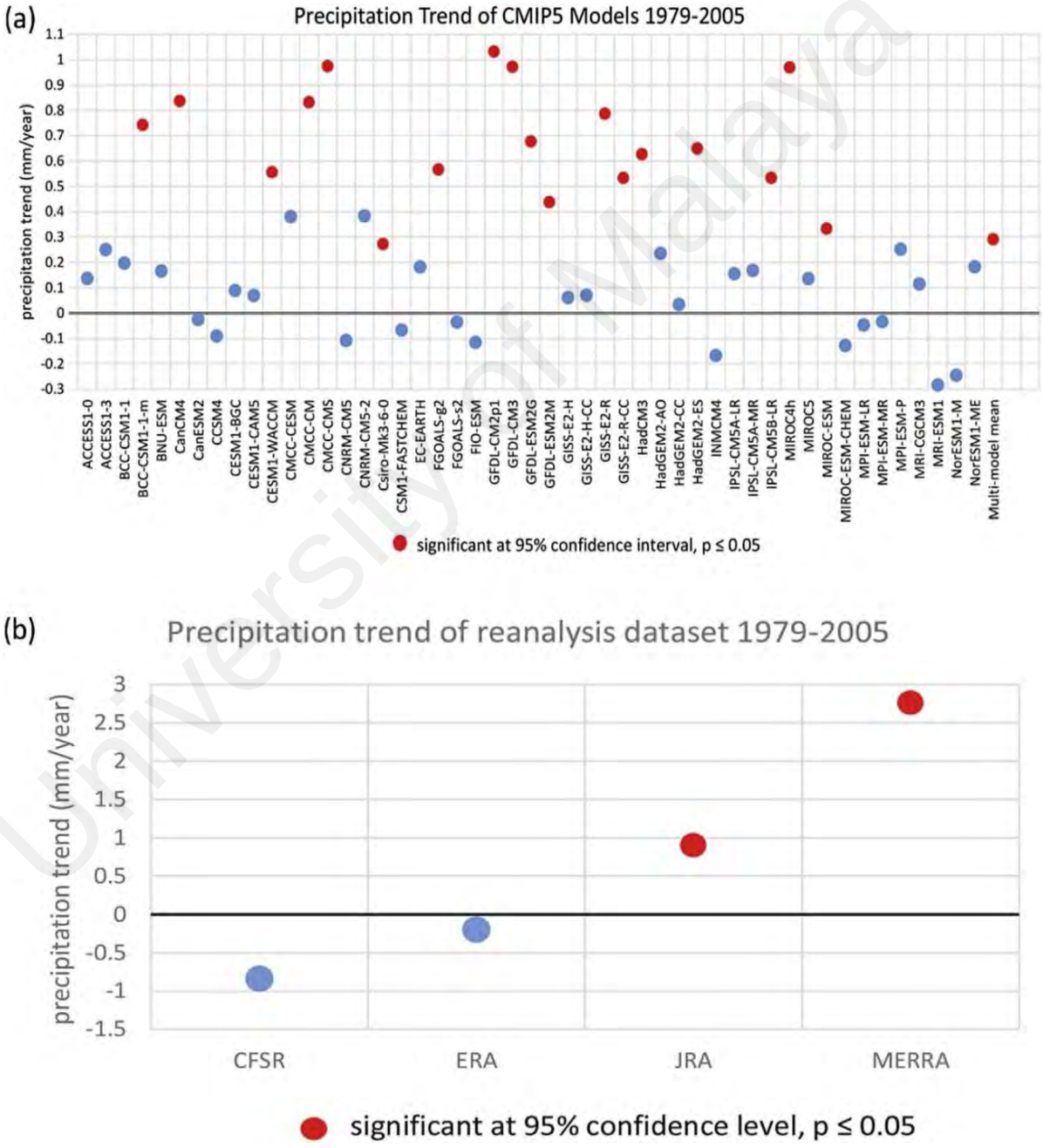

Figure 4.7 Trend of CMIP5 models, CMIP5 MMM and reanalysis datasets.

4.2.1.3 Spatial trend of precipitation

One of the most consistent observation that can be derived from the four reanalyses in Figure 4.9 is the decreasing precipitation trend (up to −0.40 mm year^{-1}) at the coast of George Land-Adélie Land (66°S, 136°E) and Enderby Land (67°S, 44°E). Apart from that, the analyses also show significant increasing precipitation trend (0.30–0.50 mm year^{-1}) ($p < .05$) at the Wilkes Land (66°S, 110°E) and Weddell Sea (71°S, 45°W). The CFSR, as a whole, shows much wider range of decreasing precipitation especially in the Bellingshausen Sea (71°S, 85°W) and the Ross Sea (74.5°S, 166°W), while the MERRA reanalysis shows that a large swath of the Southern Ocean has been experiencing increasing precipitation from 1979 to 2005. Most of the precipitation increase occurs in the peripheral regions of the continent (range from +0.10 mm year^{-1} to +0.50 mm year^{-1}) with the interior experiencing little to no significant precipitation change (up to +0.05 mm year^{-1}). This result is consistent with the result published by Nicolas and Bromwich (2011), which shows that MERRA has a positive and highly significant trend over the whole Southern Ocean poleward of 40°S, while the trends are small and insignificant in ERA-Interim and CFSR (Nicolas et al., 2011).

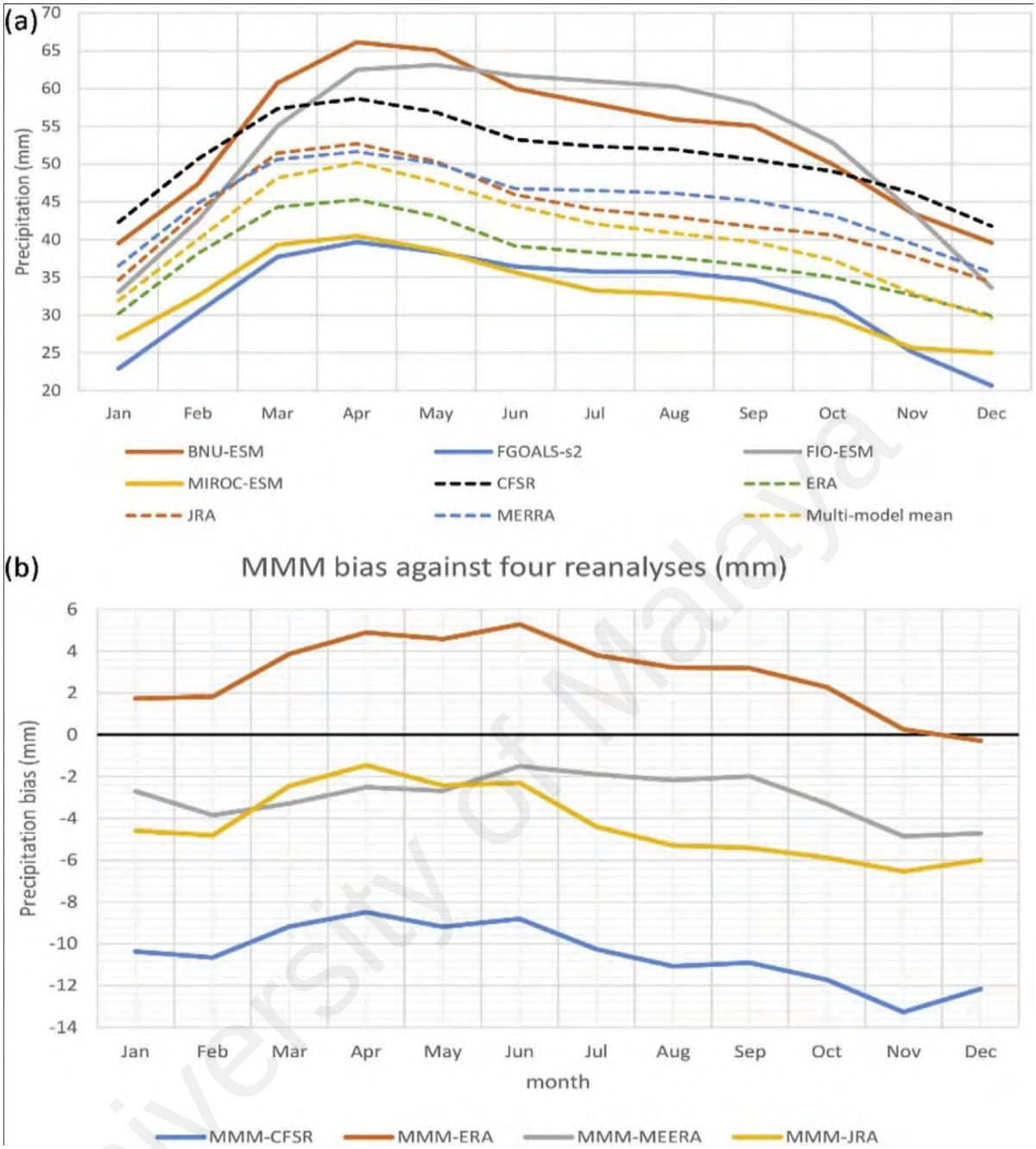

Figure 4.8 (a) Seasonal variation of precipitation (mm); (b) bias of CMIP5 MMM against four reanalyses (mm).

On the other hand, the CMIP5 MMM was able to reproduce a precipitation trend more closely resembling the reanalyses over the coastal areas as compared to that over the interior—which is consistent with earlier reports using lesser number of models—where they tend to simulate relatively higher trend than the reanalyses (Palerme et al., 2017b). For the precipitation trend of the Peninsula, the CMIP5 MMM shows an insignificant

trend +0.03 mm year^{-1} while the precipitation trend shown by the four reanalyses ranges from +0.40 to +0.50 mm year^{-1}. Of the 49 CMIP5 models, there were 15 models that showed a decreasing precipitation trend at the Peninsula region, with precipitation trend ranging from −0.10 mm year^{-1} to −0.50 mm year^{-1}. At the Adélie Land, the reanalyses and the MMM show a decreasing trend, while 17 CMIP5 models show an increasing precipitation trend. In the interior, most of the models are able to simulate the dry climate of East Antarctica. At the coastal area, some models tend to simulate extreme amount of precipitation (both high and low). This discrepancy is most likely due to the poor resolution of the CMIP5 models. The coarse grid (1.00°–3.00°) makes it difficult to properly resolve the steep orography particularly at the Peninsula region. It has been shown that resolution of approximately ∼10 km (approximately 0.01° resolution) is needed to simulate the action of Foehn winds on the lee side of the Peninsula (van Lipzig et al., 2008), which brings warm air to the region through adiabatic compression as the air descends.

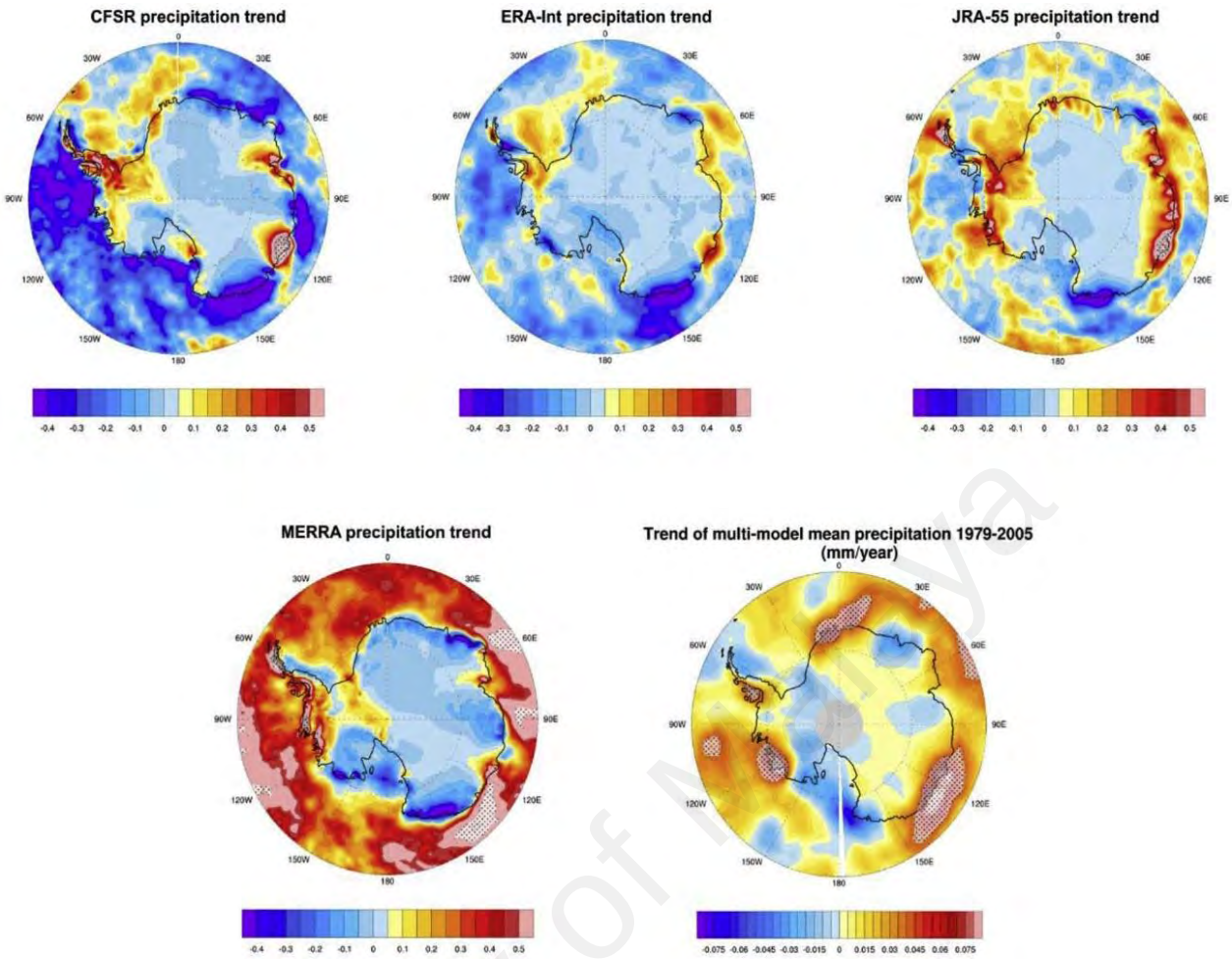

Figure 4.9 Trends (mm year^{-1}) of precipitation 1979–2005, from the four reanalyses and the CMIP5 MMM. Dotted regions are areas where the trends are statistically significant (95% confidence level). For enlarged plot please refer Supplementary 6 in the Appendix.

The CMIP5 MMM does not show a large spatial variability in terms of magnitude of the precipitation trend. Despite having a good agreement with the reanalyses—especially JRA-55 reanalysis— in simulating changing precipitation trend along the coast of the continent and some parts of the Peninsula, the MMM precipitation amount is almost an order of magnitude smaller than that of the reanalyses dataset (maximum +0.08 mm year^{-1}) due to the effect of smoothing.

When calculating the MMM, we consider the unweighted mean–giving every model equal weight— assuming that the biases of each individual model can be partially cancelled in the process and thus generating an MMM prediction that is more likely to be correct compared to that from a single model (Knuth et al., 2010). However, as explained by Zheng et al. (2013), combining ensemble simulations reduces the internal variability for some simulations while improves others. Similarly, combining different models with different precipitation variability reduces the variability and therefore the σ of resultant MMM (Zheng et al., 2013).

4.2.2 Surface air temperature

4.2.2.1 Time series of area average for 60°S -90°S

The CFSR has the highest mean SAT among the reanalyses with −15.93 °C (σ = 4.75 °C), followed by ERA-Interim −16.69 °C (σ = 6.20 °C), JRA-55 -17.20 °C (σ = 6.05 °C), and MERRA −17.62 °C (σ = 5.89 °C). The drop of SAT in the year 2004 shown in Figure 4.10 could be caused by the incorporation of data from the Moderate Resolution Imaging Spectroradiometer (MODIS) onboard the Earth Observation Systems (EOS) Aqua and Terra platforms during the mid-2004. Compared to precipitation, the correlation of SAT between the reanalyses is much higher. For instance, MERRA has a high correlation (+0.88) with the ERA-Interim, while the JRA-55 has lowest correlation with all other reanalyses (CFSR +0.48; ERA-Interim +0.68; MERRA +0.79). The MMM has a 0.43 correlation with JRA-55. The correlation between the reanalyses is tabulated in Table 4.5. The mean temperature for the CMIP5 models range from −21.72 °C (CCSM4) to −13.00 °C (GISS-E2-H) (refer Supplementary 4). The range for SAT in CMIP5 models is larger compared to reanalyses, and the MMM mean SAT is −17.78 °C. A majority of the CMIP5 models have lower mean SAT compared to the reanalyses, and hence the resultant MMM is lower than all the reanalyses. Nonetheless the difference is very small.

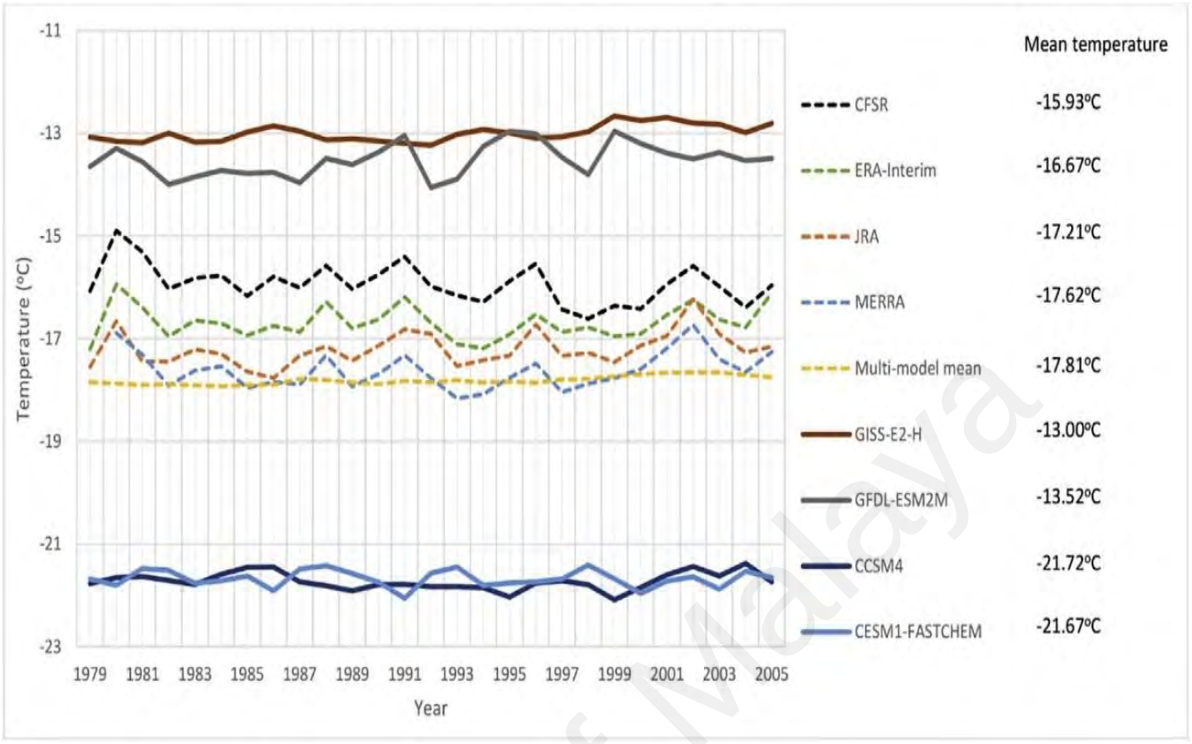

Figure 4.10 Mean annual SAT for CMIP5 and four reanalyses (°C) from 1979 to 2005.

As for the trend, The CFSR shows a negative temperature trend (−0.022 ± 0.018 °C year^{-1}) while the other reanalyses show insignificant increasing trend (+0.003 ± 0.017 °C year^{-1} to +0.015 ± 0.016 °C year^{-1}). 19 of the 49 models show a significant increase ($p \leq .05$) while 4 models show significant decrease in SAT. Over 50% of the models show no significant change in SAT trend. The model that shows that largest trend is the BCC-CSM1-1 with +0.070 ± 0.010 ℃year^{-1}. The resultant MMM shows a significant positive trend (0.009 ± 0.003 °C year^{-1}) (Figure 4.11). However, putting this value in perspective, the MMM trend only represents a rise of less than 1 °C in SAT in a century. Hence, the calculated t-value from the regression analysis is most likely due to the small value of standard error in the regression line.

Table 4.5 Correlation coefficient for between the reanalysis datasets and the CMIP5 MMM

	ERA-Interim	CFSR	JRA-55	MERRA	MMM
ERA-Interim	1.00	0.75[a]	0.68[a]	0.88[a]	0.12
CFSR		1.00	0.48[a]	0.68[a]	−0.32
JRA-55			1.00	0.79[a]	0.43[a]
MERRA				1.00	0.34
MMM					1.00

[a] Significant at 95% confidence level.

4.2.2.2 Seasonal variation of temperature

Of the 49 models, only two models exhibit correlation < +0.90 with the reanalyses: HadCM3 and HadGEM2-ES (refer Supplementary 5). The SAT profile of HadGEM2-ES is very different from that of other models (refer Supplementary 5). This is because the model has its highest SAT in February (−14.55 °C), which is a month later than all other models. Moreover, the lowest SAT for HadGEM2-ES occurs in September instead of July. HadCM3, on the other hand, reaches its lowest SAT in spring (−38.39 °C), while the other models have the lowest SAT in the mid-late winter. It should be noted that seasonal variation of the CMIP5 models falls within the σ of the reanalyses. The bias between the MMM and CFSR is the largest (close to 5 °C), while the bias between MERRA and MMM is the smallest (less than 2 °C) (see Figure 4.12(b)).

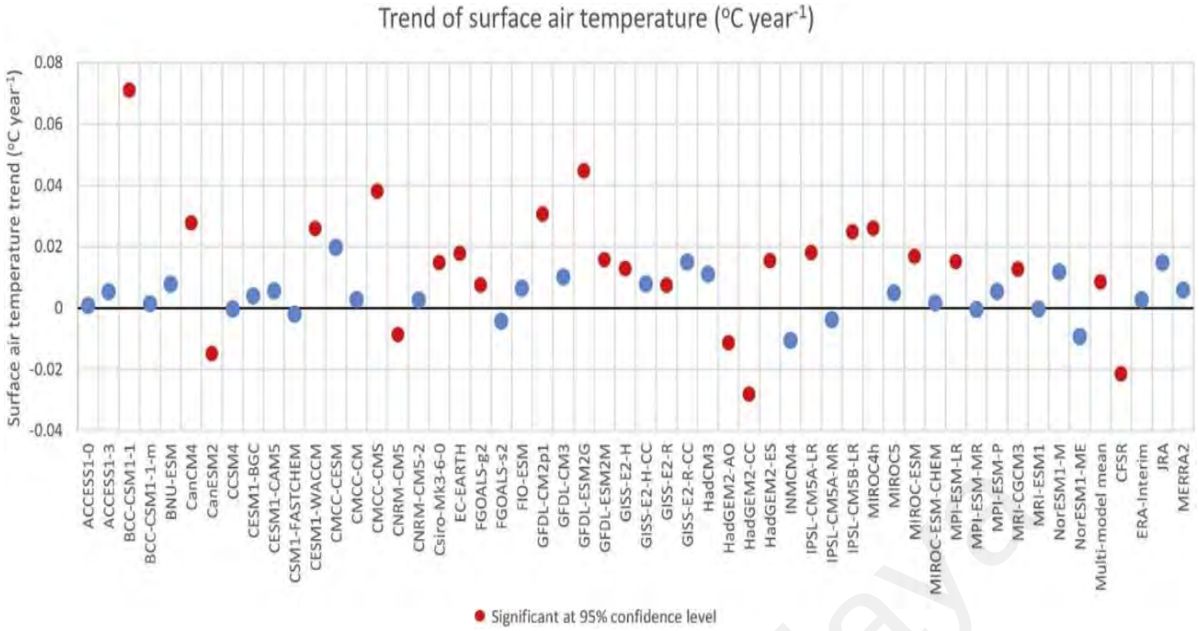

Figure 4.11 SAT Trend of CMIP5 models, CMIP5 MMM and reanalysis datasets.

4.2.2.3 Spatial trend of temperature

The reanalyses—with the exception of ERA-Interim— show that the Peninsula region has seen a net increasing SAT trend from 1979 to 2005, which is well replicated by the CMIP5 MMM. Another region that has seen increasing SAT is the Marie Byrd Land (68°S, 130°W) with +0.15 °C year^{-1}. The area off the coast of George V Land (68°30′ S, 148°E), however, has seen a slight decrease in SAT (−0.15 °C year^{-1}), and is consistent across all the reanalyses and the CMIP5 MMM. This result is in agreement with the spatial result in Figure 4.9 which shows the coastal area off Adélie Land having a decreasing precipitation trend. Similarly, the increasing SAT trend in the Peninsula region is also in agreement with the increasing precipitation trend. However, the Marie Byrd Land shown in Figure 4.9 has a decreasing precipitation, while at the same time an increasing SAT trend as shown in Figure 4.13. Generally, the reanalyses agree with one another in terms of spatial pattern of SAT. Moreover, the reanalyses and the CMIP5 MMM show that the entire Antarctica land mass shows a net SAT increase since 1979.

The largest trend observed in Figure 4.13 is the increasing SAT trend off the coast of Filchner-Ronne Ice Shelf (79°S, 40°W) (+0.20 °C $year^{-1}$) shown by the CFSR, and the decreasing SAT at the Amery Ice Shelf (68°15′ S, 74°30′ E) (−0.25 °C $year^{-1}$) by ERA-Interim.

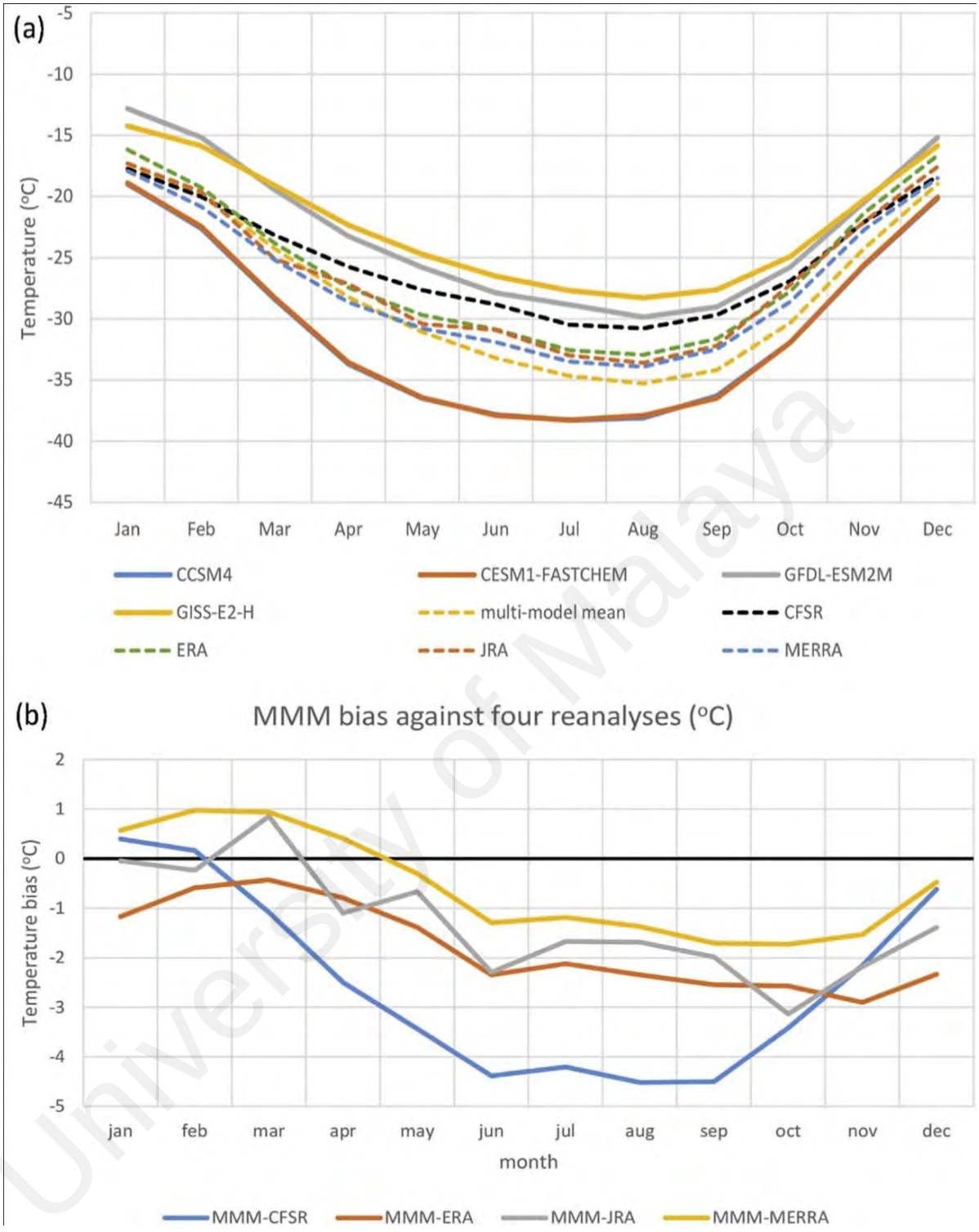

Figure 4.12 (a) Seasonality of SAT for all the models and reanalyses used in this study; (b) MMM bias against reanalysis datasets

For the CMIP5 models, there is a stark contrast between the models in terms of the SAT trend in Peninsula, West Antarctica and East Antarctica. For the Peninsula, for instance, 23 of the 49 models show a decreasing SAT trend (−0.03 °C year^{-1} to −0.15 °C

year^{-1}) from 1979 to 2005. For the West Antarctica, 20 CMIP5 models show a decreasing SAT trend (−0.03 °C year^{-1} to 0.15 °C year^{-1}) while three of the reanalyses show an increasing SAT trend (up to +0.10 °C year^{-1}). Over at the East Antarctica, all of the reanalyses and 30 CMIP5 models show an increasing SAT trend, a trend replicated by 30 of the CMIP5 models.

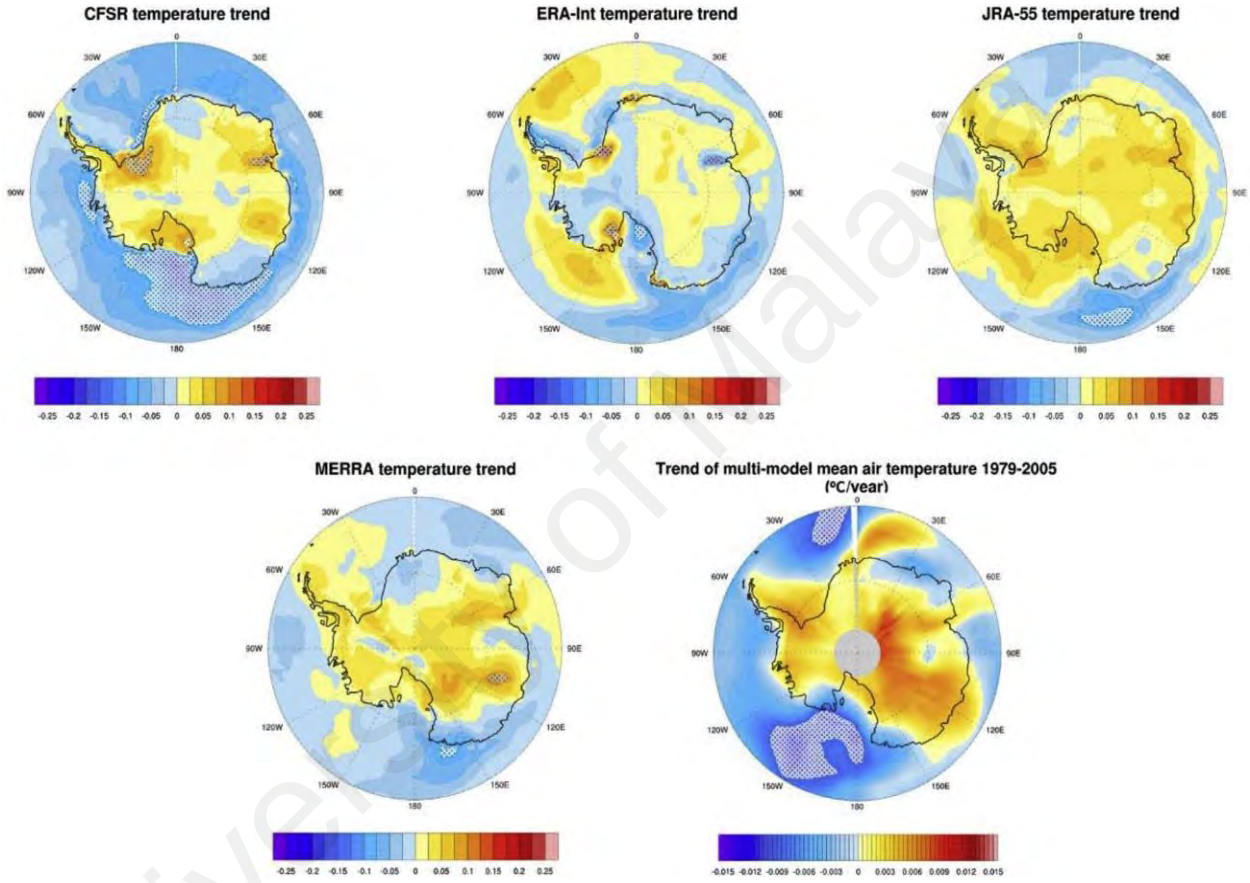

Figure 4.13 Spatial map of SAT trend from 1979 to 2005 (°C year^{-1}). Dotted regions are areas where the trends are statistically significant (95% confidence level). For enlarged plot please refer Supplementary 8 in the Appendix.

4.2.3 Relationship between temperature and precipitation

By comparing Figure 4.9 and Figure 4.13, we can see that the region with positive (negative) SAT trend is generally similar to the region with positive (negative) precipitation trend. This is because warmer SAT is able to hold more moisture (Clausius-Clapeyron relation), a phenomenon that can be more significant in relatively low

temperature region such as the Antarctic (Pall et al., 2007). When wind carries the moisture-laden air towards the Antarctic continent, the orographic lifting will cause the moisture to fall as precipitation. The Clausius-Clapeyron relation dictates that for the atmosphere, its water vapor content will increase by roughly 7% with every 1 °C increase in temperature (Kininmonth). This means that in the Antarctic, when the trend of SAT increases (decreases), the trend of precipitation should also increase (decrease).

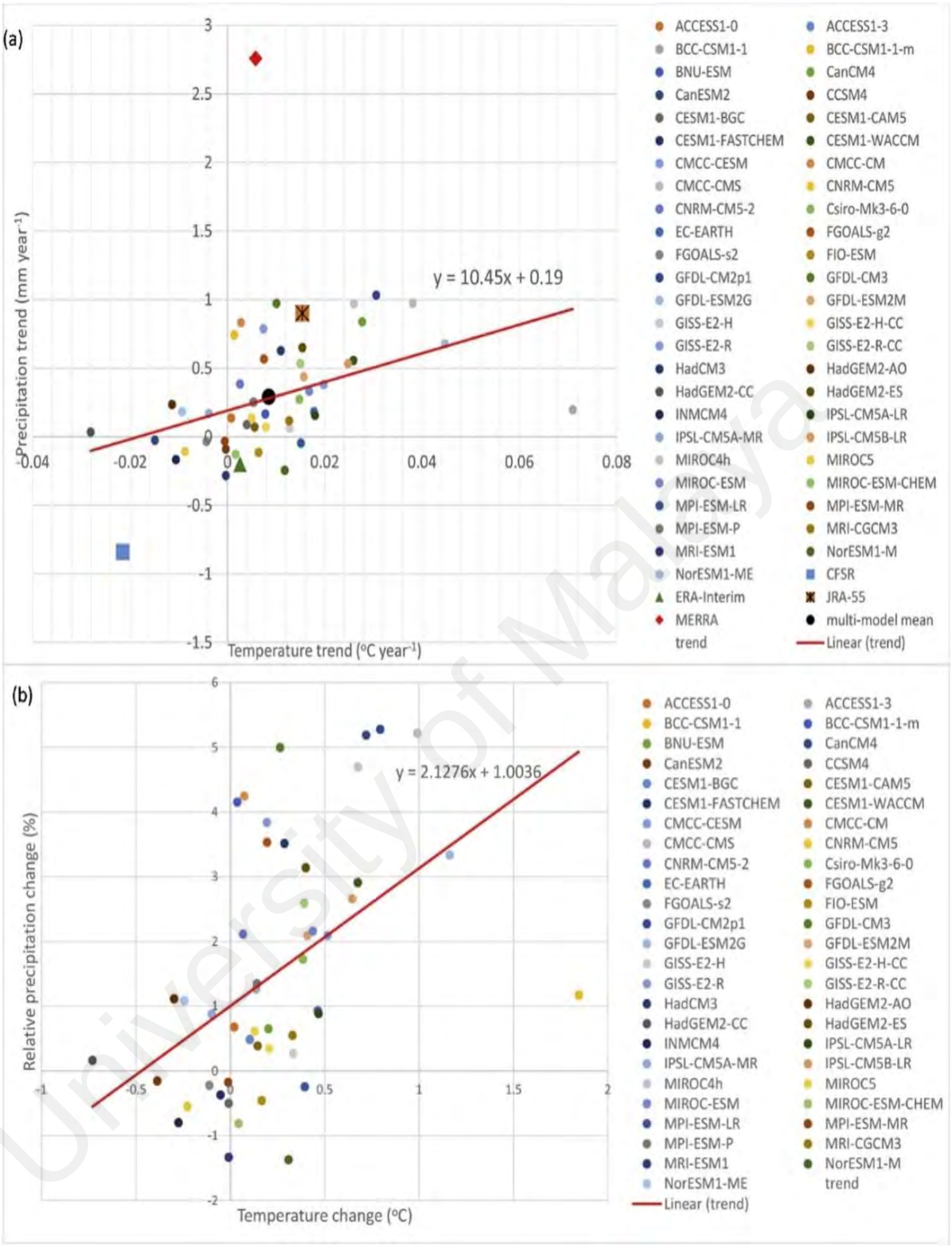

Figure 4.14 (a) Precipitation trend against SAT trend for CMIP5 models and reanalyses; (b) relative precipitation changes (%) against temperature changes (°C) for CMIP5 models.

The linear relationship between SAT and precipitation, however, does not always occur in the CMIP5 models. For instance, the two models (FIO-ESM and BNU-ESM) that show the highest precipitation amount have low mean annual SAT which are significantly lower than the MERRA reanalysis dataset (Figure 4.9). The trend of precipitation has been compared to the trend of temperature (Figure 4.14). A majority of the CMIP5 models lie within quadrant one and three, with the exception of eight models (FIO-ESM, HadGEM2-AO, HadGEM2-CC, NorESM1-M, NorESM1-ME, IPSL-CM5A-MR, MPI-ESM-LR, and MIROC-ESM-CHEM). For the reanalyses, MERRA and JRA-55 are in quadrant one while the CFSR resides in quadrant three. ERA-Interim shows a positive trend in SAT and an insignificant negative trend in precipitation. The slope of the regressed linear line, which represents precipitation change per temperature, is 10.45 mm°C^{-1}. We also derived the relative precipitation changes (Δprecipitation (%)) against the changes in surface air temperature (ΔSAT). A linear regression produces precipitation trend, $\Delta P = 2.13\ \Delta SAT + 1.00$ for the entire coverage area. At temperature −33.0 °C, the atmospheric moisture capacity is expected to be about 9.7%°C^{-1}. The slope value from Figure 4.14 is on the lower end of values reported in previous studies which range from 3%°C^{-1} to 7%°C^{-1} (Gregory et al., 2006; Krinner et al., 2007; Ligtenberg et al., 2013; Palerme et al., 2017b).

4.3 Results for future precipitation prediction under four RCP scenarios by CMIP5 models.

In order to facilitate the presentation of results in the following section, we will present the results based on different regions: West Antarctica (60°S –90°S, 90°W –195°W), East Antarctica (60°S –90°S, 165°E –45°W), Peninsula (60°S –75°S, 45°W –75°W), and the whole Antarctica (60°S -90°S).

4.3.1 Precipitation

4.3.1.1 Projected time series 2006-2100

Figure 4.15 shows the CMIP5 MMM precipitation time series from 2006-2100. The four different precipitation paths start diverging at around the year 2040. The East Antarctica receives the least amount of precipitation compared to the West Antarctica and Peninsula. This is because the high altitude of the Antarctic Plateau prevents moisture from the coasts from penetrating deep into the interior. The linear trend is calculated using linear regression. One interesting observation that can be seen from Figure 4.15 is that the trend of the RCP 2.6 for East Antarctica (0.123 mm $year^{-1}$) is higher compared to the RCP 2.6 for West Antarctica (1.50×10^{-2} mm $year^{-1}$) and Peninsula (6.40×10^{-2} mm $year^{-1}$). Apart from the West Antarctica, the trends of RCP 2.6 for Peninsula and East Antarctica are significant ($p \leq 0.05$). For East Antarctica, this is due to the relatively smaller precipitation variability of the region compared to West Antarctica or Peninsula. Therefore even a mild increase of precipitation in the long run would become statistically significant. For the other three scenarios, however, the precipitation trend is highest in the Peninsula, followed by the West Antarctica and East Antarctica. This means that under the RCP 4.5, RCP 6.0, and RCP 8.5 scenarios, the Peninsula is predicted to experience more precipitation compared to West Antarctica or East Antarctica.

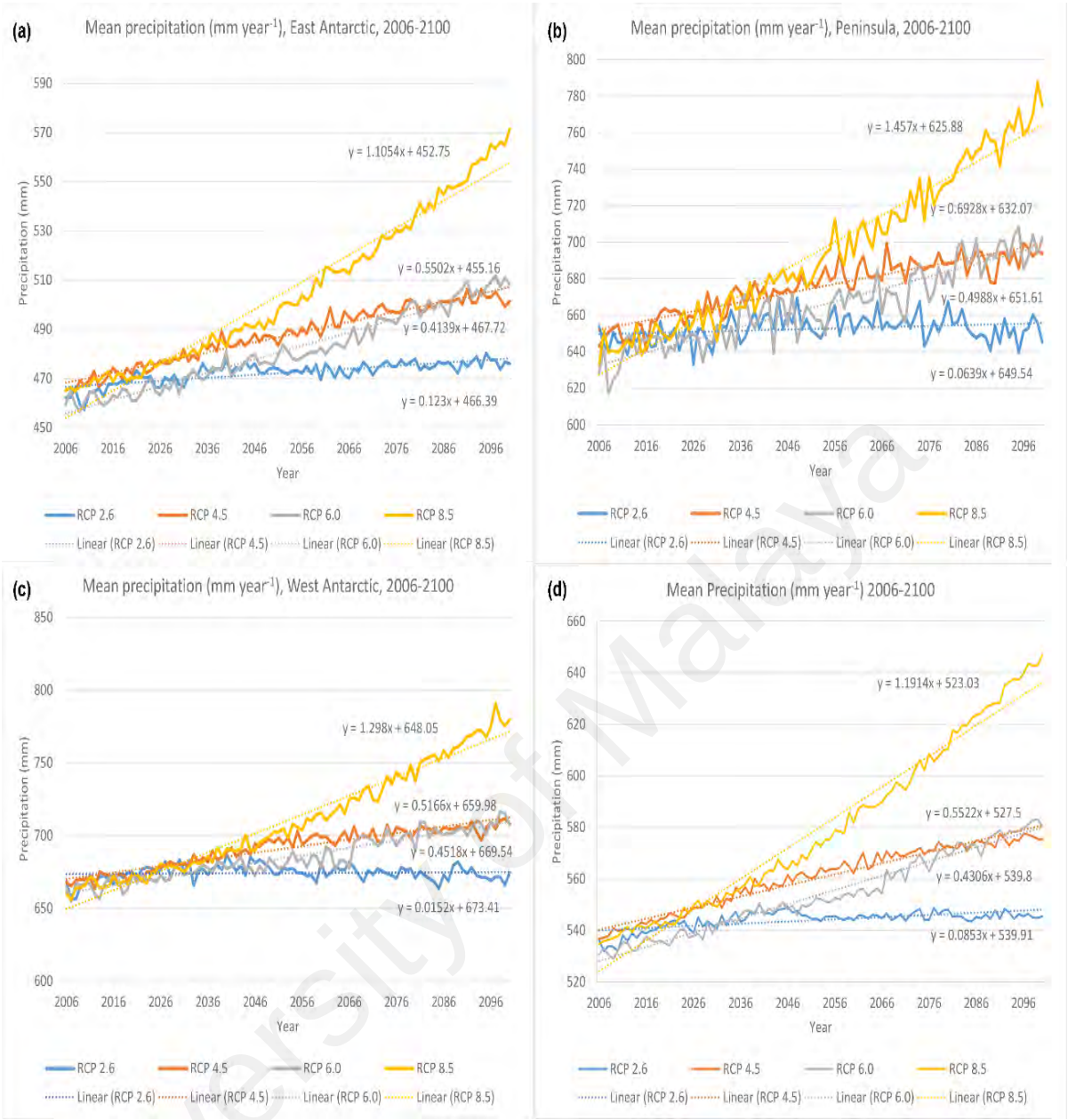

Figure 4.15 Time series of CMIP5 MMM annual precipitation 2006-2100 (mm year^{-1}) for (a) East Antarctica; (b) Peninsula; (c) West Antarctica; and (d) whole Antarctic.

For the entire continent, the model with the highest positive trend for RCP 2.6, RCP 4.5, RCP 6.0, and RCP 8.5 are CESM1-CAM5 (2.76 x 10^{-2} mm year^{-1}), CESM1-CAM5 (6.76 x 10^{-2} mm year^{-1}), CESM1-CAM5 (8.00 x 10^{-2} mm year^{-1}), and FGOALS-S2 (0.167 mm year^{-1}), respectively. The details of models with highest trends, lowest trends and multimodel trends for different region and scenario are tabulated in Table 4.6. In RCP 2.6

scenarios, there are several models that showed decreasing precipitation trends. The number of models that show negative trends decreases from RCP 2.6 to RCP 6.0. There are no models that show negative trends in RCP 8.5 experiment.

Table 4.6 CMIP5 models with highest, lowest and Multimodel precipitation trends for different scenarios and regions.

		East Antarctica	West Antarctica	Peninsula
RCP 2.6	Highest trend	**MIROC-ESM-CHEM** (3.25×10^{-2} mm year^{-1})	**CESM1-CAM5** (3.08×10^{-2} mm year^{-1})	**BCC-CSM1-1** (2.68×10^{-2}mm year^{-1})
	MMM trend	(1.03×10^{-2} mm year^{-1})	(1.27×10^{-3} mm year^{-1})	(5.33×10^{-3} mm year^{-1})
	Lowest trend	**BCC-CSM1-1-m** (-5.23×10^{-2} mm year^{-1})	**GFDL-ESM2G** (-5.19×10^{-2} mm year^{-1})	**BCC-CSM1-1-m** (-3.84×10^{-2} mm year^{-1})
RCP 4.5	Highest trend	**CESM1-CAM5** (6.42×10^{-2} mm year^{-1})	**CESM1-CAM5** (7.28×10^{-2} mm year^{-1})	**HadGEM2-ES** (8.36×10^{-2} mm year^{-1})
	MMM trend	(3.45×10^{-2} mm year^{-1})	(3.76×10^{-2} mm year^{-1})	(4.16×10^{-2} mm year^{-1})
	Lowest trend	**BCC-CSM1-1-m** (-1.12×10^{-2} mm year^{-1})	**GFDL-ESM2G** (-1.64×10^{-2} mm year^{-1})	**MRI-CGCM3** (1.02×10^{-2} mm year^{-1})
RCP 6.0	Highest trend	**CESM1-CAM5** (8.13×10^{-2} mm year^{-1})	**HadGEM2-AO** (8.08×10^{-2} mm year^{-1})	**HadGEM2-AO** (9.14×10^{-2} mm year^{-1})
	MMM trend	(4.56×10^{-2} mm year^{-1})	(4.30×10^{-2} mm year^{-1})	(5.77×10^{-2} mm year^{-1})

	Lowest trend	**BCC-CSM1-1-m** (7.70×10^{-3} mm year^{-1})	**MIROC5** (-2.69×10^{-3} mm year^{-1})	**IPSL-CM5A-LR** (1.23×10^{-2} mm year^{-1})
RCP 8.5	Highest trend	**FGOALS-s2** (0.145 mm year^{-1})	**FGOALS-s2** (0.207 mm year^{-1})	**FGOALS-s2** (0.204 mm year^{-1})
	MMM trend	(9.21×10^{-2} mm year^{-1})	(0.108 mm year^{-1})	(0.121 mm year^{-1})
	Lowest trend	**GFDL-ESM2G** (3.52×10^{-2} mm year^{-1})	**MIROC5** (3.67×10^{-2} mm year^{-1})	**BNU-ESM** (3.63×10^{-2} mm year^{-1})

It is difficult to determine the effect of the models' resolution on the trend of precipitation that they simulate. The CESM1-CAM5, for instance, has a resolution of 0.9ºx 1.25º, and is considered one of the higher resolution models in CMIP5. It consistently shows highest trend for experiments like RCP 4.5 (as shown in Table 4.6). For the low and high GHG concentration experiment like RCP 2.6 and RCP 8.5, the highest and lowest trends are given by low resolution models like BCC-CSM1-1-m (2.8º x 2.8º), FGOALS-s2 (1.7º x 2.8º), BNU-ESM (2.8º x 2.8º), and GFDL-ESM2G (2.0º x 2.5º). It is apparent that lower resolution models tend to give higher, or amplified trend, in high GHG concentration experiment i.e. RCP 8.5. For instance, all but one model with the highest and lowest trends for RCP 8.5 experiment in different regions have resolution coarser than 2.5º: FGOALS-s2 (1.7º x 2.8º) for RCP 8.5 scenarios in Peninsula, West Antarctica and East Antarctica; BNU-ESM (2.8º x 2.8º) and GFDL-ESM2G (2.0º x 2.5º). There is a lack of consensus on the effect of model resolution on simulated results. While various authors have attributed the performance of the CMIP5 models based on their improved resolution (Boyle et al., 2010; Delworth et al., 2012), studies have also shown that for precipitation, the effect of resolution on the simulated result is somewhat modest

(Mass et al., 2002; Mishra et al., 2014; Pope et al., 2002). Moreover, it can be argued that the reason why low resolution models give very high or low trend is because of the overall greater number of low-resolution models (over 2.0^{o}) among the participating models. Nonetheless, the results shown is actually in line with the historical simulation of precipitation using CMIP5 models, where models like BNU-ESM and FGOALS-s2 tend to exaggerate the values of precipitation i.e. too high or too low from the values given by reanalysis datasets (Tang et al., 2018b). It is possible that this tendency to overestimate precipitation amount gets carried into the RCPs scenarios.

The precipitation variability in different regions is very different. Precipitation variability is highly dependent on the precipitation frequency and amount, the topography of different regions, and the number of models used in the calculation of MMM. For instance, the variability of precipitation in Peninsula is much higher compared to East Antarctica or West Antarctica. This could be due to the fact that the Peninsula receives the most amount of precipitation, primarily contributed by the climatological center of low pressure located in the western side of the Peninsula, in the Bellingshausen Sea (Turner et al., 1995). In addition, the rugged topography (the spine of the Transantarctic Mountains stretches along the Peninsula) relative to the flat Antarctic plateau of the East Antarctica or the RIS of West Antarctica also contributes to the higher precipitation variability in Peninsula. The highest point in Peninsula extends beyond 2000 meters, separating the warm, maritime climate along the western coastline from the cold continental climate on the eastern side (King et al., 1997). The eastern side of the Peninsula is also affected by the presence of Foehn winds, which causes an increase in temperature and reduction in humidity along the lee side of the Peninsula (Cape et al., 2015), further reduces the precipitation on the eastern side of Peninsula, thereby increases the precipitation variability in the region. Apart from that, the variability of MMM is also affected by the number of models involved in the calculation of MMM. Studies have

shown that the variability of MMM drops with the increase in model number (Chenoli et al., 2017; Shu et al., 2015). It should be noted that the number of models that have RCP 6.0 experiment is only half of the RCP 4.5 and RCP 8.5, and hence the effect of smoothing is less apparent. Therefore the variability of RCP 6.0 is much higher compared to other scenarios. This is consistent across all the different regions shown in Figure 4.15.

4.3.1.2 Seasonal variability

Figure 4.16 shows the mean seasonal variability for different regions for different time slices: 2006-2040; 2041-2070; and 2071-2100 (to be defined as early-, mid-, and late-period, respectively, from this point henceforth). For all seasons and across all four scenarios, the amount of precipitation received by East Antarctica is the least among the different regions, ranging from 98.5mm – 113.7mm during summer (DJF) to 143.2mm – 166.3mm during autumn (MAM). During summer, the Peninsula (138.9mm-160.8mm) is expected to receive higher precipitation than the West Antarctica (136.3mm-153.3mm) across four scenarios. For autumn, winter and spring, however, the amount of precipitation in West Antarctica is projected to be higher than the Peninsula across all scenarios. The difference between the precipitation values projected for the two regions, however, is insignificant. It is reasonable to assume that the largest percentage increase in precipitation occurs under the RCP 8.5 scenario.

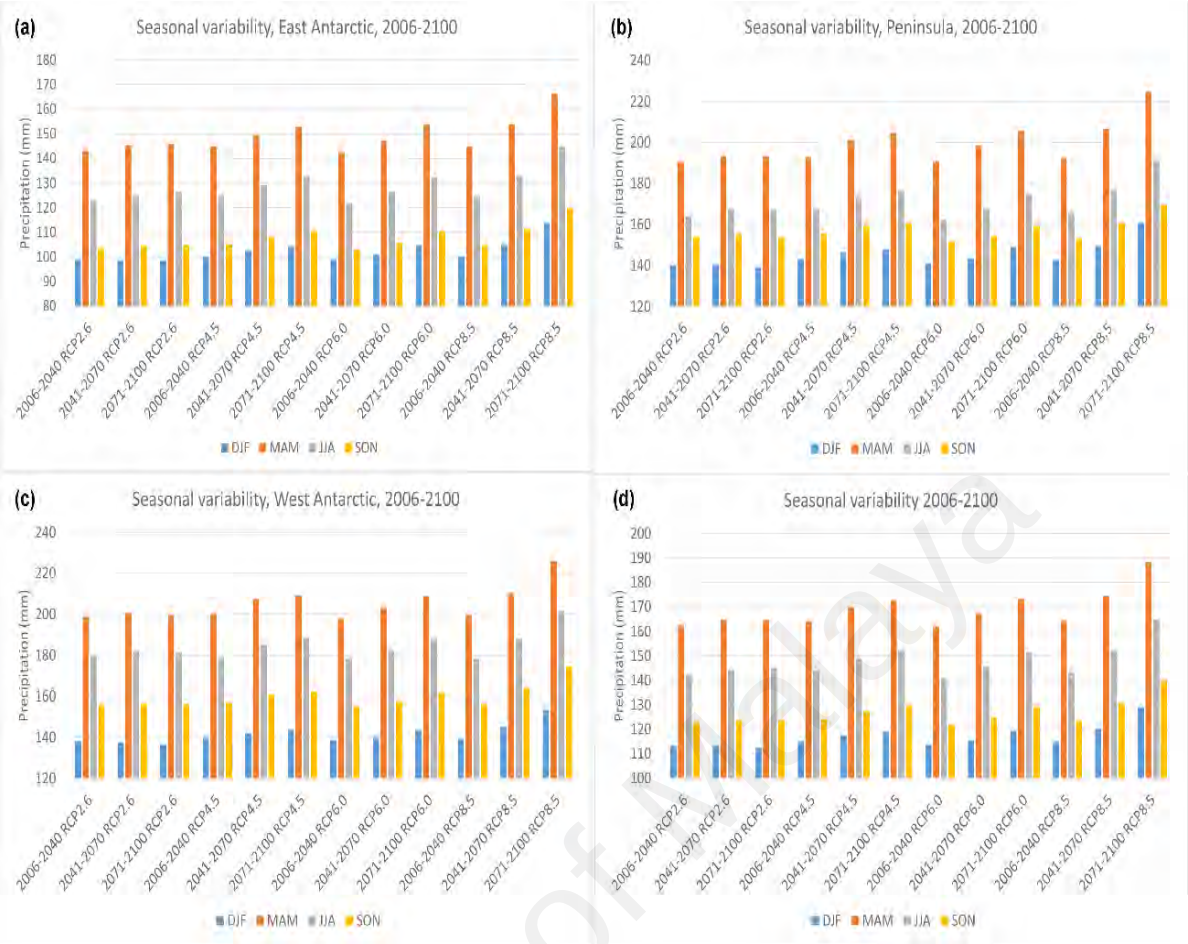

Figure 4.16 Mean seasonal variability for precipitation, 2006-2100, projected from CMIP5 MMM for (a) East Antarctica; (b) Peninsula; (c) West Antarctica; and (d) whole Antarctic.

Calculations based on Figure 4.16 show that the largest percentage precipitation increase occurs in East Antarctic in winter (JJA) during the late-period (+9.00%), followed by Peninsula in autumn of late period (+8.81%) and again in East Antarctica in summer (+8.22%). In addition, the percentage increase is generally larger during the late-period compared to mid- or early-period. For summer, the increase in precipitation can be linked to the increasing positive Southern Annular Mode (SAM) trend under the RCP 8.5 scenario. (Zheng et al., 2013) used output from CMIP5 models to project the trends of SAM index under the RCP 4.5 and RCP 8.5 scenarios. The authors found that under the RCP 8.5 scenario, all the models had significant positive SAM index trends. The trend

was observed to be larger beyond 2050, which is in agreement with the larger percentage increase in precipitation during the late-period in this work, which the author attributes to a lagged accumulative effect of the very rapid increase in radiative forcing in the 2040s. The ozone layer is expected to recover by the twenty-first century, thus contributing to a negative SAM influence (Polvani et al., 2011). However, the continual increase in GHG concentration under the RCP 8.5 scenario is likely to outweigh the influence of ozone recovery, thus contributing to the positive SAM index and consequently, more precipitation (Zheng et al., 2013).

4.3.1.3 Spatial trend of precipitation 2006-2100

One important observation that can be seen in Figure 4.17(c) is the patch of negative trend in Marie Byrd Land, which is possibly caused by the failure of MMM to eliminate the extreme values due to the relatively low number of models in RCP 6.0 experiment. Apart from the RCP 2.6 scenario, all other scenarios show that the precipitation trend is the highest in western side of Peninsula (over 0.02 mm $year^{-1}$ for RCP 8.5), followed by the coast of Enderby Land and Kemp Land, Shackleton Ice Shelf, the coastal area of Dronning Maud Land, and the coastal area of Amundsen Sea. These regions are the four climatological centers of low pressure in the Antarctic coastal region, as shown in Figure 4.17 as regions with most significant precipitation trends: in the Ross Sea, off East Antarctica, north of Dronning Maud Land, and in the Bellingshausen Sea. Compared to the coastal regions and the surrounding Southern Ocean, the precipitation trends of the landmass is relatively lower. The western side of the Peninsula is expected to receive the highest amount of precipitation (Figure 4.16), along with the highest trend in precipitation increment (Figure 4.15 and Figure 4.17), possibly because of increasing extra-tropical cyclones going into the southern Bellingshausen Sea from lower latitudes as the concentration of GHG increases, coupled with the increasing new lows in the coastal regions.

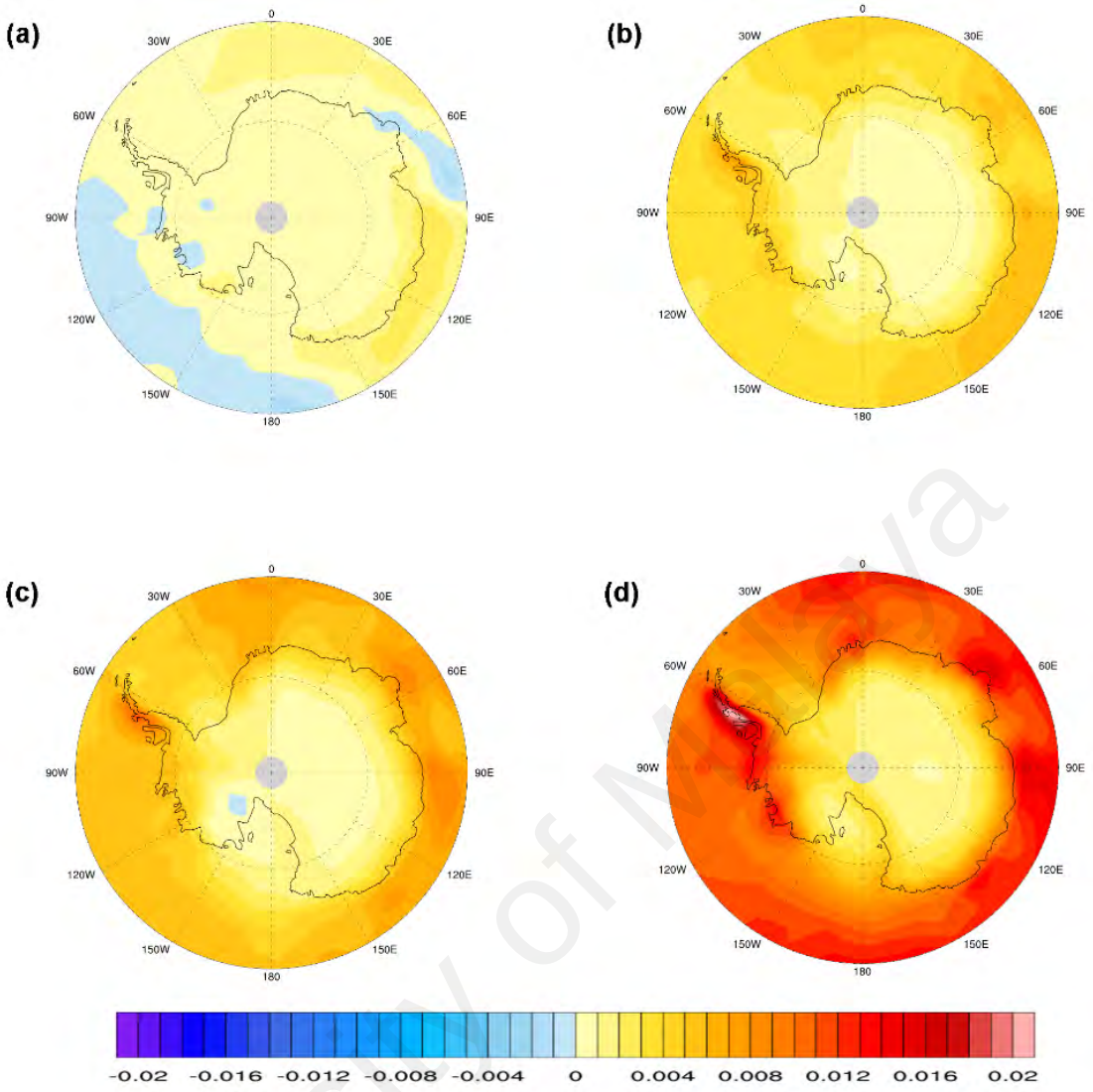

Figure 4.17 Spatial trend of precipitation (mm year^{-1}) calculated from CMIP5 MMM for (a) RCP 2.6; (b) RCP 4.5; (c) RCP 6.0; and (d) RCP 8.5.

4.3.2 Surface air temperature

4.3.2.1 Projected time series 2006-2100.

Figure 4.18 Time series of CMIP5 MMM annual SAT 2006-2100 (^{o}C year^{-1}) for (a) East Antarctica; (b) Peninsula; (c) West Antarctica; and (d) whole Antarctic

Figure 4.18 shows the CMIP5 MMM SAT time series from 2006-2100. The East Antarctica is generally the coldest region on the continent, due to the high altitude of the Antarctic plateau that prevents warm ocean air from penetrating inland. The Peninsula is the warmest region in Antarctica, while the West Antarctica has the highest SAT variability. Under three scenarios (RCP 2.6, RCP 4.5, and RCP 6.0) the East Antarctica has the highest SAT trends in Antarctic (0.067 ^{o}C decade^{-1}, 0.173 ^{o}C decade^{-1}, and 0.223 ^{o}C decade^{-1}, respectively). Under the RCP 8.5 scenario, the highest SAT trend occurs in the Peninsula (0.44 ^{o}C decade^{-1}). These result are consistent with the results obtained by Palerme (2017), whose work suggested that the largest SAT change in the RCPs scenarios

occurred at altitude of over 2250 meters, and by 2099 under the RCP 8.5 scenario the maximum SAT increase would be about 4.0 to 4.5^{o}C (Palerme et al., 2017b). An interesting observation that can be made from Figure 4.18 is that the West Antarctica appears to be having the lowest SAT trends (0.036 ^{o}C decade^{-1} and 0.426 ^{o}C decade^{-1} under RCP 2.6 and RCP 8.5 scenarios, respectively) among the different regions. For the entire continent, the model with the highest positive trend for RCP 2.6, RCP 4.5, RCP 6.0, and RCP 8.5 are CNRM-CM5 (0.188 ^{o}C decade^{-1}), CNRM-CM5 (0.318 ^{o}C decade^{-1}), CESM1-CAM5 (0.385 ^{o}C decade^{-1}), and FIO-ESM (0.741 ^{o}C decade^{-1}), respectively. The details of models with highest and lowest trends for different regions and scenario is tabulated in Table 4.7.

Table 4.7 CMIP5 models with highest trends, lowest trends and Multimodel trends for SAT for different scenarios and regions.

		East Antarctica	West Antarctica	Peninsula
RCP 2.6	Highest trend	**MIROC-ESM-CHEM** ($0.203\ ^{o}C\ decade^{-1}$)	**CNRM-CM5** ($0.159\ ^{o}C\ decade^{-1}$)	**CESM1-CAM5** ($0.187\ ^{o}C\ decade^{-1}$)
	MMM trend	($6.11 \times 10^{-2}\ ^{o}C\ decade^{-1}$)	($2.87 \times 10^{-2}\ ^{o}C\ decade^{-1}$)	($4.21 \times 10^{-2}\ ^{o}C\ decade^{-1}$)
	Lowest trend	**BCC-CSM1-1-m** ($-0.220\ ^{o}C\ decade^{-1}$)	**GFDL-ESM2G** ($-0.152\ ^{o}C\ decade^{-1}$)	**BCC-CSM1-1-m** ($-0.098\ ^{o}C\ decade^{-1}$)
RCP 4.5	Highest trend	**FGOALS-g2** ($0.338\ ^{o}C\ decade^{-1}$)	**MRI-CGCM3** ($0.365\ ^{o}C\ decade^{-1}$)	**CESM1-CAM5** ($0.336\ ^{o}C\ decade^{-1}$)
	MMM trend	($1.67 \times 10^{-1}\ ^{o}C\ decade^{-1}$)	($0.138\ ^{o}C\ decade^{-1}$)	($0.164\ ^{o}C\ decade^{-1}$)
	Lowest trend	**BCC-CSM1-1-m** ($-0.65 \times 10^{-1}\ ^{o}C\ decade^{-1}$)	**GFDL-CM3** ($-0.069\ ^{o}C\ decade^{-1}$)	**FGOALS-g2** ($9.15 \times 10^{-3}\ ^{o}C\ decade^{-1}$)
RCP 6.0	Highest trend	**FIO-ESM** ($0.405\ ^{o}C\ decade^{-1}$)	**CESM1-CAM5** ($0.312\ ^{o}C\ decade^{-1}$)	**MIROC-ESM** ($0.407\ ^{o}C\ decade^{-1}$)
	MMM trend	($2.17 \times 10^{-1}\ ^{o}C\ decade^{-1}$)	($0.162\ ^{o}C\ decade^{-1}$)	($0.211\ ^{o}C\ decade^{-1}$)
	Lowest trend	**BCC-CSM1-1-m** ($-4.77 \times 10^{-2}\ ^{o}C\ decade^{-1}$)	**GFDL-ESM2M** ($-0.0312\ ^{o}C\ decade^{-1}$)	**GFDL-CM3** ($0.082\ ^{o}C\ decade^{-1}$)
RCP 8.5	Highest trend	**FIO-ESM** ($0.786\ ^{o}C\ decade^{-1}$)	**FGOALS-g2** ($0.738\ ^{o}C\ decade^{-1}$)	**FGOALS-g2** ($0.814\ ^{o}C\ decade^{-1}$)

	MMM trend	(0.420 ^{o}C decade^{-1})	(0.379 ^{o}C decade^{-1})	(0.437 ^{o}C decade^{-1})
	Lowest trend	**GFDL-CM3** (0.150 ^{o}C decade^{-1})	**IPSL-CM5B-LR** (8.60 x 10^{-3} ^{o}C decade^{-1})	**BNU-ESM** (0.185 ^{o}C decade^{-1})

As can be seen from Table 4.7 the difference between the highest trend and the lowest trend is significant. There are several models that show negative trend in SAT even in high GHG concentration scenario like RCP 6.0. It is possible that these models overestimated the effect of ozone recovery to offset the influence of increasing GHG concentration.

4.3.2.2 Seasonal variability

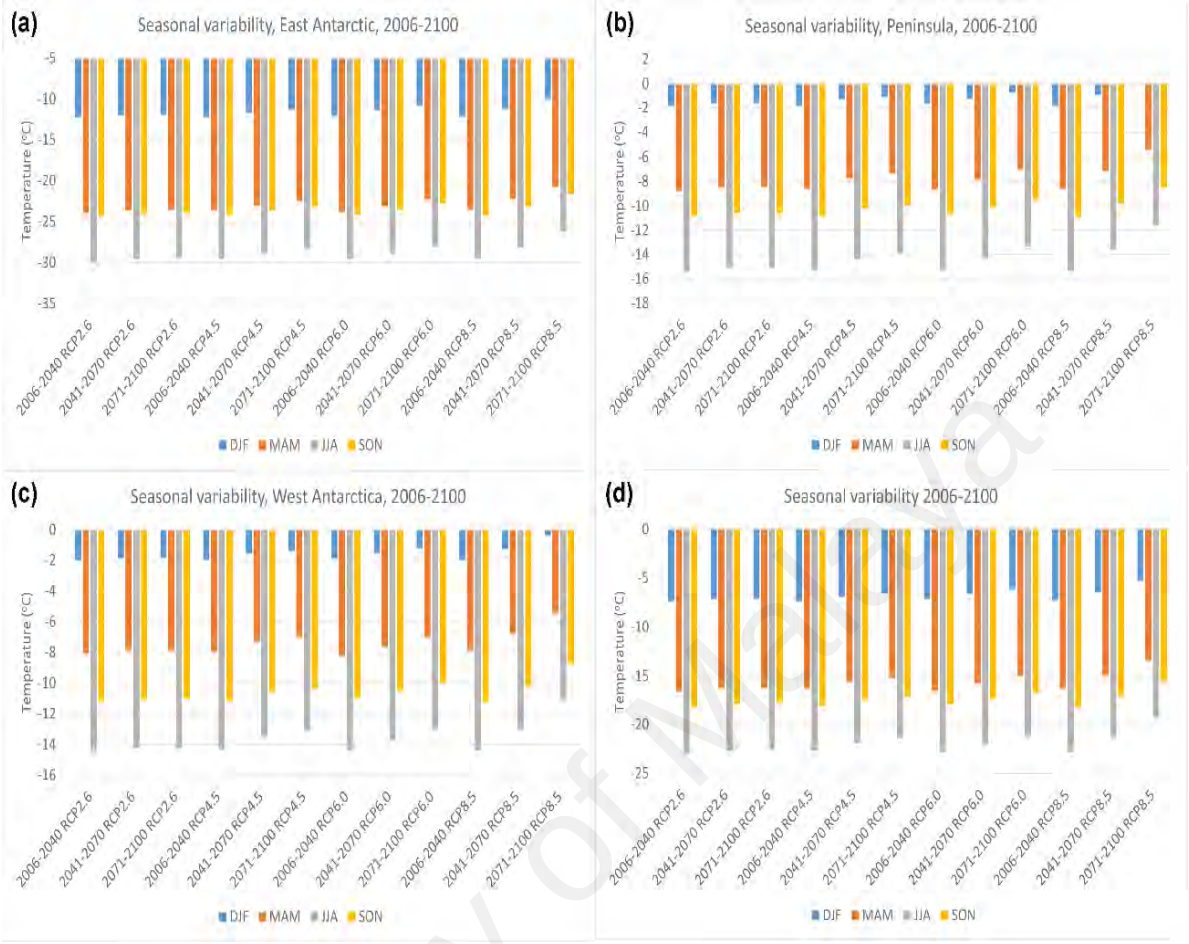

Figure 4.19 Mean seasonal variability for SAT, 2006-2100, projected from CMIP5 MMM for (a) East Antarctica; (b) Peninsula; (c) West Antarctica; and (d) whole Antarctic.

For all seasons and across all four scenarios, the SAT in the East Antarctica is the lowest among the different regions, ranging from -28.89 ºC during winter (JJA) to -9.94 ºC during summer (DJF). Compared to precipitation, the changes in SAT is relatively more significant. Winter in the Antarctic Peninsula is projected to be the most affected season and region of SAT warming. The highest increase in SAT occurs under the RCP 8.5 scenario in the second half of the 21st century in winter in all the locations. The Peninsula will experience the highest increase in SAT (2.00 ºC), followed by the West Antarctica (1.92 ºC) and the East Antarctica (1.875 ºC). Interestingly, there is also a fall

in SAT under the RCP 2.6 scenario in the late-period in Peninsula and the West Antarctica. The largest fall in SAT occurs under the RCP 2.6 in spring (SON) in Peninsula (-0.0389 ^{o}C) and the West Antarctica (-0.0259 ^{o}C). Under the RCP 4.5 and 6.0 scenarios, the Peninsula winter will be the fastest warming region in Antarctica (0.838 ^{o}C and 0.999 ^{o}C, respectively).

4.3.2.3 Spatial trend of SAT 2006-2100

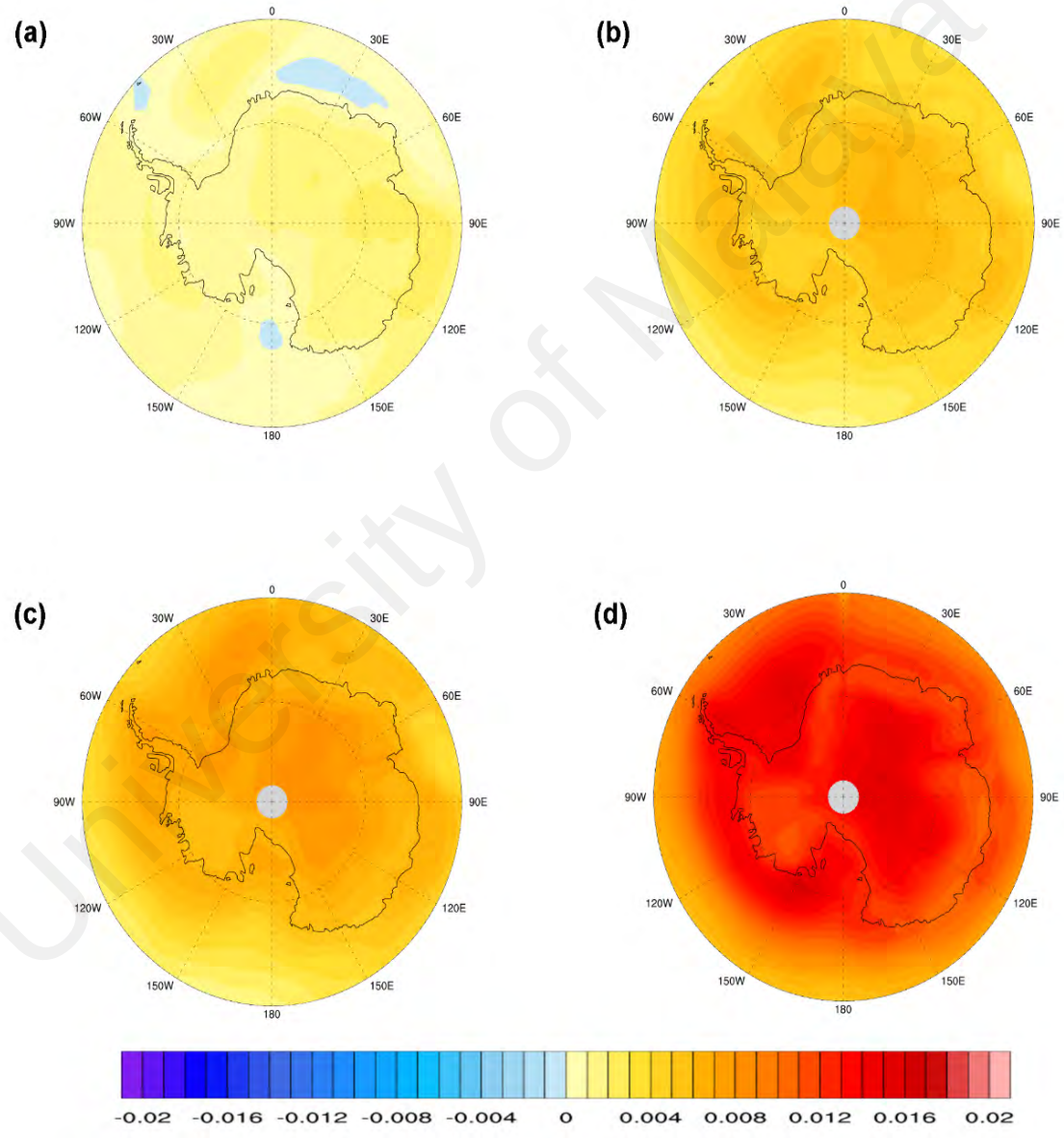

Figure 4.20 Spatial trend of SAT (^{o}C year^{-1}) calculated from CMIP5 MMM for (a) RCP 2.6; (b) RCP 4.5; (c) RCP 6.0; and (d) RCP 8.5.

One important observation that can be seen in Figure 4.20 is the high SAT trend in the interior extending northward from the South Pole. Apart from that, other regions that are expected to experience high SAT trends include the Weddell Sea off the coast of Halley station, the western side of the Peninsula, extending along the coast towards Marie Byrd Land, and the coast off Wilkes Land. There are several spots where the SAT shows a negative trend in the RCP 2.6 scenario: the Ross Sea, north of Dronning Maud Land, and at the tip of Peninsula. The "hotspots" shown in Figure 4.20(b)-(d) are not identical to the four climatological centers of low pressure in the Antarctic coastal region that are responsible for precipitation. Figure 4.20 gives a more in-depth insight into the time series of SAT shown in Figure 4.18 and Figure 4.19: the relatively lower trends in Marie Byrd Land compared to the coastal regions lowers the overall SAT trend in the West Antarctica. Similarly, the East Antarctica is much larger in land area compared to either the Peninsula or the West Antarctica, covering approximately 66% of the landmass area in the continent. With only a single spot that experiences relatively high trend while the rest of the East Antarctica has relatively lower trend, the overall trend of the East Antarctica SAT will therefore be lower. Comparatively, the Peninsula is much smaller in size, and the tip of the Peninsula extends beyond the Antarctic Circle. More area in Peninsula is projected to have higher SAT trend, thus driving up the overall SAT trend of Peninsula. It is also interesting to see that under the RCP 8.5 scenario, the eastern side of the Peninsula has a higher SAT trend compared to the western side.

CHAPTER 5: DISCUSSIONS

For chapter five, the discussions will be conducted according to the different works: the first part being the precipitation instruments work; followed by the assessment of historical precipitation; and finally the assessment of future precipitation. Following the discussion, there will be a conclusion for the work.

5.1 Discussion: Precipitation instruments in Rothera Station, Antarctic Peninsula, A comparative study

5.1.1 The effects of wind

Our study indicates that wind has a profound effect on the TBGs and the LBSs. The TBGs are generally less sensitive to precipitation compared to the LBSs, which can be attributed to effects of the funnel and the nature of snow particles in Antarctica. In the Antarctic, snow particles consist of ice crystals that can be very small and light (Lachlan-Cope et al., 2001), and therefore susceptible to even the slightest breeze. It is not uncommon to see snow particles travelling horizontally or even upward in strong wind. Therefore, the TBGs, which rely heavily on gravitational pull to bring precipitation particles into the funnel, can only be efficient under low wind conditions. Moreover, wind tends to blow the snow particles, even those already falling down the funnel, out of the snow gauge. Folland (1988) proposed that the design of precipitation gauges would cause an updraft at the leading edge, creating an upward deflection of snow particles (Folland, 1988). One method to reduce the effect of wind is to install a wind shield around the TBG. One of the most widely used wind shields is the Alter shield. Installation of the Alter shield helps to reduce the flow speed and distortion around the precipitation instrument, improving snow detection (Rasmussen et al., 2012).

Wind also affects the LBSs by blowing the snow particles in multiple directions, sometimes travelling up and down or in a loop. This could cause a snow particle to cross

the beam of the sensor multiple times, introducing error to the measurement. Moreover, strong wind can blow ground snow towards an LBS, which reads every particle that passes through the beam path, resulting in false readings. During periods of low wind, the precipitation measurements given by the LBSs were very close to the value given by the GPCP. During strong wind events, the GPCP 1DD precipitation values were relatively low. This could be caused by the GPCP's inability to capture the effect of wind as accurately as in situ instruments. Wind effects interfere with our ability to accurately record precipitation in Antarctica.

5.1.2 Instrumental problems

One of the main observations of our study was the failure of the CS700H to function properly and deliver reliable precipitation measurements. After the first month of observations, a significant difference between the data obtained from the CS700H and the other instruments was observed. While the five gauges did not yield precisely the same precipitation amounts, the results obtained by the CS700H were markedly lower than that of all other instruments. An inspection revealed that the heating element of the CS700H required higher-than expected power input in order to function properly. Based on its specification, the CS700H requires 10 to 30 VDC or 12 to 28 VAC, while the PWS-100 requires only 9 to 24 VDC (or 9 to 16 VDC with CS215-PWS Temperature and Relative Humidity (RH) sensor) and the LPM 12 VDC version requires an additional heater 230VAC/150 VA. The CS700H can be a power-saving option as it can turn on its heater only when needed. Subsequent repair was insufficient to keep the instrument working properly, which accounts for the different results from this instrument compared to other instruments.

The LBS also had problems in the harsh environment of the Antarctic. There were multiple instances (10 readings) when blowing snow blocked the sensor head of the LPM,

causing unrealistic readings. At one point the error registered by the LPM was 1317.84 mm in a single day. After removing observations that had registered blockage of the sensor head by snow, the daily mean precipitation for the LPM became 5.83 mm, a marked reduction compared to the original reading and a value much closer to the readings reported by the VPF-730, the PWS-100 and the UPG-1000. The LPM has an internal heating feature similar to that of the UPG-1000 and the CS700H, as mentioned above. However, the LPM installed at Rothera did not have the internal heater turned on.

5.1.3 Heating feature

One of the major problems observed on the CS700H was the formation of ice that blocked the funnel. This blocking did not happen to the UPG-1000. The two instruments use the same working principle and heating element, but the UPG-1000 has a wide, bowl-shaped bucket that absorbs sufficient heat to ensure that freezing does not occur, whereas the CS700H has a much narrower design and a funnel that slopes heavily towards the tipping bucket. Under heavy precipitation conditions, a snow particle that falls into the CS700H slides quickly towards the tipping bucket and can refreeze before dropping into the tipping bucket. The narrower design of the CS700H could also be the reason why the CS700H measured less precipitation compared to the UPG-1000 when the two instruments were active during the first month of operation.

The heating function of the TBGs can also be a disadvantage. The air of the Antarctic is relatively dry compared to the mid-latitudes and tropics. Water, therefore, can evaporate easily under the right conditions. While the process of evaporation is not entirely temperature dependent, the rate of evaporation is positively correlated with temperature. When the heating function of the CS700H is turned on – when it is meant to maintain the temperature of funnel at around 10°C – it could possibly provide enough heat not only to melt, but also evaporate, the precipitation. The UPG-1000, on the other hand, turns on the

heater when the ambient temperature approaches zero and maintains the temperature at around 3°C. This would result in much higher loss to evaporation in the CS700H, leading to inaccurate measurements. The heating element on the LBSs does not cause a loss in measured precipitation because it functions only to prevent snow from blocking the sensor head and the measured snow particles are not in direct contact with the heated sensor head.

5.1.4 Conclusion

Quantifying precipitation in Antarctica involves unique challenges, such as wind and technical difficulties associated with the harsh environment. This study compared a variety of precipitation measurements in Antarctica, including field instruments, satellite data and available reanalysis data sets. Among the instruments, the TBGs were generally less sensitive than the LBSs. The most sensitive LBS (VPF-730) registered 276 precipitation days out of a total of 348 days, while the most sensitive TBG (UPG-1000) detected 152 precipitation days. The LPM had the highest mean daily precipitation during the study period, followed by other LBSs – the PWS-100 and the VPF-730 (5.102 mm) – and the TBGs UPG-1000 and CS700H. Case studies of the precipitation results and seasonal accumulation results show that the VPF-730 may be the most reliable precipitation instrument. The precipitation amounts given by the reanalyses were significantly correlated with wind speed. JRA-55 was the most affected by wind speed, giving precipitation amounts significantly higher than the other reanalysis as well as instrument measurements. It should be noted that the measurement included blowing snow and real precipitation. The comparison between the instruments, reanalyses, model and the GPCP 1DD shows that the GPCP 1DD results were closest to CFSv2, while for the instruments the measurements from GPCP 1DD were closest to the UPG-1000. The LPM and the CS700H experienced instrumental error during the study, which caused precipitation readings to be exceedingly high and low, respectively. Installing multiple

LBSs in different locations (in close proximity) can help identify inconsistencies in the readings.

5.2 Discussion: Assessment of historical precipitation in Antarctica using CMIP5 models, reanalysis datasets and GPCP.

5.2.1 Discussions and summary

For the precipitation time series, the large model spread is significant, up to 260.96 mm year^{-1} between the highest and lowest mean precipitation. The precipitation amount shown by the reanalyses is also significantly different from each other, for instance the difference between mean CFSR precipitation and ERA-Interim precipitation is 196.68 mm year^{-1}. Most CMIP5 and reanalyses models are unable to simulate a consistent spatial and temporal precipitation pattern for the Antarctic (Tang et al., 2018b). This weakness in both the reanalyses and CMIP5 models to simulate precipitation has recently becoming more well-known among scientists, with various authors calling for caution when using the reanalyses as a measuring standard (Bromwich et al., 2011; Nicolas et al., 2011). Nonetheless, the use of reanalyses as by researchers as the standard of measurement for precipitation is still prevalent. More importantly, our calculation shows that the CMIP5 MMM shows a significant increase in precipitation (2.90 ± 0.61 mm decade^{-1}), which is in contrast to earlier studies published by different authors. This discrepancy could be due to the inclusion of more CMIP5 models compared to earlier studies.

For SAT, the difference in mean SAT between the reanalyses is insignificant (1.68 °C). There are certain peaks and trough in SAT that can be seen in the reanalyses data which are caused by the integration of new observation system in the satellite. As for the CMIP5 models, the difference between the highest and lowest model is also significant (difference up to 8 °C). However, the reanalyses SAT time series is more uniform and has high correlation with one another. This consistency is due to the assimilation of

temperature observation data in the reanalysis datasets. 19 of the 49 models show a significant increase while 3 models show significant decrease. Over half of the CMIP5 models show no significant change in SAT trend. More importantly, our calculation shows that the MMM has a significant increase in SAT.

One important caveat to note when comparing the historical time series shown in Figure 4.6 and Figure 4.10 is that for the CMIP5 models, the years are somewhat nominal i.e. the climate models for the year 1990 are not the same as the reanalyses for the year 1990. This is because the drivers of CMIP5 output are the effect of GHG, aerosols, ozone and other factors, while the reanalyses are driven by numerical models anchored by real-world measurements. It is therefore not possible to expect the time series in the historical CMIP5 runs to follow the reanalyses'. For the trend plots (Figure 4.7, Figure 4.11 and Figure 4.14), however, the CMIP5 runs are merely responses to the forcings without taking into account any natural variability and hence can be compared against the reanalyses.

One of the reasons for the large differences in precipitation amount is the resolution of each models. It should be noted that the CMIP5 models used in this work were retained in their native resolution to preserve the accuracy of the simulated results. The lack of resolution means the CMIP5 models were unable to capture and resolve the topographic features of the Antarctic, especially in region such as the Peninsula. This could explain why the CMIP5 models fail to replicate properly the spatial trend of precipitation discussed in earlier sections. While some models could simulate a highly-detailed spatial map of Antarctic precipitation by themselves, the calculation of MMM requires all the models to be regridded to a common 2.50° × 2.50° resolution. This step severely sacrificed the high resolution models and consequently affected the resulting MMM precipitation amount. The alteration of the resolution not only cost the MMM the ability

to resolve the effect of topography, but also the effect of other meteorological factors, for example wind and sea-ice extent.

Higher resolution models, theoretically, could better resolve the topography of the continent and hence could better produce a more convincing precipitation and SAT pattern. Nonetheless, we observed that the higher resolution models did not necessarily simulate a better or more convincing spatial trend of precipitation. Among the three highest resolution models (1.0° × 1.0°) were BCC-CSM1-1-m, EC-EARTH and MRI-CGCM3. The BCC-CSM1-1-m, for example, was incapable of simulating the decreasing trend in Adélie Land that was featured on every spatial map of the reanalyses. The EC-EARTH, on the other hand, simulated a much higher precipitation increase in the coast of West Antarctica than the Peninsula, while the MRI-CGCM3 simulated a decreasing precipitation trend at the coast of West Antarctica—all of which were different compared to the results from the reanalyses. It is impossible to identify one factor that causes these differences in the models because different models handle the forcing of GHG and ozone recovery differently (Zheng et al., 2013), and this difference in the forcing would result in simulations of other phenomenon that have an influence on precipitation, for example the variability of teleconnections such as SAM, cyclones, the variability of sea ice, and many more.

The relationship between SAT and precipitation was examined in Figure 4.14. A large number of the CMIP5 models were within quadrant one and three, with the exception of eight models. We calculated the slope of the regressed linear line (Δprecipitation (%) per temperature) to be 10.45 mm $°C^{-1}$. For relative precipitation changes (Δprecipitation (%)) against the changes in surface air temperature (ΔSAT), a linear regression produces precipitation trend, $\Delta P = 2.13\ \Delta SAT + 1.00$ for the entire coverage area. In comparison with previous works, the value of the slope reported by (Palerme et al., 2017b), for

instance, was 7.4 for the whole continent, 7.0 for the coastal region, and 9.3 for the interior of the continent. One of the reasons the value of our calculated slope is on the lower end of values reported in previous studies is because it covered the entire study area of 60-90^{o}S including the Southern Ocean. The surrounding ocean plays a major role in the climate of Antarctica. The effect of sea level pressure and sea surface temperature, for instance, form the basis for SAM and ENSO. These teleconnections have significant effect on the climate of Antarctica especially on the western coast of the continent (Clem et al., 2016; Fogt et al., 2011; Rahaman et al., 2019). The dynamic of the atmosphere-ocean interaction could affect or offset the dynamic of the atmospheric-land interaction, thereby altering the result of this calculation

Moreover, the number of CMIP5 models used in this work also exceeded that of previous work (Palerme et al., 2017b). A larger number of model could result in more variability in the result as different models behave differently in terms of physics. In addition, this study used the CMIP5 suite of models while previous works included results generated from limited number of AOGCM models (Gregory et al., 2006) or a different type of model (LMDZ4 atmospheric general circulation model) (Krinner et al., 2007).

Another important observation that we noted throughout our work is the small σ of MMM. For the MMM of 49 models, we considered the unweighted mean, giving every model an equal weight in the calculation. Many researchers cite the advantage of having less error as the main reason for using the MMM (Chenoli et al., 2017; Shu et al., 2015). However, as we often see in our work, the large variation of each model often cancel each other out, thus creating a dampened MMM with a very small σ value, a phenomenon that is commonly known among researchers (Deser et al., 2012; Zheng et al., 2013). For instance, Shu et al. (2015)— in a study of sea ice simulation using CMIP5 models— investigated the reliability of using MMM as a measuring metric, calculated the ratio of

sea ice extend (SIE) and sea ice volume (SIV) RMSE between the errors calculated using different number of CMIP5 models and the error calculated from 49 models. The study concluded that the model errors do indeed reduce with increasing model numbers. However, this trend gradually decrease when the model number exceeds 40 models and eventually the model errors become constant. The author wrote that for the study of Antarctic sea ice, the maximum number of models that should be included in a study should be less than or equal to around 40 CMIP5 models (Shu et al., 2015). However, different parameters would have different variability, and hence more study is needed to investigate the ideal number of models suitable for the study of precipitation.

5.2.2 Conclusion

49 CMIP5 models and four reanalysis datasets were used to examine the historical trends of Antarctic precipitation and SAT for the year 1979 to 2005. The results suggest that there is a relationship between the changes in precipitation and SAT. The time series show that the MERRA and JRA-55 precipitations have increased significantly since 1979, while the ERA-Interim and CFSR precipitations have only changed insignificantly. The reanalyses have low correlation with one another (generally less than +0.69). 37 of the 49 CMIP5 models have shown increasing trend, 18 of which are significant. CMIP5 models has mean precipitation that range from 33.63 mm month^{-1} (FGOALS-s2) to 55.38 mm month^{-1} (BNU-ESM), with the MMM precipitation of 41.91 mm month^{-1}. The resulting CMIP5 MMM also has a significant increasing trend of 0.29 ± 0.06 mm year^{-1}. For SAT, the CFSR shows the highest mean SAT (−15.93 °C) while the MERRA has the lowest mean SAT (−17.62 °C). The CMIP5 model spread for SAT range from −21.72 °C to−4.0 °C with the MMM SAT -17.78 °C. The reanalyses show insignificant changes and have high correlation with one another, while the CMIP5 MMM shows a significant increasing trend. Nonetheless, the variability of precipitation and SAT MMM could affect the significance of its trend. The variability of the MMM decreases rapidly with increasing

participating models. More study is needed to investigate the optimum number of models that is advisable for study of precipitation MMM.

5.3 Discussion: Future precipitation in Antarctica under four RCP scenarios using CMIP5 models.

5.3.1 Discussions and summary

From the projection of precipitation and SAT shown in Figure 4.17, it can be seen that the Peninsula will be receiving higher precipitation regardless of scenarios. The projection of SAT also shows a similar result (Figure 4.20). Under the RCP 6.0 and RCP 8.5 scenario, the effect of the winds is especially apparent—low humidity with elevated temperature, as shown in Figure 4.17(c), (d) and Figure 4.20(c), (d). This notion is supported by the work of Zheng et al. (2013), who used 43 CMIP5 models to project future SAM index and found that the SAM will become stronger towards the end of the century. Stronger upwind flow during the positive SAM phase is believed to aid the advection of air over the Antarctic peninsula, which leads to a buildup of surface temperature as the air descends over the Larsen region (Zheng et al., 2013). However, it is important to note that the effect is only apparent under the RCP 6.0 and RCP 8.5 scenario, and less visible in the other scenarios.

One of the reasons —apart from low GHG concentration— the effect of wind is less apparent in other scenarios is probably because of the low resolution of the CMIP5 models. The commonly used grid (1.0^o to 3.0^o) of the CMIP5 models is not fine enough to resolve the complicated topography particularly in the Peninsula region. Studies have shown that a resolution of around ~10 km (about 0.01^o resolution) is required in order for the model to simulate the effect of Foehn winds on the lee side of the Peninsula (van Lipzig et al., 2008). In addition, most of the CMIP5 models have different level of resolution between themselves. Higher resolution models would naturally be able to simulate the RCP runs with higher degree of accuracy and precision. The calculation of MMM, however, requires all the models to be regridded to a common $2.50° \times 2.50°$ resolution. This step severely downgraded the overall resolution of the MMM and

consequently affected the outcome of the simulation. The downgrade of the resolution affected the MMM's ability to simulate the influence of topography and the surrounding ocean, which could then affect other meteorological factors such as temperature, wind, sea level pressure and so on.

The initial list of models used in this work comprises of 46 CMIP5 models. However, not all models contain a complete list of RCP 2.6, RCP 4.5, RCP 6.0, ad RCP 8.5 dataset. Moreover, during data analysis, some models do not have a complete run of the RCPs experiment that range from the year 2006-2100. Some models have datasets that end in the year 2035, while some have dataset that span 2006-2095. Therefore, some models were discarded from the MMM calculation during data analysis in order to preserve the 2006-2100 study period. This may have an effect on the resulting trends of the different experiment. For example, the trends of the MMM in East Antarctica and Peninsula under RCP 2.6 is significant, while the trend of MMM in West Antarctica is not. The number of participating models and the variability of MMM can affect the resulting trend. It is hard to pinpoint one particular reason for the discrepancies observed in the models because each model forces GHG concentration and ozone recovery differently. This difference in the forcing would lead to simulations of other phenomenon such as teleconnections, cyclones, the variability of sea-ice, and others that would in turn have an influence on precipitation.

5.3.2 Consistency of CMIP5 projections

The consistency of CMIP5 models' simulation is an important factor to consider when interpreting the results of projection. It is a common practice to include models that have high level of similarity to a standard of comparison (for example, reanalysis dataset or satellite observation) in the historical experiment to be used to project future scenarios. The ability of the CMIP5 models to simulate historical SAT results accurately is well-

documented (Agosta et al., 2015; Palerme et al., 2017b; Tang et al., 2018b). In the historical experiment, different CMIP5 models are able to simulate similar SAT climatology, trends, and seasonal variability, with high degree of correlations (over +0.90) with one another. This means that all the models, despite all their differences in physics and algorithms, are able to simulate more or less similar results compared to the standard of comparison (for instance, reanalysis datasets or satellite observations) and to one another. Given the exceptional performance of CMIP5 models in simulating SAT under the historical experiment, most models will no doubt be included in the projection of future scenario. Under the RCPs experiments, however, the models do not project consistent simulation of neither SAT nor of precipitation. The differences between the models are significant, the correlations between the models are low, and the trends of the projections are also very different, particularly for lower GHG concentration scenarios.

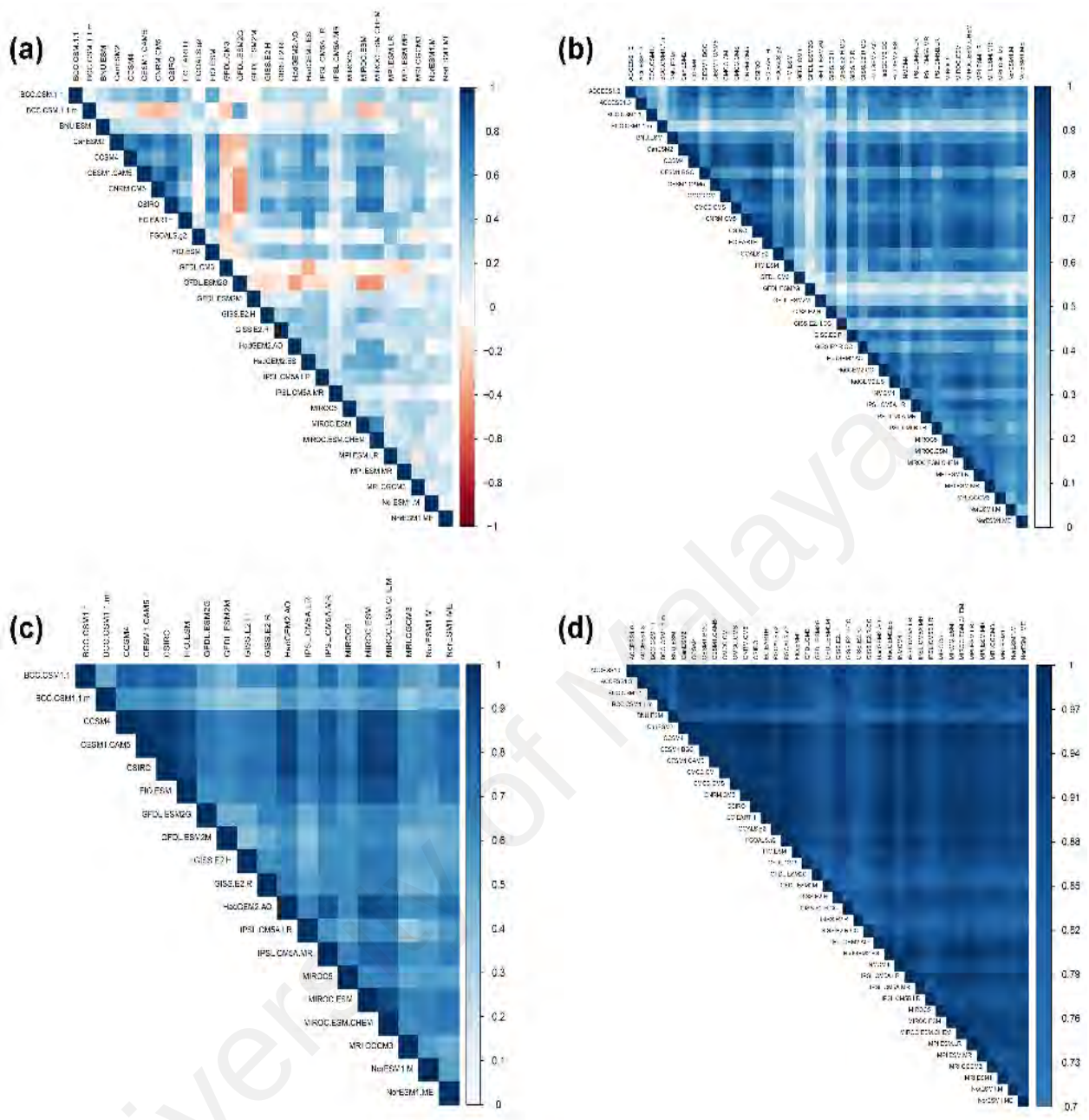

Figure 5.1 Correlation between the models in simulating precipitation under (a) RCP 2.6; (b) RCP 4.5; RCP 6.0; RCP 8.5 scenario. For enlarged plot please refer Supplementary 10 in the Appendix.

In the RCP 2.6 precipitation scenario, for instance, there are several instances where the correlation between the models is negative (Figure 5.1 (a)), and many instances where the correlation is zero. As the concentration of GHG increases from RCP 4.5 to RCP 8.5, the results from the models begin to become more consistent with one another. In the

RCP 8.5 scenario, most of the models have correlation of +0.70 with one another, which means that the models are able to provide a consistent projection under high GHG concentration scenario. The same phenomenon also occurs in the SAT simulation: in the RCP 2.6 and RCP 4.5 scenarios, there are several models that have negative correlations with one another, and some with zero correlation. As the GHG concentration increases from RCP 2.6 to RCP 8.5, the correlation between the models begin to become consistent (mostly over +0.80).

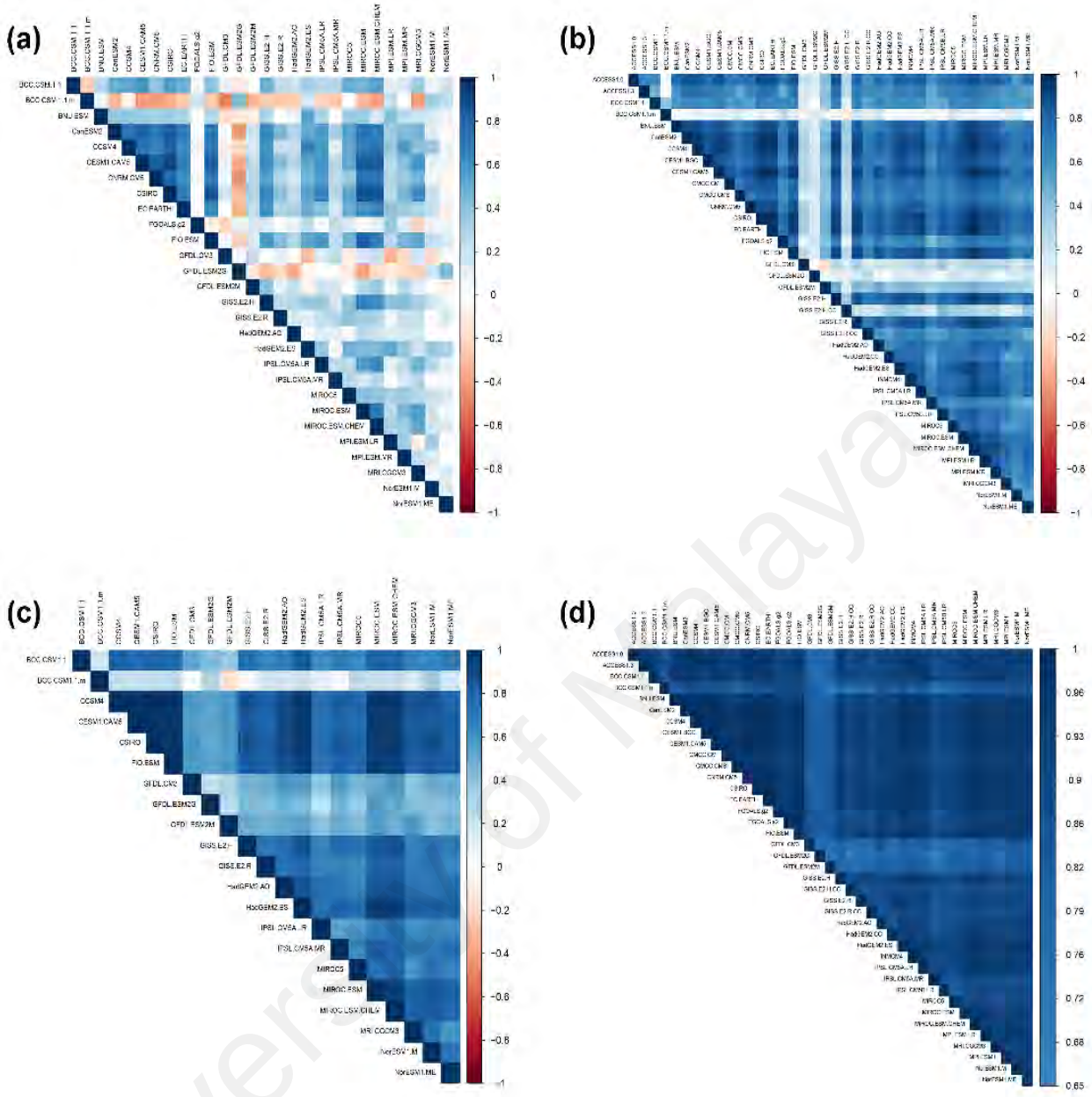

Figure 5.2 Correlation between the models in simulating SAT under (a) RCP 2.6; (b) RCP 4.5; RCP 6.0; RCP 8.5 scenario. For enlarged plot please refer Supplementary 11 in the Appendix.

From Figure 5.1 and Figure 5.2, the lowest correlation between the models can be seen clearly by noting the faintest-colored band across and down in the figures. The GFDL suite of models, in particular, have the lowest correlations with other models. The GFDL-ESM2M and GFDL-ESM2G, for example, have the lowest precipitation correlation

against other models in RCP 4.5 scenario, while the GFDL-CM3 has the lowest correlation in the RCP 2.6 scenario. The GFDL models are also the lowest correlating models in simulating the SAT with one additional model: BCC-CSM-1-1m. There are very few models that have high correlation (over +0.80) with one another for RCP 2.6 and RCP 4.5, for example CanESM2, CCSM4, CSIRO and EC-EARTH. Further study is needed to investigate the reason for the failure of the CMIP5 models to simulate a uniform SAT and precipitation result under RCP scenarios.

5.3.3 Relationship between SAT and precipitation

The relation between SAT and precipitation is governed by the Clausius-Clapeyron relation. Warmer SAT contains higher level of moisture, which can become more significant under relatively low temperature circumstances (Pall et al., 2007). As the moisture-rich air travels towards the Antarctic continent, the high topography of the region lifts the warm air (orographic lifting) and causes the moisture to condensate and fall as precipitation. In the real world, however, the relationship between SAT and precipitation may not be so straightforward, as precipitation can be affected by many other factors such as sea-ice distribution (Weatherly, 2004), cyclone activities (Turner et al., 1995), orographic effect (van Lipzig et al., 2004), or teleconnections like the SAM and ENSO (Marshall, 2003). Under the RCP 2.6 scenario, the correlation between SAT and precipitation can be either positive or negative, which means that the role of SAT is merely complementary to other precipitation factors such as SST and SAM.

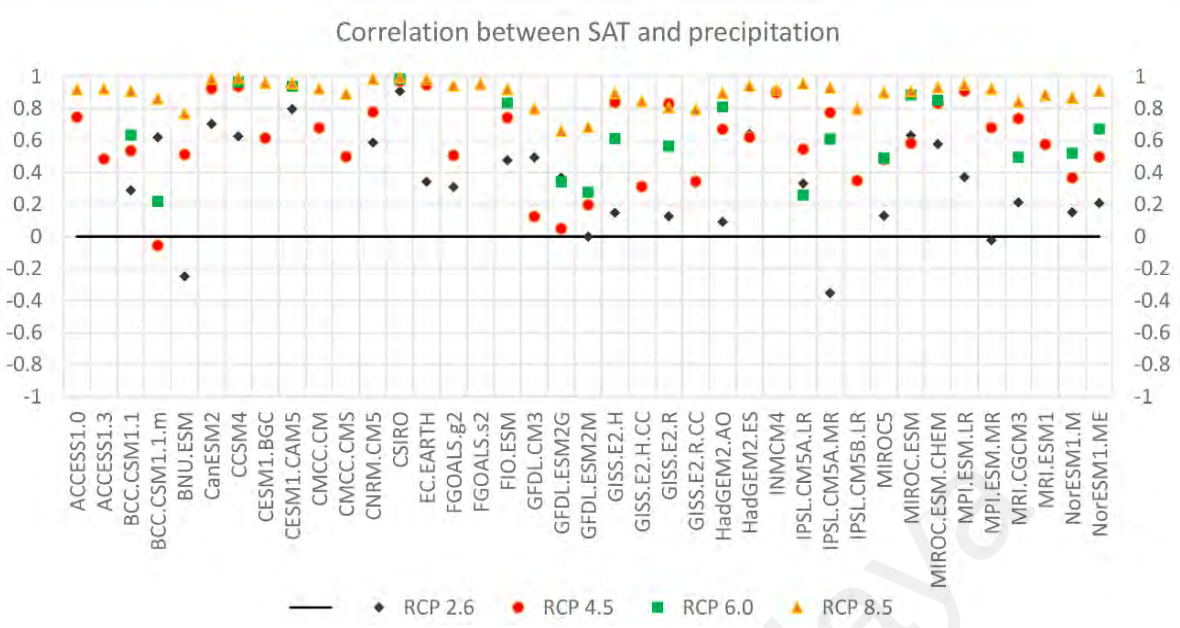

Figure 5.3 Correlation between SAT and precipitation under RCP 2.6, RCP 4.5, RCP 6.0, and RCP 8.5 scenarios. Note that this list is made up of models that have both precipitation and SAT data only.

For RCP 4.5 scenario, there are also several models that show negative SAT-precipitation correlations, but generally most models show positive SAT-precipitation correlation. As the concentration of GHG increases further, the correlations between SAT and precipitation increases (Figure 5.3). Under the RCP 8.5 scenario, all models show correlation above +0.60 between SAT and precipitation. Another interesting observation that can be made is the large variation of the correlation index between RCP 2.6 to RCP 8.5. For RCP 8.5, the differences in the correlation index is relatively smaller compared to either RCP 2.6 or RCP 4.5. It is possible that as GHG concentration continues to increase (RCP 8.5), the subsequent rise in SAT will become the dominant factor in affecting precipitation.

5.3.4 Conclusion

This work uses using 46 CMIP5 global climate models to study the projected precipitation and SAT temporal and spatial trends for 2006-2100 (95 years) under four different RCPs scenarios. For precipitation, the Peninsula has the highest trend regardless of scenario (over 0.02 mm $year^{-1}$ for RCP 8.5), followed by the coast of Enderby Land and Kemp Land, Shackleton Ice Shelf, the coastal area of Dronning Maud Land, and the coastal area of Amundsen Sea. For SAT, the interior region will have the highest trend (over +0.016^{o}C $year^{-1}$), followed by the Weddell Sea off the coast of Halley station, the western side of the Peninsula, extending along the coast towards Marie Byrd Land, and the coast off Wilkes Land. The effect of heightened wind is most apparent under the RCP 8.5 scenario—signaled by increasing temperature and decreasing precipitation along the lee side of Peninsula. For the projection of SAT, the consistency of the CMIP5 models in simulating accurate historical SAT climatology no longer appear in the RCP experiments. However, the consistency of the projection from different models increases as the GHG concentration increases. The correlation between SAT and precipitation increases as the GHG concentration increases. Further study is needed to investigate the reason for the failure of the CMIP5 models to simulate a consensual SAT and precipitation result under RCP scenarios.

CHAPTER 6: CONCLUSIONS

6.1 Main Findings

The work completed in this thesis has resulted in the first published work on

1) The comparison of precipitation instruments in Antarctica;
2) A study on historical precipitation of Antarctica using output from CMIP5 models, reanalysis datasets and satellite data;

and a study on future Antarctic precipitation as well as surface temperature using CMIP5 models under four RCPs scenarios.

The main findings from this research are:

1. Laser-based precipitation sensors are much more reliable compared to tipping bucket gauges. The most sensitive laser-based sensor (VPF-730) detection is almost twice as sensitive as the best tipping bucket gauge (UPG-1000). The LBS also registered higher mean daily precipitation compared to TBGs. Detailed case studies of the precipitation and seasonal accumulation results with wind and temperature data show that the VPF-730 may be the most reliable precipitation instrument for measuring blowing snow and precipitation.
2. The LPM and the CS700H encountered instrumental malfunction during the course of the work, which produced erroneous precipitation readings. The LPM was blocked by drifting snow, which caused extremely high readings. The CS700H, on the other hand, experienced failure in its heating element, causing snow to accumulate, freeze and subsequently block the funnel. As a result, the readings from CS700H were extremely low. Installing multiple LBSs in different locations (in close proximity) can help identify inconsistencies in the readings.

3. For the study of precipitation instruments, the precipitation amount of reanalysis datasets was significantly correlated with wind speed. Among the reanalysis datasets the JRA-55 was most affected by wind speed, giving significantly higher precipitation amounts than the other reanalysis during windy period. Precipitation from the satellite data GPCP 1DD was closest to the value produced by CFSv2 and the UPG-1000.
4. For the study of historical precipitation and temperature in Antarctica using CMIP5 and reanalysis dataset, the results show that there is a relationship between precipitation and SAT. The results show that the precipitation trend for MERRA and JRA-55 have increased markedly since 1979.The ERA-Interim and CFSR precipitation trends are insignificant. 37 of the 49 CMIP5 models show increasing trend, 18 of which are significant. The CMIP5 MMM has a significant increasing trend of 0.29 ± 0.06 mm year^{-1}. For SAT, the CMIP5 MMM is -17.78 °C. The results show that the reanalysis datasets' SAT has insignificant trends and have high correlation with one another, while the CMIP5 MMM has a significant increasing trend. It is important to note that the variability of precipitation and SAT MMM has a profound influence on the significant level of its trend. The variability of the MMM decreases rapidly with increasing participating models.
5. In order to assess the relationship between precipitation and SAT, we derived the relative precipitation changes (Δprecipitation (%)) against the variation in air temperature (ΔSAT). A linear regression produces precipitation trend, $\Delta P = 2.13\ \Delta SAT + 1.00$, or 2.13% $^{o}C^{-1}$.
6. For the study of future precipitation and SAT in Antarctica under four RCPs scenarios of CMIP5, the work is intended for submission for publication in the near future. For precipitation, the Peninsula has the highest increasing trend under all four scenarios, followed by the coast of Enderby Land and Kemp Land,

Shackleton Ice Shelf, the coastal area of Dronning Maud Land, and the coastal area of Amundsen Sea. For SAT, the high plateau of East Antarctica will have the highest increasing trend for the year 2006-2100 under all four scenarios, followed by the Weddell Sea off the coast of Halley station, the western side of the Peninsula, extending along the coast towards Marie Byrd Land, and the coast off Wilkes Land.

7. Different CMIP5 models can simulate similar historical SAT climatology. However, in the RCP experiments the CMIP5 models output can be significantly different from one another. This phenomenon reduces as the GHG concentration increases from RCP2.6 to RCP 8.5. In addition, the correlation between SAT and precipitation increases as the GHG concentration increases.

6.2 Recommendations for future work

The work described herein presents several recommendations for further research.

1. One suggestion of future work involves installing precipitation instruments for longer period of time in Antarctica. In our work, the study period was only for one year. However, it would be interesting to increase the study period to three or five years and compare the precipitation values with that of reanalysis datasets and satellite data.
2. Secondly, the coverage of the instrumental study could also be expanded to several different stations located several kilometers apart. In this work, all five precipitation instruments were installed at the Rothera station in Antarctic Peninsula, which can be represented as a single point value. However, installing several instruments in several research stations located a few kilometers apart can properly simulate a grid in a reanalysis dataset, and therefore can become a more comprehensive study of the comparison between in-situ measurement and reanalysis dataset.
3. We also recommend researchers to collaborate with manufacturers to come up with better instrument designs for enhancing precipitation measurement in Antarctica. The Alter Shield, one of the most commonly used wind shield for tipping bucket gauges, was developed in 1937. In order to improve the process of precipitation measurement, new technologies should be engaged. Researchers may also include automation in their work to detect instrument malfunction and systematic error that could occur due to harsh weather or electrical outage. In this way, researchers can easily eliminate erroneous data and outlier values in the measurement.
4. For the study of precipitation output from CMIP5 models, it is recommended to study the optimum number of models for the calculation of multi-model mean. As already shown in chapter 4.4, using too many models in the calculation of MMM

may actually reduce the variability of precipitation and cause small trends to become significant. Therefore, future researchers should consider doing statistical study on the optimum number of models that could give the best representative of MMM values in the entire suite of CMIP models.

5. The use of reanalysis datasets as the standard of measurement should be practiced with caution. As shown in chapter 3 and chapter 4, some reanalysis datasets like the JRA-55 and MERRA can give spurious results and sometimes be unreliable, especially for short term study that involves only several months or years. This is because reanalysis datasets are generally more reliable for long term climatology study.
6. Future researchers should also consider exploiting the GPCP-1DD dataset as the primary satellite product for the high latitudes. The product is of much higher spatial (1^{o}) and temporal resolution (daily) as compared to other satellite products.
7. Lastly, this work has been based on a low spatial (up to 3.0^{o} in CMIP5 models) and temporal resolution of precipitation model output (monthly precipitation from CMIP5 models and reanalysis datasets, daily precipitation from precipitation instruments). It would therefore be beneficial if future researchers could utilize more refined data (e.g. GPCP-1DD) which provide higher spatial and temporal resolution that can provide a clearer picture of the state of climate in Antarctica. It is my hope that the WCRP would push the agenda to encourage modeling groups to develop higher resolution models in the future, and that these higher spatial and temporal resolution models could better simulate the hydrological processes in the high latitudes.

REFERENCES

Adler, R. F., Negri, A. J., Keehn, P. R., & Hakkarinen, I. M. (1993). Estimation of Monthly Rainfall over Japan and Surrounding Waters from a Combination of Low-Orbit Microwave and Geosynchronous IR Data. *Journal of Applied Meteorology, 32*(2), 335-356.

Agosta, C., Fettweis, X., & Datta, R. (2015). Evaluation of the CMIP5 models in the aim of regional modelling of the Antarctic surface mass balance. *Cryosphere, 9*, 2311-2321.

Arkin, P., & Meisner, B. N. (1987). *The Relationship between Large-Scale Convective Rainfall and Cold Cloud over the Western Hemisphere during 1982-84*.

Arrigo, K. R., & van Dijken, G. L. (2003). Phytoplankton dynamics within 37 Antarctic coastal polynya systems. *Journal of Geophysical Research: Oceans, 108*(C8). doi: 10.1029/2002jc001739

Bacmeister, J. T., Suarez, M. J., & Robertson, F. R. (2006). Rain Reevaporation, Boundary Layer–Convection Interactions, and Pacific Rainfall Patterns in an AGCM. *Journal of the Atmospheric Sciences, 63*(12), 3383-3403. doi: 10.1175/jas3791.1

Behrangi, A., Lebsock, M., Wong, S., & Lambrigtsen, B. (2012). On the quantification of oceanic rainfall using spaceborne sensors. *Journal of Geophysical Research: Atmospheres, 117*(D20). doi: 10.1029/2012jd017979

Behrangi, A., Tian, Y., Lambrigtsen, B. H., & Stephens, G. L. (2014). What does CloudSat reveal about global land precipitation detection by other spaceborne sensors? *Water Resources Research, 50*(6), 4893-4905. doi: 10.1002/2013wr014566

Bellot, H., Trouvilliez, A., Naaim-Bouvet, F., Genthon, C., & Gallée, H. (2011). Present weather-sensor tests for measuring drifting snow. *Annals of Glaciology, 52*(58), 176-184. doi: Doi: 10.3189/172756411797252356

Bendix, J., Rollenbeck, R., Göttlicher, D., Nauß, T., & Fabian, P. (2008). Seasonality and diurnal pattern of very low clouds in a deeply incised valley of the eastern tropical Andes (South Ecuador) as observed by a cost-effective WebCam system. *Meteorological Applications, 15*(2), 281-291. doi: 10.1002/met.72

Benning, J., & Yang, D. (2005). Adjustment of Daily Precipitation Data at Barrow and Nome Alaska for 1995–2001. *Arctic, Antarctic, and Alpine Research, 37*(3), 276-283.

Bernstein, L., Bosch, P., Canziani, O., Chen, Z., Christ, R., & Riahi, K. (2008). IPCC, 2007: climate change 2007: synthesis report: IPCC.

Biasutti, M., Held, I. M., Sobel, A. H., & Giannini, A. (2008). SST Forcings and Sahel Rainfall Variability in Simulations of the Twentieth and Twenty-First Centuries. *Journal of Climate, 21*(14), 3471-3486. doi: 10.1175/2007jcli1896.1

Bindschadler, R., Choi, H., Shuman, C., & Markus, T. (2005). Detecting and measuring new snow accumulation on ice sheets by satellite remote sensing. *Remote Sensing of Environment, 98*(4), 388-402. doi: https://doi.org/10.1016/j.rse.2005.07.014

Bloom, S. C., Takacs, L. L., da Silva, A. M., & Ledvina, D. (1996). Data Assimilation Using Incremental Analysis Updates. *Monthly Weather Review, 124*(6), 1256-1271.

Boersma, P. D., & Rebstock, G. A. (2014). Climate Change Increases Reproductive Failure in Magellanic Penguins. *PLOS ONE, 9*(1), e85602. doi: 10.1371/journal.pone.0085602

Boyle, J., & Klein, S. A. (2010). Impact of horizontal resolution on climate model forecasts of tropical precipitation and diabatic heating for the TWP-ICE period. *Journal of Geophysical Research: Atmospheres, 115*(D23). doi: 10.1029/2010jd014262

Bromwich, D., Guo, Z., Bai, L., & Chen, Q. (2004). Modeled Antarctic precipitation. Part I: Spatial and temporal variability. *Journal of Climate, 17*(3), 427-447.

Bromwich, D., Nicolas, J., & Monaghan, A. (2011). An Assessment of Precipitation Changes over Antarctica and the Southern Ocean since 1989 in Contemporary Global Reanalyses*. *Journal of Climate, 24*, 4189-4209. doi: 10.1175/2011jcli4074.1

Bromwich, D. H. (1988). Snowfall in high southern latitudes. *Reviews of Geophysics, 26*(1), 149-168. doi: 10.1029/RG026i001p00149

Bromwich, D. H. (1989). Satellite Analyses of Antarctic Katabatic Wind Behavior*. *Bulletin of the American Meteorological Society, 70*(7), 738-749.

Bromwich, D. H., Monaghan, A. J., Powers, J. G., Cassano, J. J., Wei, H.-L., Kuo, Y.-H., & Pellegrini, A. (2003). Antarctic Mesoscale Prediction System (AMPS): A Case Study from the 2000–01 Field Season*. *Monthly Weather Review, 131*(2), 412-434.

Buzzii, A., Cadelli, R., & Malguzzi, P. (1997). Low-level jet simulation over the Southern Ocean in Antarctica. *Tellus A, 49*(2), 263-276. doi: 10.1034/j.1600-0870.1997.t01-1-00007.x

Cape, M. R., Vernet, M., Skvarca, P., Marinsek, S., Scambos, T., & Domack, E. (2015). Foehn winds link climate-driven warming to ice shelf evolution in Antarctica. *Journal of Geophysical Research: Atmospheres, 120*(21), 11,037-011,057. doi: 10.1002/2015jd023465

Carleton, A., McMurdie, L., Zhao, H., Katsaros, K., Mognard, N., & Claud, C. (1993). *Satellite microwave sensing of Antarctic Ocean mesocyclones.* Paper presented at the Proceedings of the Fourth International Conference on Southern Hemisphere Meteorology and Oceanography.

Carrasco, J. F., Bromwich, D. H., & Monaghan, A. J. (2003). Distribution and Characteristics of Mesoscale Cyclones in the Antarctic: Ross Sea Eastward to the Weddell Sea*. *Monthly Weather Review, 131*(2), 289-301.

Chenoli, S. N., Ahmad Mazuki, M. Y., Turner, J., & Samah, A. A. (2017). Historical and projected changes in the Southern Hemisphere Sub-tropical Jet during winter from the CMIP5 models. *Climate Dynamics, 48*(1), 661-681. doi: 10.1007/s00382-016-3102-y

Chenoli, S. N., Turner, J., & Samah, A. A. (2013). A climatology of strong wind events at McMurdo station, Antarctica. *International Journal of Climatology, 33*(12), 2667-2681. doi: 10.1002/joc.3617

Chou, M.-D., Suarez, M. J., Liang, X.-Z., Yan, M. M.-H., & Cote, C. (2001). A thermal infrared radiation parameterization for atmospheric studies.

Chou, M. D. (1999). *A Solar Radiation Parameterization for Atmospheric Studies*: National Aeronautics and Space Administration, Goddard Space Flight Center, Laboratory for Atmospheres, Climate and Radiation Branch.

Clem, K. R., Renwick, J. A., McGregor, J., & Fogt, R. L. (2016). The relative influence of ENSO and SAM on Antarctic Peninsula climate. *Journal of Geophysical Research: Atmospheres, 121*(16), 9324-9341. doi: 10.1002/2016jd025305

Cohen, L., & Dean, S. (2013). Snow on the Ross Ice Shelf: comparison of reanalyses and observations from automatic weather stations. *The Cryosphere, 7*(5), 1399-1410. doi: 10.5194/tc-7-1399-2013

Comiso, J. C. (2000). Variability and Trends in Antarctic Surface Temperatures from In Situ and Satellite Infrared Measurements. *Journal of Climate, 13*(10), 1674-1696.

Connolley, W. M., & Bracegirdle, T. J. (2007). An Antarctic assessment of IPCC AR4 coupled models. *Geophysical Research Letters, 34*(22). doi: 10.1029/2007gl031648

Covey, C., AchutaRao, K. M., Cubasch, U., Jones, P., Lambert, S. J., Mann, M. E., . . . Taylor, K. E. (2003). An overview of results from the Coupled Model Intercomparison Project. *Global and Planetary Change, 37*(1), 103-133. doi: https://doi.org/10.1016/S0921-8181(02)00193-5

Cullather, R. I., Bromwich, D. H., & Van Woert, M. L. (1998). Spatial and Temporal Variability of Antarctic Precipitation from Atmospheric Methods*. *Journal of Climate, 11*(3), 334-367.

Dee, D. P., Uppala, S. M., Simmons, A. J., Berrisford, P., Poli, P., Kobayashi, S., . . . Vitart, F. (2011). The ERA-Interim reanalysis: configuration and performance of the data assimilation system. *Quarterly Journal of the Royal Meteorological Society, 137*(656), 553-597. doi: 10.1002/qj.828

Delworth, T. L., Rosati, A., Anderson, W., Adcroft, A. J., Balaji, V., Benson, R., . . . Zhang, R. (2012). Simulated Climate and Climate Change in the GFDL CM2.5

High-Resolution Coupled Climate Model. *Journal of Climate, 25*(8), 2755-2781. doi: 10.1175/jcli-d-11-00316.1

Deser, C., Phillips, A., Bourdette, V., & Teng, H. (2012). Uncertainty in climate change projections: the role of internal variability. *Climate Dynamics, 38*(3), 527-546. doi: 10.1007/s00382-010-0977-x

Dirmeyer, P. A. (2013). Characteristics of the water cycle and land–atmosphere interactions from a comprehensive reforecast and reanalysis data set: CFSv2. *Climate Dynamics, 41*(3), 1083-1097. doi: 10.1007/s00382-013-1866-x

Dutton, M., Jenkins, T., & Strangeways, I. (2008). *A heated aerodynamic universal precipitation gauge*.

Ebita, A., Kobayashi, S., Ota, Y., Moriya, M., Kumabe, R., Onogi, K., . . . Ishimizu, T. (2011). The Japanese 55-year Reanalysis ``JRA-55'': An Interim Report. *SOLA - Scientific Online Letters on the Atmosphere, 7*, 149. doi: 10.2151/sola.2011-038

Eyring, V., Arblaster, J. M., Cionni, I., Sedláček, J., Perlwitz, J., Young, P. J., . . . Watanabe, S. (2013). Long-term ozone changes and associated climate impacts in CMIP5 simulations. *Journal of Geophysical Research: Atmospheres, 118*(10), 5029-5060. doi: 10.1002/jgrd.50316

Fisher, M., & Courtier, P. (1995). *Estimating the covariance matrices of analysis and forecast error in variational data assimilation*: ECMWF.

Flato, G., Marotzke, J., Abiodun, B., Braconnot, P., Chou, S. C., Cox, P., . . . Rummukaines, M. (2013). Evaluation of Climate Models. In: Climate Change 2013: The Physical Science Basis. Contribution of Working Group I to the Fifth Assessment Report of the Intergovernmental Panel on Climate Change.

Fogt, R. L., Bromwich, D. H., & Hines, K. M. (2011). Understanding the SAM influence on the South Pacific ENSO teleconnection. *Climate Dynamics, 36*(7), 1555-1576. doi: 10.1007/s00382-010-0905-0

Folland, C. K. (1988). Numerical models of the raingauge exposure problem, field experiments and an improved collector design. *Quarterly Journal of the Royal Meteorological Society, 114*(484), 1485-1516. doi: 10.1002/qj.49711448407

Fyfe, J. C., Gillett, N. P., & Marshall, G. J. (2012). Human influence on extratropical Southern Hemisphere summer precipitation. *Geophysical Research Letters, 39*(23). doi: 10.1029/2012gl054199

Fyfe, J. C., Gillett, N. P., & Zwiers, F. W. (2013). Overestimated global warming over the past 20 years. *Nature Climate Change, 3*(9), 767-769.

Gates, W. L. (1992). An AMS Continuing Series: Global Change--AMIP: The Atmospheric Model Intercomparison Project. *Bulletin of the American Meteorological Society, 73*(12), 1962-1970.

Genthon, C., Krinner, G., & Sacchettini, M. (2003). Interannual Antarctic tropospheric circulation and precipitation variability. *Climate Dynamics, 21*(3), 289-307. doi: 10.1007/s00382-003-0329-1

Gregory, J. M., & Huybrechts, P. (2006). Ice-sheet contributions to future sea-level change. *Philosophical Transactions of the Royal Society A: Mathematical, Physical and Engineering Sciences, 364*(1844), 1709-1732. doi: doi:10.1098/rsta.2006.1796

Gultepe, I., Isaac, G. A., Joe, P., Kucera, P. A., Theriault, J. M., & Fisico, T. (2014). Roundhouse (RND) Mountain Top Research Site: Measurements and Uncertainties for Winter Alpine Weather Conditions. *Pure and Applied Geophysics, 171*(1), 59-85. doi: 10.1007/s00024-012-0582-5

Haimberger, L., Tavolato, C., & Sperka, S. (2008). Toward Elimination of the Warm Bias in Historic Radiosonde Temperature Records—Some New Results from a Comprehensive Intercomparison of Upper-Air Data. *Journal of Climate, 21*(18), 4587-4606. doi: 10.1175/2008jcli1929.1

Huffman, G. J., Adler, R. F., Arkin, P., Chang, A., Ferraro, R., Gruber, A., . . . Schneider, U. (1997). The Global Precipitation Climatology Project (GPCP) Combined Precipitation Dataset. *Bulletin of the American Meteorological Society, 78*(1), 5-20.

Hulme, M., Barrow, E., Arnell, N., Harrison, P., Johns, T., & Downing, T. (1999a). Relative impacts of human-induced climate change and natural climate variability. *Nature, 397*(6721), 688-691. doi: 10.1038/17789

Hulme, M., Mitchell, J., Ingram, W., Lowe, J., Johns, T., New, M., & Viner, D. (1999b). Climate change scenarios for global impacts studies. *Global Environmental Change, 9*, S3-S19.

Huybrechts, P., Letreguilly, A., & Reeh, N. (1991). The Greenland ice sheet and greenhouse warming. *Global and Planetary Change, 3*(4), 399-412. doi: https://doi.org/10.1016/0921-8181(91)90119-H

Iserloh, T., Fister, W., Seeger, M., Willger, H., & Ries, J. B. (2012). A small portable rainfall simulator for reproducible experiments on soil erosion. *Soil and Tillage Research, 124*, 131-137. doi: https://doi.org/10.1016/j.still.2012.05.016

Jean-Noël, T., & Kelly, G. A. (2006). Assimilation only surface pressure observations in 3D and 4DVAR.

Jones, R. W., Renfrew, I. A., Orr, A., Webber, B. G. M., Holland, D. M., & Lazzara, M. A. (2016). Evaluation of four global reanalysis products using in situ observations in the Amundsen Sea Embayment, Antarctica. *Journal of Geophysical Research: Atmospheres, 121*(11), 6240-6257. doi: 10.1002/2015jd024680

King, J. C., & Turner, J. (1997). *Antarctic Meteorology and Climatology*. Cambridge: Cambridge University Press.

Kininmonth, W. (2010). Clausius-clapeyron and the regulation of global warming.

Kirchgäßner, A. (2011). An analysis of precipitation data from the Antarctic base Faraday/Vernadsky. *International Journal of Climatology, 31*(3), 404-414. doi: 10.1002/joc.2083

Knuth, S. L. (2007). *Estimation of snow accumulation in Antarctica using automated acoustic depth gauge measurements.* Citeseer.

Knuth, S. L., Tripoli, G. J., Thom, J. E., & Weidner, G. A. (2010). The Influence of Blowing Snow and Precipitation on Snow Depth Change across the Ross Ice Shelf and Ross Sea Regions of Antarctica. *Journal of Applied Meteorology and Climatology, 49*(6), 1306-1321. doi: 10.1175/2010jamc2245.1

Knutti, R., Masson, D., & Gettelman, A. (2013). Climate model genealogy: Generation CMIP5 and how we got there. *Geophysical Research Letters, 40*(6), 1194-1199. doi: 10.1002/grl.50256

Kobayashi, S., Ota, Y., Harada, Y., Ebita, A., Moriya, M., Onoda, H., . . . Takahashi, K. (2015). The JRA-55 Reanalysis: General Specifications and Basic Characteristics. *Journal of the Meteorological Society of Japan. Ser. II, 93*(1), 5-48. doi: 10.2151/jmsj.2015-001

Kochendorfer, J., Rasmussen, R., Wolff, M., Baker, B., Hall, M. E., Meyers, T., . . . Brækkan, R. (2017). The quantification and correction of wind-induced precipitation measurement errors. *Hydrology and Earth System Sciences, 21*(4), 1973.

Köhler, M., Ahlgrimm, M., & Beljaars, A. (2011). Unified treatment of dry convective and stratocumulus-topped boundary layers in the ECMWF model. *Quarterly Journal of the Royal Meteorological Society, 137*(654), 43-57. doi: 10.1002/qj.713

Krinner, G., Magand, O., Simmonds, I., Genthon, C., & Dufresne, J. L. (2007). Simulated Antarctic precipitation and surface mass balance at the end of the twentieth and twenty-first centuries. *Climate Dynamics, 28*(2), 215-230. doi: 10.1007/s00382-006-0177-x

Krzeminski, B., Bormann, N., Kelly, G., McNally, T., & Bauer, P. (2009). Revision of the HIRS cloud detection at ECMWF.

Lachlan-Cope, T., Ladkin, R., Turner, J., & Davison, P. (2001). Observations of cloud and precipitation particles on the Avery Plateau, Antarctic Peninsula. *Antarctic Science, 13*(3), 339-348. doi: Doi: 10.1017/s0954102001000475

Laepple, T., Jewson, S., & Coughlin, K. (2008). Interannual temperature predictions using the CMIP3 multi-model ensemble mean. *Geophysical Research Letters, 35*(10). doi: 10.1029/2008gl033576

Lambert, S. J., & Boer, G. J. (2001). CMIP1 evaluation and intercomparison of coupled climate models. *Climate Dynamics, 17*(2), 83-106. doi: 10.1007/pl00013736

Lassu, T., Seeger, M., Peters, P., & Keesstra, S. D. (2015). The Wageningen Rainfall Simulator: Set-up and Calibration of an Indoor Nozzle-Type Rainfall Simulator

for Soil Erosion Studies. *Land Degradation & Development, 26*(6), 604-612. doi: 10.1002/ldr.2360

Lenaerts, J. T. M., Medley, B., van den Broeke, M. R., & Wouters, B. (2019). Observing and Modeling Ice Sheet Surface Mass Balance. *Reviews of Geophysics, 57*(2), 376-420. doi: 10.1029/2018rg000622

Li, L., & Pomeroy, J. W. (1997). Probability of occurrence of blowing snow. *Journal of Geophysical Research: Atmospheres, 102*(D18), 21955-21964. doi: 10.1029/97jd01522

Ligtenberg, S. R. M., van de Berg, W. J., van den Broeke, M. R., Rae, J. G. L., & van Meijgaard, E. (2013). Future surface mass balance of the Antarctic ice sheet and its influence on sea level change, simulated by a regional atmospheric climate model. *Climate Dynamics, 41*(3), 867-884. doi: 10.1007/s00382-013-1749-1

Little, C. M., & Urban, N. M. (2016). CMIP5 temperature biases and 21st century warming around the Antarctic coast. *Annals of Glaciology, 57*(73), 69-78. doi: DOI: 10.1017/aog.2016.25

Liu, G. (2008). Deriving snow cloud characteristics from CloudSat observations. *Journal of Geophysical Research: Atmospheres, 113*(D8). doi: 10.1029/2007jd009766

Liu, J., Liu, X., Zhu, X., & Yuan, S. (2016). Droplet characterisation of a complete fluidic sprinkler with different nozzle dimensions. *Biosystems Engineering, 148*, 90-100. doi: https://doi.org/10.1016/j.biosystemseng.2016.05.008

Marshall, G. J. (2003). Trends in the Southern Annular Mode from Observations and Reanalyses. *Journal of Climate, 16*(24), 4134-4143.

Marshall, G. J., & Bracegirdle, T. J. (2015). An examination of the relationship between the Southern Annular Mode and Antarctic surface air temperatures in the CMIP5 historical runs. *Climate Dynamics, 45*(5), 1513-1535. doi: 10.1007/s00382-014-2406-z

Mass, C. F., Ovens, D., Westrick, K., & Colle, B. A. (2002). Does increasing horizontal resolution produce more skillful forecasts? The results of two years of real-time numerical weather prediction over the Pacific Northwest. *Bulletin of the American Meteorological Society, 83*(3), 407-430.

Meehl, G. A., Covey, C., Delworth, T., Latif, M., McAvaney, B., Mitchell, J. F. B., . . . Taylor, K. E. (2007). THE WCRP CMIP3 Multimodel Dataset: A New Era in Climate Change Research. *Bulletin of the American Meteorological Society, 88*(9), 1383-1394. doi: 10.1175/bams-88-9-1383

Meehl, G. A., Covey, C., McAvaney, B., Latif, M., & Stouffer, R. J. (2005). Overview of the coupled model intercomparison project. *Bulletin of the American Meteorological Society, 86*(1), 89-93.

Meehl, G. A., Goddard, L., Murphy, J., Stouffer, R. J., Boer, G., Danabasoglu, G., . . . Hawkins, E. (2009). Decadal prediction: Can it be skillful? *Bulletin of the American Meteorological Society, 90*(10), 1467-1486.

Meehl, G. A., Karl, T., Easterling, D. R., Changnon, S., Pielke, R., Jr., Changnon, D., . . . Zwiers, F. (2000). An Introduction to Trends in Extreme Weather and Climate Events: Observations, Socioeconomic Impacts, Terrestrial Ecological Impacts, and Model Projections*. *Bulletin of the American Meteorological Society, 81*(3), 413-416. doi: 10.1175/1520-0477(2000)081<0413:aittie>2.3.co;2

Michaelides, S., Levizzani, V., Anagnostou, E., Bauer, P., Kasparis, T., & Lane, J. E. (2009). Precipitation: Measurement, remote sensing, climatology and modeling. *Atmospheric Research, 94*(4), 512-533. doi: https://doi.org/10.1016/j.atmosres.2009.08.017

Miles, G. M., Marshall, G. J., McConnell, J. R., & Aristarain, A. J. (2008). Recent accumulation variability and change on the Antarctic Peninsula from the ERA40 reanalysis. *International Journal of Climatology, 28*(11), 1409-1422. doi: 10.1002/joc.1642

Mishra, V., Kumar, D., Ganguly, A. R., Sanjay, J., Mujumdar, M., Krishnan, R., & Shah, R. D. (2014). Reliability of regional and global climate models to simulate precipitation extremes over India. *Journal of Geophysical Research: Atmospheres, 119*(15), 9301-9323. doi: 10.1002/2014jd021636

Mo, K. C., Shukla, S., Lettenmaier, D. P., & Chen, L.-C. (2012). Do Climate Forecast System (CFSv2) forecasts improve seasonal soil moisture prediction? *Geophysical Research Letters, 39*(23). doi: 10.1029/2012gl053598

Monaghan, A. J., Bromwich, D. H., Fogt, R. L., Wang, S.-H., Mayewski, P. A., Dixon, D. A., . . . Isaksson, E. (2006). Insignificant change in Antarctic snowfall since the International Geophysical Year. *Science, 313*(5788), 827-831.

Monaghan, A. J., Bromwich, D. H., Powers, J. G., & Manning, K. W. (2005). The Climate of the McMurdo, Antarctica, Region as Represented by One Year of Forecasts from the Antarctic Mesoscale Prediction System*. *Journal of Climate, 18*(8), 1174-1189. doi: 10.1175/jcli3336.1

Montero-Martínez, G., Torres-Pérez, E. F., & García-García, F. (2016). A comparison of two optical precipitation sensors with different operating principles: The PWS100 and the OAP-2DP. *Atmospheric Research, 178-179*, 550-558. doi: https://doi.org/10.1016/j.atmosres.2016.05.007

Moorthi, S., & Suarez, M. J. (1992). Relaxed Arakawa-Schubert. A Parameterization of Moist Convection for General Circulation Models. *Monthly Weather Review, 120*(6), 978-1002. doi: 10.1175/1520-0493(1992)120<0978:rasapo>2.0.co;2

Moss, R. H., Edmonds, J. A., Hibbard, K. A., Manning, M. R., Rose, S. K., van Vuuren, D. P., . . . Wilbanks, T. J. (2010). The next generation of scenarios for climate change research and assessment. *Nature, 463*(7282), 747-756. doi: 10.1038/nature08823

Neale, R. B., Richter, J., Park, S., Lauritzen, P. H., Vavrus, S. J., Rasch, P. J., & Zhang, M. (2013). The Mean Climate of the Community Atmosphere Model (CAM4) in Forced SST and Fully Coupled Experiments. *Journal of Climate, 26*(14), 5150-5168. doi: 10.1175/jcli-d-12-00236.1

New, M., Todd, M., Hulme, M., & Jones, P. (2001). Precipitation measurements and trends in the twentieth century. *International Journal of Climatology, 21*(15), 1889-1922. doi: 10.1002/joc.680

Nicolas, J. P., & Bromwich, D. H. (2011). Precipitation Changes in High Southern Latitudes from Global Reanalyses: A Cautionary Tale. *Surveys in Geophysics, 32*(4), 475-494. doi: 10.1007/s10712-011-9114-6

Nitu, R., Roulet, Y.-A., Wolff, M., Earle, M. E., Reverdin, A., Smith, C. D., . . . Wong, K. (2019). WMO Solid Precipitation Intercomparison Experiment (SPICE)(2012-2015).

Nylen, T. H., Fountain, A. G., & Doran, P. T. (2004). Climatology of katabatic winds in the McMurdo dry valleys, southern Victoria Land, Antarctica. *Journal of Geophysical Research: Atmospheres, 109*(D3). doi: 10.1029/2003jd003937

O'Connor, W. P., Bromwich, D. H., & Carrasco, J. F. (1994). Cyclonically Forced Barrier Winds along the Transantarctic Mountains near Ross Island. *Monthly Weather Review, 122*(1), 137-150. doi: 10.1175/1520-0493(1994)122<0137:cfbwat>2.0.co;2

Onogi, K. (1998). A Data Quality Control Method Using Forecasted Horizontal Gradient and Tendency in a NWP System. *Journal of the Meteorological Society of Japan. Ser. II, 76*(4), 497-516.

Oshima, K., & Yamazaki, K. (2017). Atmospheric hydrological cycles in the Arctic and Antarctic during the past four decades. *Czech Polar Reports, 7*(2), 169-180.

Pachauri, R. K., Allen, M. R., Barros, V. R., Broome, J., Cramer, W., Christ, R., . . . Dasgupta, P. (2014). *Climate change 2014: synthesis report. Contribution of Working Groups I, II and III to the fifth assessment report of the Intergovernmental Panel on Climate Change*: Ipcc.

Palerme, C., Claud, C., Dufour, A., Genthon, C., Wood, N. B., & L'Ecuyer, T. (2017a). Evaluation of Antarctic snowfall in global meteorological reanalyses. *Atmospheric Research, 190*, 104-112. doi: https://doi.org/10.1016/j.atmosres.2017.02.015

Palerme, C., Genthon, C., Claud, C., Kay, J. E., Wood, N. B., & L'Ecuyer, T. (2017b). Evaluation of current and projected Antarctic precipitation in CMIP5 models. *Climate Dynamics, 48*(1), 225-239. doi: 10.1007/s00382-016-3071-1

Palerme, C., Kay, J., Genthon, C., L'Ecuyer, T., Wood, N., & Claud, C. (2014). How much snow falls on the Antarctic ice sheet? *Cryosphere, 8*(4).

Pall, P., Allen, M. R., & Stone, D. A. (2007). Testing the Clausius–Clapeyron constraint on changes in extreme precipitation under CO2 warming. *Climate Dynamics, 28*(4), 351-363. doi: 10.1007/s00382-006-0180-2

Parish, T. R. (1988). Surface winds over the Antarctic continent: A review. *Reviews of Geophysics, 26*(1), 169-180. doi: 10.1029/RG026i001p00169

Parish, T. R., & Bromwich, D. H. (1986). The Inversion Wind Pattern over West Antarctica. *Monthly Weather Review, 114*(5), 849-860. doi: 10.1175/1520-0493(1986)114<0849:tiwpow>2.0.co;2

Parish, T. R., & Bromwich, D. H. (1998). A Case Study of Antarctic Katabatic Wind Interaction with Large-Scale Forcing*. *Monthly Weather Review, 126*(1), 199-209. doi: 10.1175/1520-0493(1998)126<0199:acsoak>2.0.co;2

Parish, T. R., & Cassano, J. J. (2003). The Role of Katabatic Winds on the Antarctic Surface Wind Regime. *Monthly Weather Review, 131*(2), 317-333. doi: 10.1175/1520-0493(2003)131<0317:trokwo>2.0.co;2

Parish, T. R., Cassano, J. J., & Seefeldt, M. W. (2006). Characteristics of the Ross Ice Shelf air stream as depicted in Antarctic Mesoscale Prediction System simulations. *Journal of Geophysical Research: Atmospheres, 111*(D12). doi: 10.1029/2005jd006185

Petoukhov, V., Claussen, M., Berger, A., Crucifix, M., Eby, M., Eliseev, A. V., . . . Weaver, A. J. (2005). EMIC Intercomparison Project (EMIP–CO2): comparative analysis of EMIC simulations of climate, and of equilibrium and transient responses to atmospheric CO2 doubling. *Climate Dynamics, 25*(4), 363-385. doi: 10.1007/s00382-005-0042-3

Pham, D. H., Chu, T. T. H., & Ngo, B. T. (2013). Design and implementation of an automatic hydrological monitoring system for hydropower plants. *Journal of Vietnamese Environment, 4*(2), 34-42.

Polvani, L. M., Waugh, D. W., Correa, G. J. P., & Son, S.-W. (2011). Stratospheric Ozone Depletion: The Main Driver of Twentieth-Century Atmospheric Circulation Changes in the Southern Hemisphere. *Journal of Climate, 24*(3), 795-812. doi: 10.1175/2010jcli3772.1

Pope, V., & Stratton, R. (2002). The processes governing horizontal resolution sensitivity in a climate model. *Climate Dynamics, 19*(3), 211-236. doi: 10.1007/s00382-001-0222-8

Rabier, F., Thépaut, J.-N., & Courtier, P. (1998). Extended assimilation and forecast experiments with a four-dimensional variational assimilation system. *Quarterly Journal of the Royal Meteorological Society, 124*(550), 1861-1887. doi: 10.1002/qj.49712455005

Rahaman, W., Chatterjee, S., Ejaz, T., & Thamban, M. (2019). Increased influence of ENSO on Antarctic temperature since the Industrial Era. *Scientific Reports, 9*(1), 6006. doi: 10.1038/s41598-019-42499-x

Rasmussen, R., Baker, B., Kochendorfer, J., Meyers, T., Landolt, S., Fischer, A. P., . . . Gutmann, E. (2012). How Well Are We Measuring Snow: The NOAA/FAA/NCAR Winter Precipitation Test Bed. *Bulletin of the American Meteorological Society, 93*(6), 811-829. doi: 10.1175/bams-d-11-00052.1

Renfrew, I. A., & Anderson, P. S. (2002). The surface climatology of an ordinary katabatic wind regime in Coats Land, Antarctica. *Tellus A: Dynamic Meteorology and Oceanography, 54*(5), 463-484.

Rienecker, M. M., Suarez, M. J., Gelaro, R., Todling, R., Bacmeister, J., Liu, E., . . . Woollen, J. (2011). MERRA: NASA's Modern-Era Retrospective Analysis for Research and Applications. *Journal of Climate, 24*(14), 3624-3648. doi: 10.1175/jcli-d-11-00015.1

Saha, S., Moorthi, S., Pan, H.-L., Wu, X., Wang, J., Nadiga, S., . . . Goldberg, M. (2010). The NCEP Climate Forecast System Reanalysis. *Bulletin of the American Meteorological Society, 91*(8), 1015-1058. doi: 10.1175/2010bams3001.1

Saha, S., Moorthi, S., Wu, X., Wang, J., Nadiga, S., Tripp, P., . . . Becker, E. (2014). The NCEP Climate Forecast System Version 2. *Journal of Climate, 27*(6), 2185-2208. doi: 10.1175/jcli-d-12-00823.1

Salby, M. L., Titova, E. A., & Deschamps, L. (2012). Changes of the Antarctic ozone hole: Controlling mechanisms, seasonal predictability, and evolution. *Journal of Geophysical Research: Atmospheres, 117*(D10). doi: 10.1029/2011jd016285

Scambos, T. A., Campbell, G. G., Pope, A., Haran, T., Muto, A., Lazzara, M., . . . van den Broeke, M. R. (2018). Ultralow Surface Temperatures in East Antarctica From Satellite Thermal Infrared Mapping: The Coldest Places on Earth. *Geophysical Research Letters, 45*(12), 6124-6133. doi: 10.1029/2018gl078133

Schiffer, R. A., & Rossow, W. B. (1983). The International Satellite Cloud Climatology Project (ISCCP): The First Project of the World Climate Research Programme. *Bulletin of the American Meteorological Society, 64*(7), 779-784. doi: 10.1175/1520-0477-64.7.779

Schubert, S. D., Rood, R. B., & Pfaendtner, J. (1993). An assimilated dataset for earth science applications. *Bulletin of the American meteorological Society, 74*(12), 2331-2342.

Seefeldt, M. W., & Cassano, J. J. (2012). A description of the Ross Ice Shelf air stream (RAS) through the use of self-organizing maps (SOMs). *Journal of Geophysical Research: Atmospheres, 117*(D9). doi: 10.1029/2011jd016857

Seefeldt, M. W., Cassano, J. J., & Parish, T. R. (2007). Dominant Regimes of the Ross Ice Shelf Surface Wind Field during Austral Autumn 2005. *Journal of Applied Meteorology and Climatology, 46*(11), 1933-1955. doi: 10.1175/2007jamc1442.1

Sheffield, J., Barrett, A. P., Colle, B., Nelun Fernando, D., Fu, R., Geil, K. L., . . . Yin, L. (2013). North American Climate in CMIP5 Experiments. Part I: Evaluation of Historical Simulations of Continental and Regional Climatology*. *Journal of Climate, 26*(23), 9209-9245. doi: 10.1175/jcli-d-12-00592.1

Shepherd, A., Wingham, D., Wallis, D., Giles, K., Laxon, S., & Sundal, A. V. (2010). Recent loss of floating ice and the consequent sea level contribution. *Geophysical Research Letters, 37*(13). doi: 10.1029/2010gl042496

Shu, Q., Song, Z., & Qiao, F. (2015). Assessment of sea ice simulations in the CMIP5 models. *The Cryosphere, 9*(1), 399-409. doi: 10.5194/tc-9-399-2015

Silva, G. A., Dutra, L. M., da Rocha, R. P., Ambrizzi, T., & Leiva, É. (2014). Preliminary analysis on the global features of the NCEP CFSv2 seasonal hindcasts. *Advances in Meteorology, 2014*.

Simmons, A., Uppala, S., Dee, D., & Kobayashi, S. (2007). ERAInterim: New ECMWF reanalysis products from 1989 onwards. *ECMWF Newsletter, 110*, 25-35.

Steinhoff, D. F., Chaudhuri, S., & Bromwich, D. H. (2009). A Case Study of a Ross Ice Shelf Airstream Event: A New Perspective*. *Monthly Weather Review, 137*(11), 4030-4046. doi: 10.1175/2009mwr2880.1

Stephens, G. L., Vane, D. G., Boain, R. J., Mace, G. G., Sassen, K., Wang, Z., . . . Team, t. C. S. (2002). The CloudSat Mission and the A-Train: A New Dimension of Space-Based Observations of Clouds and Precipitation. *Bulletin of the American Meteorological Society, 83*(12), 1771-1790. doi: 10.1175/bams-83-12-1771

Stephens, G. L., Vane, D. G., Tanelli, S., Im, E., Durden, S., Rokey, M., . . . Marchand, R. (2008). CloudSat mission: Performance and early science after the first year of operation. *Journal of Geophysical Research: Atmospheres, 113*(D8). doi: 10.1029/2008jd009982

Stephenson, D., Pavan, V., & participating, C. m. g. (2003). The North Atlantic Oscillation in coupled climate models: a CMIP1 evaluation. *Climate Dynamics, 20*(4), 381-399. doi: 10.1007/s00382-002-0281-5

Stocker, T. F., Qin, D., Plattner, G.-K., Tignor, M., Allen, S. K., Boschung, J., . . . Midgley, P. M. (2013). Climate change 2013: The physical science basis.

Tang, M. S. Y., Chenoli, S. N., Colwell, S., Grant, R., Simms, M., Law, J., & Abu Samah, A. (2018a). Precipitation instruments at Rothera Station, Antarctic Peninsula: a comparative study. *Polar Research, 37*(1), 1503906. doi: 10.1080/17518369.2018.1503906

Tang, M. S. Y., Chenoli, S. N., Samah, A. A., & Hai, O. S. (2018b). An assessment of historical Antarctic precipitation and temperature trend using CMIP5 models and reanalysis datasets. *Polar Science, 15*, 1-12. doi: https://doi.org/10.1016/j.polar.2018.01.001

Taylor, K. E., Stouffer, R. J., & Meehl, G. A. (2012). An Overview of CMIP5 and the Experiment Design. *Bulletin of the American Meteorological Society, 93*(4), 485-498. doi: 10.1175/bams-d-11-00094.1

Thépaut, J.-N., Courtier, P., Belaud, G., & Lemaître, G. (1996). Dynamical structure functions in a four-dimensional variational assimilation: A case study. *Quarterly Journal of the Royal Meteorological Society, 122*(530), 535-561. doi: 10.1002/qj.49712253012

Turner, J., Anderson, P., Lachlan-Cope, T., Colwell, S., Phillips, T., Kirchgaessner, A., . . . Orr, A. (2009a). Record low surface air temperature at Vostok station,

Antarctica. *Journal of Geophysical Research: Atmospheres, 114*(D24). doi: 10.1029/2009jd012104

Turner, J., Bracegirdle, T. J., Phillips, T., Marshall, G. J., & Hosking, J. S. (2013). An Initial Assessment of Antarctic Sea Ice Extent in the CMIP5 Models. *Journal of Climate, 26*(5), 1473-1484. doi: 10.1175/jcli-d-12-00068.1

Turner, J., Chenoli, S. N., abu Samah, A., Marshall, G., Phillips, T., & Orr, A. (2009b). Strong wind events in the Antarctic. *Journal of Geophysical Research: Atmospheres, 114*(D18). doi: 10.1029/2008jd011642

Turner, J., Lachlan-Cope, T. A., Thomas, J. P., & Colwell, S. R. (1995). The synoptic origins of precipitation over the Antarctic Peninsula. *Antarctic Science, 7*(3), 327-337. doi: Doi: 10.1017/s0954102095000447

Turner, J., Marshall, G. J., & Lachlan‐Cope, T. A. (1998). Analysis of synoptic‐scale low pressure systems within the Antarctic Peninsula sector of the circumpolar trough. *International Journal of Climatology: A Journal of the Royal Meteorological Society, 18*(3), 253-280.

Uotila, P., Lynch, A. H., Cassano, J. J., & Cullather, R. I. (2007). Changes in Antarctic net precipitation in the 21st century based on Intergovernmental Panel on Climate Change (IPCC) model scenarios. *Journal of Geophysical Research: Atmospheres, 112*(D10). doi: 10.1029/2006jd007482

Uppala, S. M., Kållberg, P. W., Simmons, A. J., Andrae, U., Bechtold, V. D. C., Fiorino, M., . . . Woollen, J. (2005). The ERA-40 re-analysis. *Quarterly Journal of the Royal Meteorological Society, 131*, 2961. doi: 10.1256/qj.04.176

van Lipzig, N. P. M., King, J. C., Lachlan-Cope, T. A., & van den Broeke, M. R. (2004). Precipitation, sublimation, and snow drift in the Antarctic Peninsula region from a regional atmospheric model. *Journal of Geophysical Research: Atmospheres, 109*(D24). doi: 10.1029/2004jd004701

van Lipzig, N. P. M., Marshall, G. J., Orr, A., & King, J. C. (2008). The Relationship between the Southern Hemisphere Annular Mode and Antarctic Peninsula Summer Temperatures: Analysis of a High-Resolution Model Climatology. *Journal of Climate, 21*(8), 1649-1668. doi: 10.1175/2007jcli1695.1

Wang, Y., Ding, M., van Wessem, J. M., Schlosser, E., Altnau, S., van den Broeke, M. R., . . . Sun, W. (2016). A Comparison of Antarctic Ice Sheet Surface Mass Balance from Atmospheric Climate Models and In Situ Observations. *Journal of Climate, 29*(14), 5317-5337. doi: 10.1175/jcli-d-15-0642.1

Watterson, I. G., Bathols, J., & Heady, C. (2014). What Influences the Skill of Climate Models over the Continents? *Bulletin of the American Meteorological Society, 95*(5), 689-700. doi: 10.1175/bams-d-12-00136.1

Weatherly, J. W. (2004). Sensitivity of Antarctic Precipitation to Sea Ice Concentrations in a General Circulation Model. *Journal of Climate, 17*(16), 3214-3223. doi: 10.1175/1520-0442(2004)017<3214:soapts>2.0.co;2

Whitaker, J. S., Compo, G. P., & Thépaut, J.-N. (2009). A Comparison of Variational and Ensemble-Based Data Assimilation Systems for Reanalysis of Sparse Observations. *Monthly Weather Review, 137*(6), 1991-1999. doi: 10.1175/2008mwr2781.1

Willmott, C. J., Rowe, C. M., & Philpot, W. D. (1985). Small-Scale Climate Maps: A Sensitivity Analysis of Some Common Assumptions Associated with Grid-Point Interpolation and Contouring. *The American Cartographer, 12*(1), 5-16. doi: 10.1559/152304085783914686

Wu, Y., & Polvani, L. M. (2015). Contrasting short-and long-term projections of the hydrological cycle in the southern extratropics. *Journal of Climate, 28*(14), 5845-5856.

Yang, D. (1999). An improved precipitation climatology for the Arctic Ocean. *Geophysical Research Letters, 26*(11), 1625-1628. doi: 10.1029/1999gl900311

Yin, L., Fu, R., Shevliakova, E., & Dickinson, R. E. (2013). How well can CMIP5 simulate precipitation and its controlling processes over tropical South America? *Climate Dynamics, 41*(11), 3127-3143. doi: 10.1007/s00382-012-1582-y

Yuan, X., Wood, E. F., Luo, L., & Pan, M. (2011). A first look at Climate Forecast System version 2 (CFSv2) for hydrological seasonal prediction. *Geophysical Research Letters, 38*(13). doi: 10.1029/2011gl047792

Yue, Y., Niu, S., Zhao, L., Zhang, Y., & Xu, F. (2012). Chemical Composition of Sea Fog Water Along the South China Sea. *Pure and Applied Geophysics, 169*(12), 2231-2249. doi: 10.1007/s00024-012-0486-4

Zhang, L., Kumar, A., & Wang, W. (2012). Influence of changes in observations on precipitation: A case study for the Climate Forecast System Reanalysis (CFSR). *Journal of Geophysical Research: Atmospheres, 117*(D8). doi: 10.1029/2011jd017347

Zhang, L., Zhao, L., Xie, C., Liu, G., Gao, L., Xiao, Y., . . . Qiao, Y. (2015). Intercomparison of Solid Precipitation Derived from the Weighting Rain Gauge and Optical Instruments in the Interior Qinghai-Tibetan Plateau. *Advances in Meteorology, 2015*, 936724. doi: 10.1155/2015/936724

Zheng, F., Li, J., Clark, R. T., & Nnamchi, H. C. (2013). Simulation and Projection of the Southern Hemisphere Annular Mode in CMIP5 Models. *Journal of Climate, 26*(24), 9860-9879. doi: 10.1175/jcli-d-13-00204.1

Zhou, T., Zou, L., Wu, B., Jin, C., Song, F., Chen, X., & Zhang, L. (2014). Development of earth/climate system models in China: A review from the Coupled Model Intercomparison Project perspective. *Journal of Meteorological Research, 28*(5), 762-779. doi: 10.1007/s13351-014-4501-9

LIST OF PUBLICATIONS AND PAPERS PRESENTED

1. An assessment of historical Antarctic precipitation and temperature trend using CMIP5 models and reanalysis datasets, MSY Tang, SN Chenoli, AA Samah, OS Hai, Polar Science 15, 1-12
2. Precipitation instruments at Rothera Station, Antarctic Peninsula: a comparative study, MSY Tang et al., Polar Research 37 (1), 1503906
3. Precipitation and temperature trend in Antarctica under four different representative concentration pathways in CMIP5 models, MSY Tang, SN Chenoli, AA Samah (in progress).
4. ARIMA modeling of precipitation in Rothera Station, Antarctic Peninsula (in progress).